Report of Investigations No. 121

SAN ANDRES CARBONATES IN THE TEXAS PANHANDLE:

Sedimentation and Diagenesis Associated with Magnesium-Calcium-Chloride Brines

by Amos Bein and Lynton S. Land

1982
Bureau of Economic Geology
W. L. Fisher, Director
The University of Texas at Austin
Austin, Texas 78712

Report of Investigations No. 121

SAN ANDRES CARBONATES IN THE TEXAS PANHANDLE:

Sedimentation and Diagenesis Associated with Magnesium-Calcium-Chloride Brines

by Amos Bein[1] and Lynton S. Land[2]

[1]Visiting Research Scientist, Bureau of Economic Geology, 1980-1981; currently at the Geological Survey of Israel, Jerusalem, 95501, Israel.
[2]Professor, Department of Geological Sciences, The University of Texas at Austin, Austin, Texas 78712.

Funding provided by the U.S. Department of Energy
under Contract No. DE-AC97-80ET-46615
and the National Science Foundation
under Contract No. EAR-7824081

1982
Bureau of Economic Geology
W. L. Fisher, Director
The University of Texas at Austin
Austin, Texas 78712

CONTENTS

ILLUSTRATIONS

Figures

Tables

ABSTRACT

The San Andres evaporitic sequence in the Palo Duro Basin comprises several thick carbonate units in its lower part and many thin units in its upper part. To the south, across the Northern Shelf of the Midland Basin, evaporites pinch out and carbonates predominate. Six lithofacies were differentiated in the Palo Duro and Northern Shelf carbonates: dolomudstone, pellet-oolite packstone-grainstone, filamentous (*Girvanella*-like) grainstone, sponge spicule packstone, wispy-laminated crinoid packstone, and skeletal packstone-grainstone. Facies distribution was controlled by water-body salinity, which increased from south to north. Within the Palo Duro Basin, the carbonates in the upper part of the sequence differ from those in the lower part in that the former lack skeletal lithofacies and have higher manganese, iron, and terrestrial organic matter content. Bromide (Br) content in halite in the lower part of the sequence is consistently high, whereas halite in the upper part is mostly depleted in bromide. Strontium (Sr) in dolomite, calcite and anhydrite, $\delta^{18}O$, $\delta^{13}C$ values, and early diagenetic oxidizing conditions deduced from high pristane/phytane ratios are about the same throughout the entire San Andres Formation in the Palo Duro Basin. Depleted $\delta^{13}C$ values in dolomites associated with low pristane/phytane ratios in the Northern Shelf formed under more reducing conditions in which organically derived carbon in the carbonates increased because of sulfate-reducing bacterial activity. Sodium/chloride and potassium/chloride ratios attributed to liquid inclusions in almost all carbonates are characteristic of marine brines evaporated beyond the level of halite saturation. Sodium content in the dolomite lattice is generally low and increases from north to south at the same stratigraphic levels.

Varied sedimentologic and geochemical properties of the rocks throughout the area reflect different primary depositional regimes. Properties that do not vary are attributed to diagenetic modification of the rocks in contact with brines having similar compositions. The lower part of the formation was deposited in a broad shelf basin or lagoon sufficiently deep to maintain long periods of steady-state circulation. During these periods neither halite dissolution nor potash-magnesia mineral precipitation occurred. The upper part of the formation was deposited in smaller water bodies sensitive to inflow fluctuations. Increased proportion of meteoric water in the depositional environment during this period is evidenced by high content of manganese, iron, and terrestrial organic matter, and the meteoric water was a source of dissolved carbonate for the deposition of many of the thin carbonate units.

Diagenesis of the San Andres carbonates occurred in contact with saline magnesium-calcium-chloride brines, which evolved from seawater by anhydrite and halite precipitation. Skeletal mold formation and subsequent anhydrite cementation, dolomitization, and high-strontium calcite cementation associated with celestite precipitation are all cogenetic processes controlled by this brine-rock interaction. The $\delta^{18}O$ composition of dolomite, calcite, and chert indicates apparent equilibrium relations with the same solution. Possible low temperatures of 40° to 45° C (105° to 110° F) imply $\delta^{18}O$ of such a solution to be about 2 to 3‰. The somewhat light $\delta^{18}O$ composition of the proposed halite-saturated brine may have resulted from the reversal in the positive correlation between $\delta^{18}O$ and increased evaporation in highly saline brines.

San Andres carbonates in the Palo Duro Basin that were diagenetically altered in a halite-saturated magnesium-calcium chloride brine were plugged by precipitating salt and remain unchanged and isolated in a closed sedimentary basin. The Northern Shelf carbonates were modified by similar brines intermittently undersaturated with respect to halite because of mixing with seawater. As a result, some original porosity remained, and pressure solution occurred in the more deeply buried and more skeletal-rich sequence.

INTRODUCTION

The replacement nature of most dolomite and the inability to simulate dolomite formation under normal sedimentary conditions in laboratory experiments create uncertainty in relating a rock composition to its depositional and diagenetic environment. Ancient dolomite is especially complex because of late diagenetic modification in the subsurface. Dolomite may recrystallize and reequilibrate with solutions of unknown compositions under a variety of ill-defined conditions. These basic limitations complicate every attempt to reconstruct the depositional and diagenetic sequence of ancient rocks and to differentiate the various models that may account for dolomite formation. Heterogeneous strata, in which dolomites are associated with other lithic components such as evaporite minerals, chert, and organic matter, can probably be more accurately interpreted than can homogeneous dolomite strata. Independent information provided by each lithic component and its relation to the others provides a clearer understanding of the dolomitization process.

The Permian San Andres Formation in the Palo Duro Basin and Northern Shelf, Texas, is one such heterogeneous sedimentary system. It consists of closely associated halite, anhydrite, dolomite, and mudstone together with small amounts of calcite, quartz silt, celestite, chert, and organic matter. The stratigraphy, facies analysis, and spatial distribution of the main rock types within the formation have been studied by Presley (1979, 1981), Handford and others (in press), and Ramondetta (in press). Their studies provide a well-established framework; this study provides more details concerning the process by which the carbonate fabric was shaped and modified through time. Our investigation includes optical and scanning electron microscopy, whole-rock and electron probe chemical analysis, detailed X-ray diffraction of dolomites, bromine analysis of salt, strontium analysis of anhydrite, stable isotopic analysis of carbonates and chert, and organic matter analysis by gas chromatography and total organic carbon determination.

This study is part of the analysis of Permian bedded salt sequences in the Texas Panhandle funded by the U.S. Department of Energy. Basin analysis is designed to evaluate the feasibility of isolating nuclear wastes in subsurface salt beds. Establishing diagenetic sequences in the carbonates intercalated with the salts may assist in answering two basic questions, namely, how hydrologically isolated is the system and how does it relate to the prolific San Andres petroleum reservoirs along the northern margin of the Midland Basin?

GEOLOGIC SETTING

The San Andres Formation is the middle part of the Permian salt-bearing sequence throughout northwest Texas and New Mexico. The Texas Panhandle is underlain by several sedimentary basins bounded by uplifted basement blocks. The Palo Duro Basin is separated from the Midland Basin to the south by the Matador Arch and from the Dalhart and Anadarko Basins to the north by the Amarillo Uplift (fig. 1). The regional structure was shaped mainly during Pennsylvanian and Early Permian time (Wickman, 1978). Continuous subsidence of the area during the Middle and Late Permian enabled thick evaporites to accumulate within the area, masking many early structural elements along the Matador Arch and Amarillo Uplift. Isopach maps of the San Andres Formation (fig. 1, Presley, 1981; P. Ramondetta, personal communication, 1981) indicate an overall thickening from north to south without significant thinning over the formerly uplifted areas (fig. 1). In the study area the thickness of the formation ranges from about 166 m (800 ft) in the north to about 533 m (1,600 ft) in the south, and depth of burial increases in the same direction from about 370 m (1,110 ft) to more than 1,670 m (5,010 ft) (fig. 2).

North of the Midland Basin, the San Andres Formation is normally considered to be a shallow marine to supratidal sabkha facies tract, composed of cyclic evaporites, carbonates, and terrigenous sediments that accumulated during a general regression. To the south, in the Midland Basin, the formation is composed mainly of oolitic and sponge spiculite limestones. Studies of the San Andres Formation or its time equivalents throughout the entire area include those by Chuber and Pusey (1972), Meissner (1972), Jacka and Franco (1973), Smith (1974), Milner (1976), Todd (1976), Mejia (1977), Ramondetta (in press), Presley (1981), and Handford and others (in press).

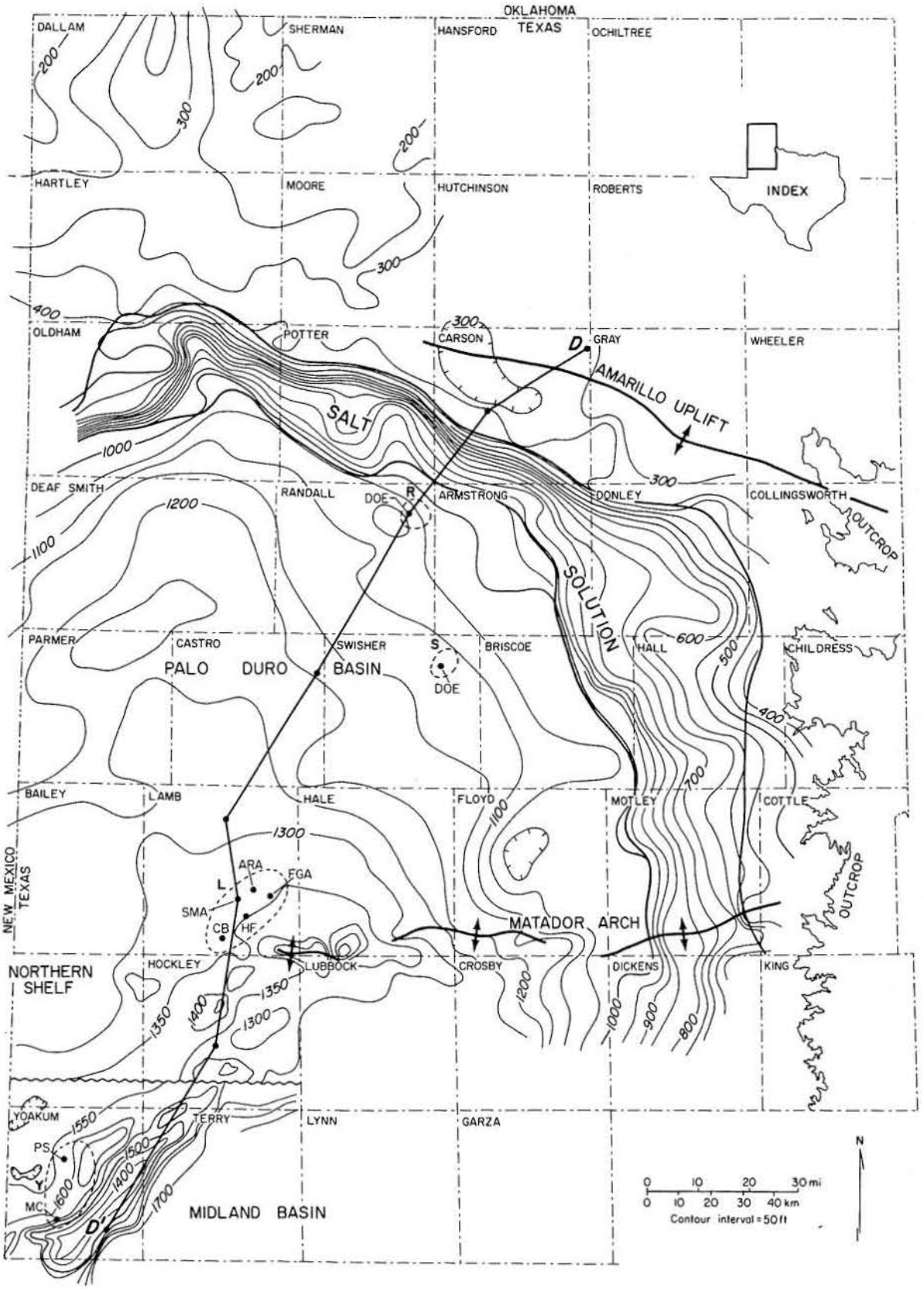

Figure 1. Location and isopach map of the San Andres Formation in the study area (after Presley, 1979, and P. Ramondetta, personal communication, 1981). The wavy line in southern Hockley County marks a change in the basal San Andres electric log marker. Wells sampled for detailed study are: Randall *D.O.E.* – Gruy Federal No. 1 Rex White; Swisher *D.O.E.* – Gruy Federal No. 1 Grabbe; Lamb *ARA* – Atlantic Oil Ryan No. 1; Lamb *FGA* – Felmont Gray No. 1; Lamb *HF* – Humble Oil Fowler No. 1; Lamb *CB* – Crown Baumgart No. 1; Lamb *SMA* – Shell Ivey McCary No. 1; Yoakum *PS* – Sun Oil Pharr No. 1; and Yoakum *MC* – Moor Bros. Cleveland No. 1.

METHODS OF STUDY

Technique

Cores used in this study are from wells concentrated in four sites along a north-south line in Randall, Swisher, Lamb, and Yoakum Counties, Texas (fig. 1). Data are grouped by samples defined according to stratigraphic position and geographic location (fig. 2). Data groups and their codes are given in table 1. Several groups combined together are designated by letters standing for geographic locations or the numbers that mark the stratigraphic position, or both (for example, LSR4 stands for cycle 4 in Lamb, Swisher, and Randall Counties).

After split cores were described in detail, samples were cut for petrographic and chemical analyses. Samples for whole-rock analysis were ground finer than 0.15 mm. Carbonate samples (~4 g) were stirred twice for 20-minute periods in 1 liter of distilled water and thereafter centrifuged and decanted until all soluble Cl^- and much of the $SO_4^=$ was eliminated, as determined by conductivity monitoring of the solutions and by direct indicators. Anhydrite samples were washed for shorter periods to remove only soluble salts. After acid digestion, multielement chemical analysis was conducted using inductively coupled plasma atomic emission spectrometry (ICP). Samples were analyzed twice in different concentrations to account for major (calcium and magnesium) and trace element constituents. ICP calibration included standards and atomic absorption spectrophotometric cross checks of duplicate samples. Solutions used in ICP analysis were further analyzed for chloride content by colorimetry and for SO_4 concentration by turbidimetry. The amount of bromine in halite was determined by hypochloric oxidation and titration and was calculated relative to chloride values in the same solutions. Stable isotope ratios of carbon and oxygen in carbonates and oxygen in chert were determined by standard techniques (McCrea, 1950; Clayton and Mayeda, 1963). Quartz was separated from anhydrite, carbonates, and other silicates by fusion with $NaHSO_4$ (Syers and others, 1968).

Total organic carbon was analyzed after acid digestion by combustion in a LECO Carbon Analyzer. Bituminous matter was Soxhlet extracted with chloroform and was liquid chromatographed on a silicic acid column. Saturated hydrocarbons were differentiated on a capillary column in a gas chromatograph.

Table 1. Rock unit symbols used in this study.

	N		Location	S		
	Randall County	Swisher County	Lamb County	Yoakum County		
San Andres Formation	R5,6	S5,6	–	Y5,6	Cycle 5, 6 (fig. 6)	Stratigraphic Interval
	R4	S4	L4	–	Cycle 4 (fig. 5)	
	R3	S3	L3	–	Cycle 3 (fig. 4)	
	R2	S2	–	–	Cycle 2 (fig. 3)	

Petrographic and chemical analysis of undisturbed rock samples included optic and scanning electron microscopy (SEM) as well as electron microprobe. X-ray diffraction was routinely used to check the mineralogical composition of samples before and after separation procedures. Lattice parameters of dolomite were determined by least-squares analysis of detailed X-ray diffractometer data. The SPSS computer program was used for data handling.

Interpretation

Since the trace element content of most of the samples is near or below the detection limit of the electron probe, basic chemical data were derived by whole-rock analysis. Pre-analysis treatment eliminated from the samples any brine or soluble salts other than liquid inclusions in the carbonate crystals. Most of the sulfate minerals (primarily anhydrite and some celestite) were also removed by this procedure, but residues of these minerals were still detected by the rock analysis. Clay, quartz, and organic matter, which together compose up to about 5 percent of most of the samples, are by definition insoluble residues in water and acid. However, some leaching of clays occurred during carbonate analyses, as indicated by the release of aluminum, titanium, and potassium into solution.

Interpretation of basic data, which included values for chloride, sulfate, and 20 cations, involved a two-step procedure. First, the main mineralogic composition and insoluble residue content were calculated by considering all sulfate as derived from anhydrite, all magnesium as dolomite, and the remaining calcium (after subtracting the appropriate amounts of calcium for anhydrite and dolomite) as calcite. A low deviation from stoichiometric dolomite composition, based on X-ray diffraction and electron probe data, appears to justify this mode of calculation. Trace element composition was calibrated to a pure soluble phase, which in most of the samples corresponds to 95 to 100 percent dolomite and less than 0.5 percent anhydrite. Second, the trace elements were correlated with the aluminum content in the same samples. High correlations clearly demonstrate the relatively high contribution of trace elements by clays. Such high correlations provide zero-aluminum intercept values that may approximate the average values of trace elements in the carbonate system.

Strontium content in anhydrite was calculated after correcting the $CaSO_4$ content by subtracting amounts of calcium equivalent to magnesium considered to be derived from dolomite impurities. True magnesium substitution for calcium in anhydrite (apparently less than 500 ppm) may have created a small error in the calibrated values.

Bromide content in halite samples was calculated from either chloride or sodium analysis of the same solution. Two samples from below the San Andres Formation, in which sodium chloride content was only about 30 percent of the total rock, exhibited very high calculated bromine values (~280 ppm), indicating a possible bromine release from some of the associated clay. In all San Andres halite samples, sodium chloride composed over 90 percent of the sample; bromine derived from minerals other than halite was apparently negligible.

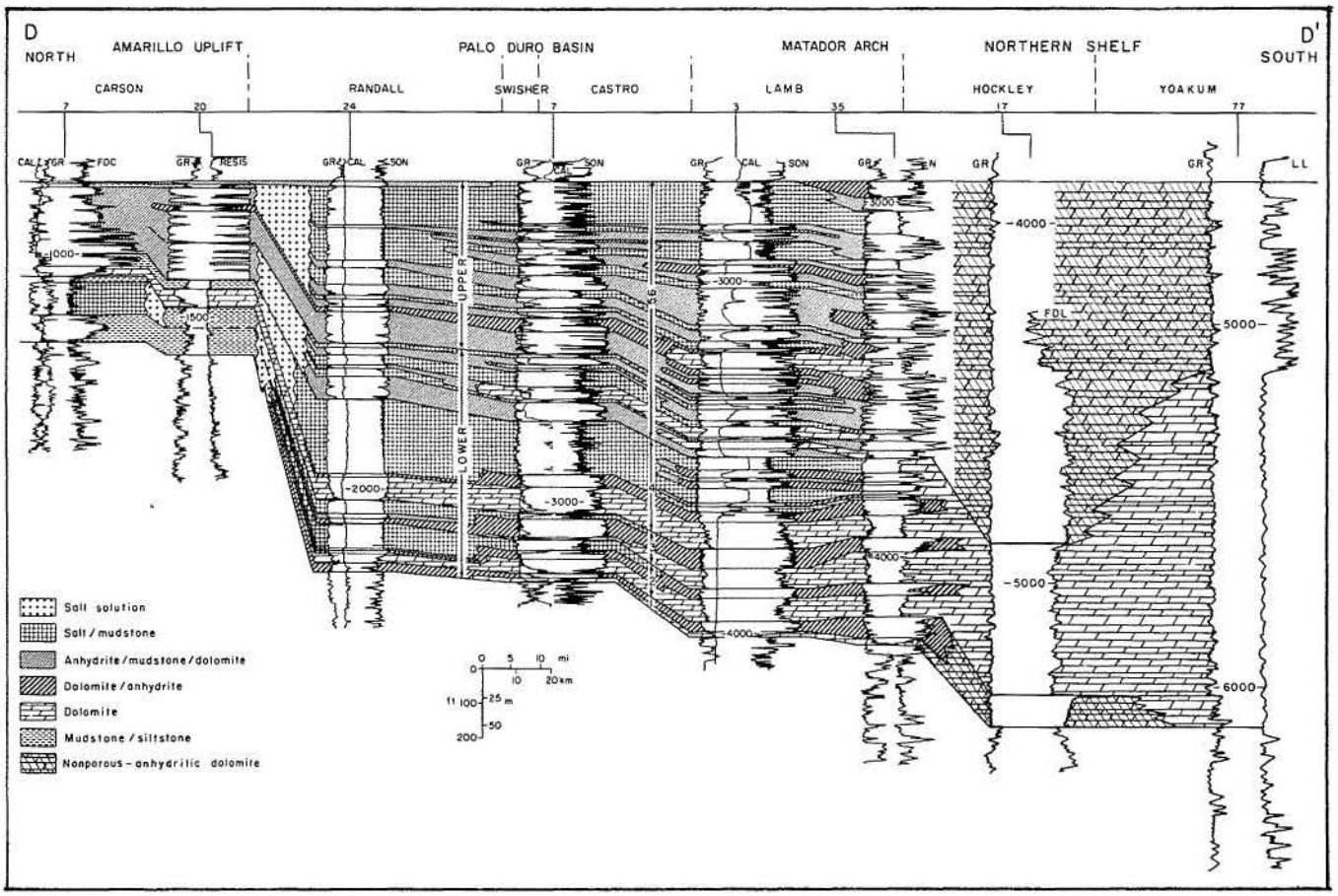

Figure 2. North-south cross section through the study area (after Presley, 1979, and P. Ramondetta, personal communication, 1981). Pinch-out of salt and anhydrite preclude detailed log correlation to the south. Datum: Top San Andres. See figure 1 for line of section.

CARBONATE LITHOFACIES

Six lithofacies were identified on the basis of petrographic studies of the cored sequences. Each is briefly described and its distribution is illustrated by several cross sections (figs. 3, 4, 5, and 6). Because large parts of the San Andres Formation are composed of chemical precipitates, environmental interpretations in this study were made principally by analyses of relative salinity, energy level, and ecology rather than by application of the recent physiography of tidal-sabkha environments to the Palo Duro Permian sequence, as was done by Handford and others (in press) and Presley (1981). Many criteria traditionally used to identify the various components of a tidal-sabkha setting (such as anhydrite nodules, algal mats, fenestral fabrics, upward shoaling, and evaporitic sequences) may be explained alternatively by changes in water chemistry and energy conditions. These, in turn, may be affected by the efficiency of the basin inflow and outflow, evaporation rates, storms, amount of continental runoff, and so on, and not necessarily by shoaling of the water body and exposing of the sequence to intertidal and supratidal conditions. The depositional and diagenetic model will be discussed further after presentation of chemical data on the carbonates, anhydrite, and salt, and after evaluation of the constraints involved in the deposition of such a widespread, thick evaporite sequence.

Dolomudstones

A scarcity of allochems and a more or less homogeneous, fine-crystalline texture characterize the dolomudstones. Dolomite crystal size normally ranges between 2 and 5μm, but commonly may reach 10μm or more (fig. 7b). Many dolomudstones exhibit some lamination. Laminations are dark and light bands, reflecting different amounts of clay, organic matter, and quartz silt, or alternations of crystal fabric density and dolomite-anhydrite intergrowth (fig. 7a, 7b). Laminations are of two types: current lamination (parallel and low-angle cross-lamination), and wavy algal lamination. Some of the current laminae display clear-cut lower boundaries with rare, minute, cut-and-fill features. Silt-sized pellets, skeletal grains, and burrows are occasionally observed in these rocks.

Mudstones are normally attributed to low-energy environments, but since many recent carbonate mudstones are actually deposited as pelletal sands that collapse or amalgamate early during diagenesis, higher energy conditions must be considered. In some of the San Andres rocks, a pelletal sand origin is evident owing to differential pellet preservation in protected areas such as in early skeletal molds (fig. 7d, 7g). In most others, however, early geopetal mud in skeletal molds (fig. 7c, 7e), fine laminae combined with rare but only silt-sized allochems (pellets, skeletal fragments, quartz), and close association with well-preserved pelletal grainstones (fig. 7f) apparently support a relatively low-energy mud environment for most of the San Andres dolomudstones. Low biogenic contribution or activity, other than algal mats, indicates unfavorable ecological conditions, mostly caused by elevated or reduced salinity relative to normal seawater. For the dolomudstone-anhydrite intergrowth association, salinities above normal are evident, indicating that the muds originated in hypersaline brines as chemical precipitates, presumably originally aragonite. The absence of desiccation cracks, solution breccia, caliche crusts, flat pebble conglomerates, small-scale tepees, pisolites, or other clear-cut indicators of contemporaneous subaerial exposure, points to a subtidal depositional regime.

Pellet-Oolite Packstones and Grainstones

Pellets and ooids are the main allochem types in these rocks, but mixtures of the two, sometimes associated with skeletal fragments, also exist. It is commonly hard to distinguish between grain types because of diagenetic effects such as micritization and dissolution.

Pellets: Pellets range in size from 30μm to 300μm; shapes include round, oval, and somewhat elongated equant forms. Many of the pelletal rocks exist as thin (a few mm to tens of mm) bands in mudstones (fig. 7f). Although some of the rocks are different in grain shape and size, most are well sorted. Sorting by size and shape in pelletal rocks is partly attributed to low diversity of pellet-producing fauna. Removal of mud from grainstones must have involved some moderate-energy conditions.

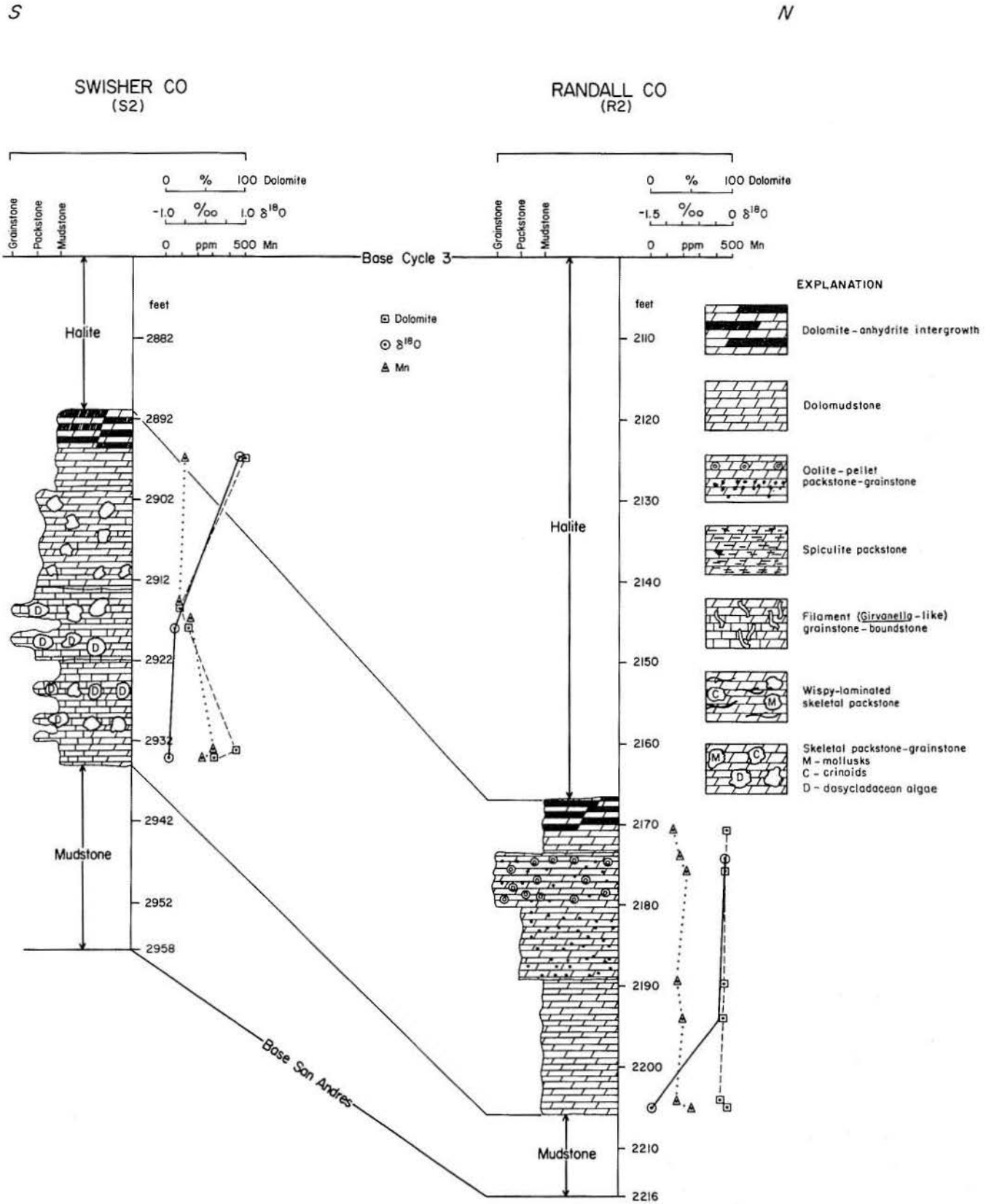

Figure 3. Lithofacies distribution of SR2 rock units.

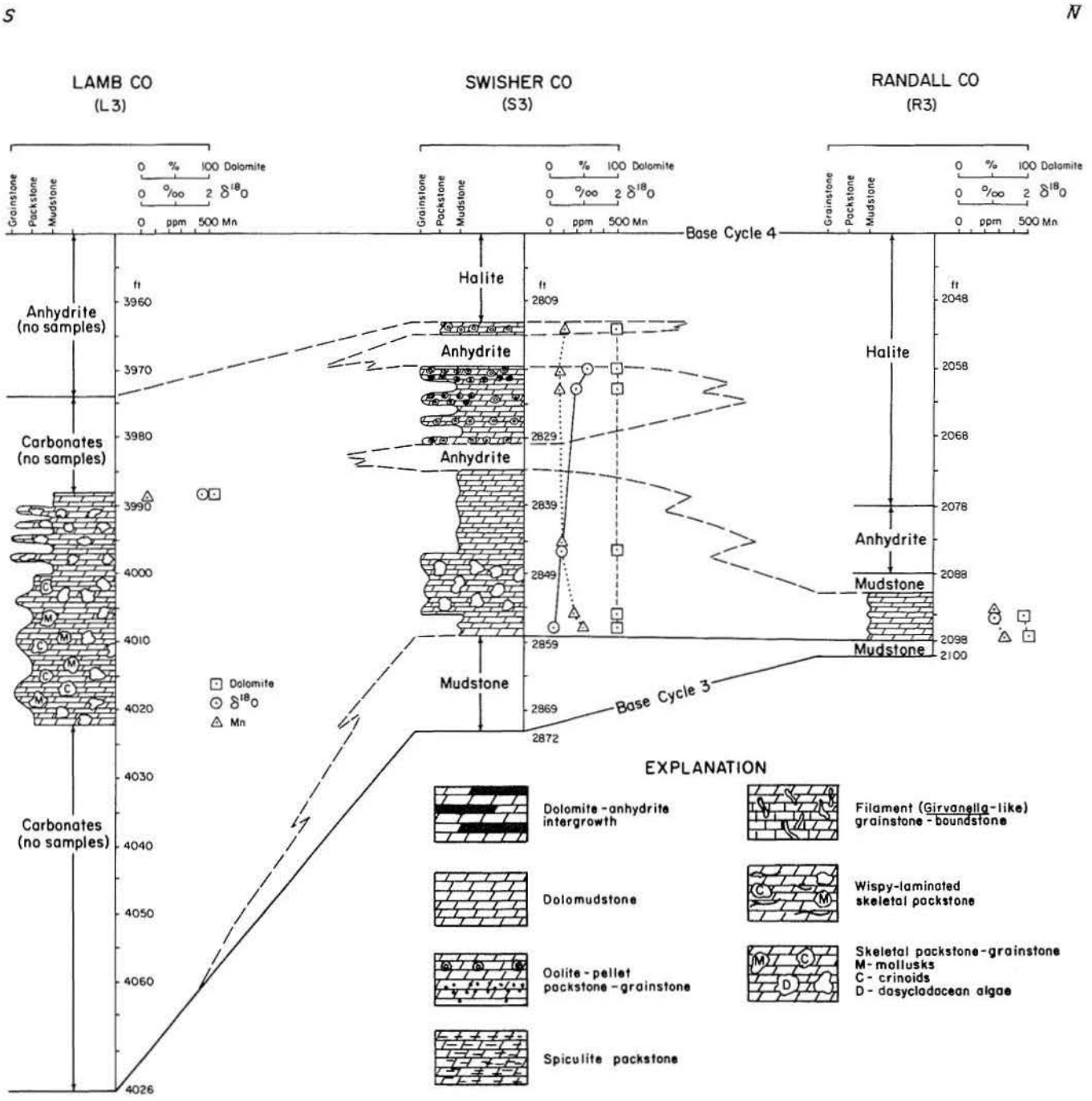

Figure 4. Lithofacies distribution of LSR3 rock units. L3 description from SMA well.

Ooids: Ooids range between 50μm and 300μm. Some of the grainstones are well sorted and cross-laminated, and a few exhibit small (millimeter-size) grading. Ooids in the packstones (and a few wackestones) are less sorted and include smaller ooids that are somewhat more densely packed (fig. 8c, 8e, 8f). Many of the larger ooids are composed of a dense nucleus similar in texture to the smaller ooids and coated with more loosely packed concentric layers (fig. 9a). Deformed ooids, sometimes extremely deformed, occur in the oolitic grainstones (fig. 8a, 8d). A one-crystal-thick cement layer fringes almost every ooid, including the most deformed ones (fig. 8b, 8d). Cement crystals are generally large (15 to 20μm) and almost equant (fig. 9c). A cement-like internal layer (fig. 9b) is a common feature of the concentric ooid layers. Some of the ooids and pellets in packstones are coated with a thin, one-crystal-thick, dolomite cement layer and are embedded in a mud matrix. The only ooids

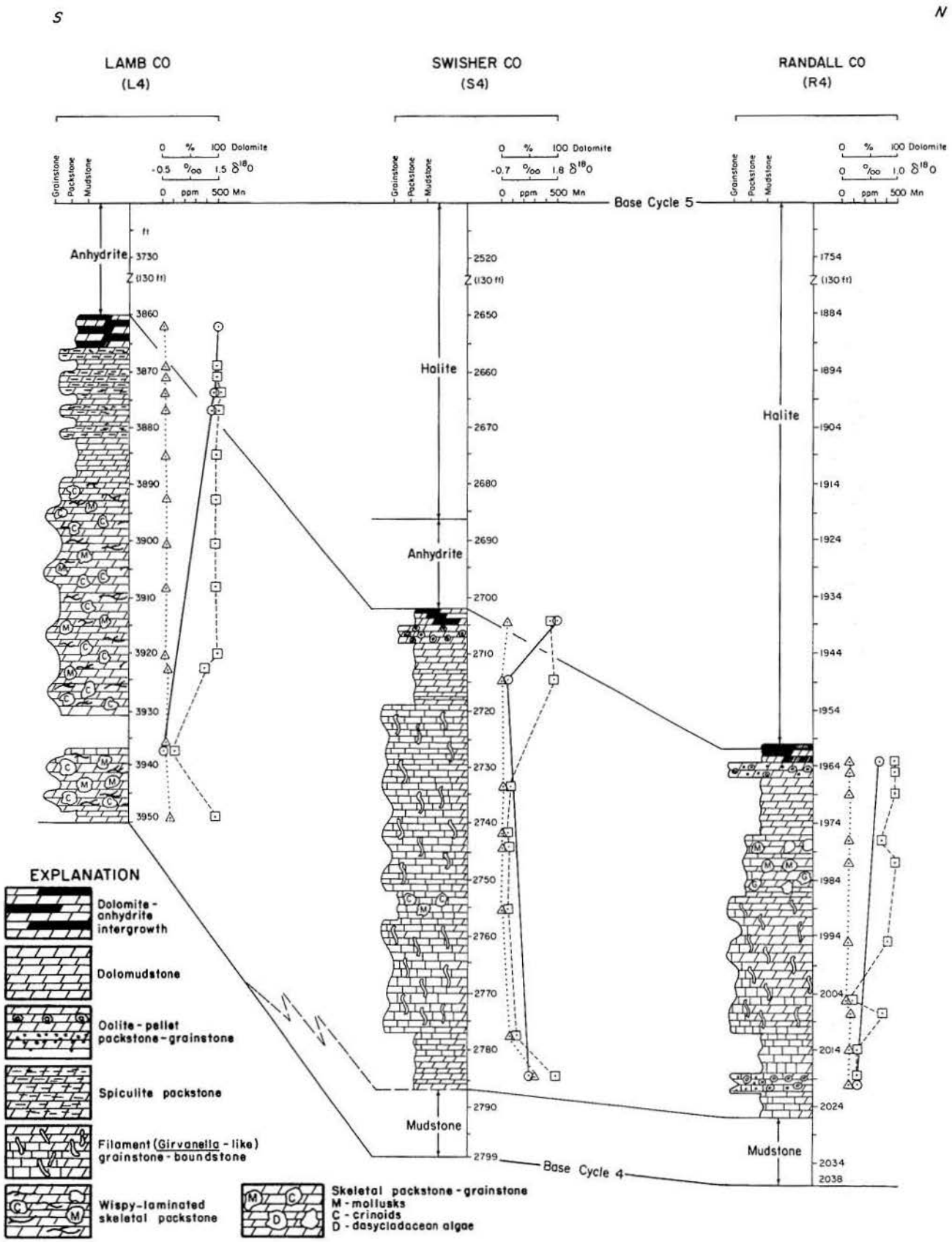

Figure 5. Lithofacies distribution of LSR 4 rock units. L4 description from ARA, CB, HF, and FGA wells.

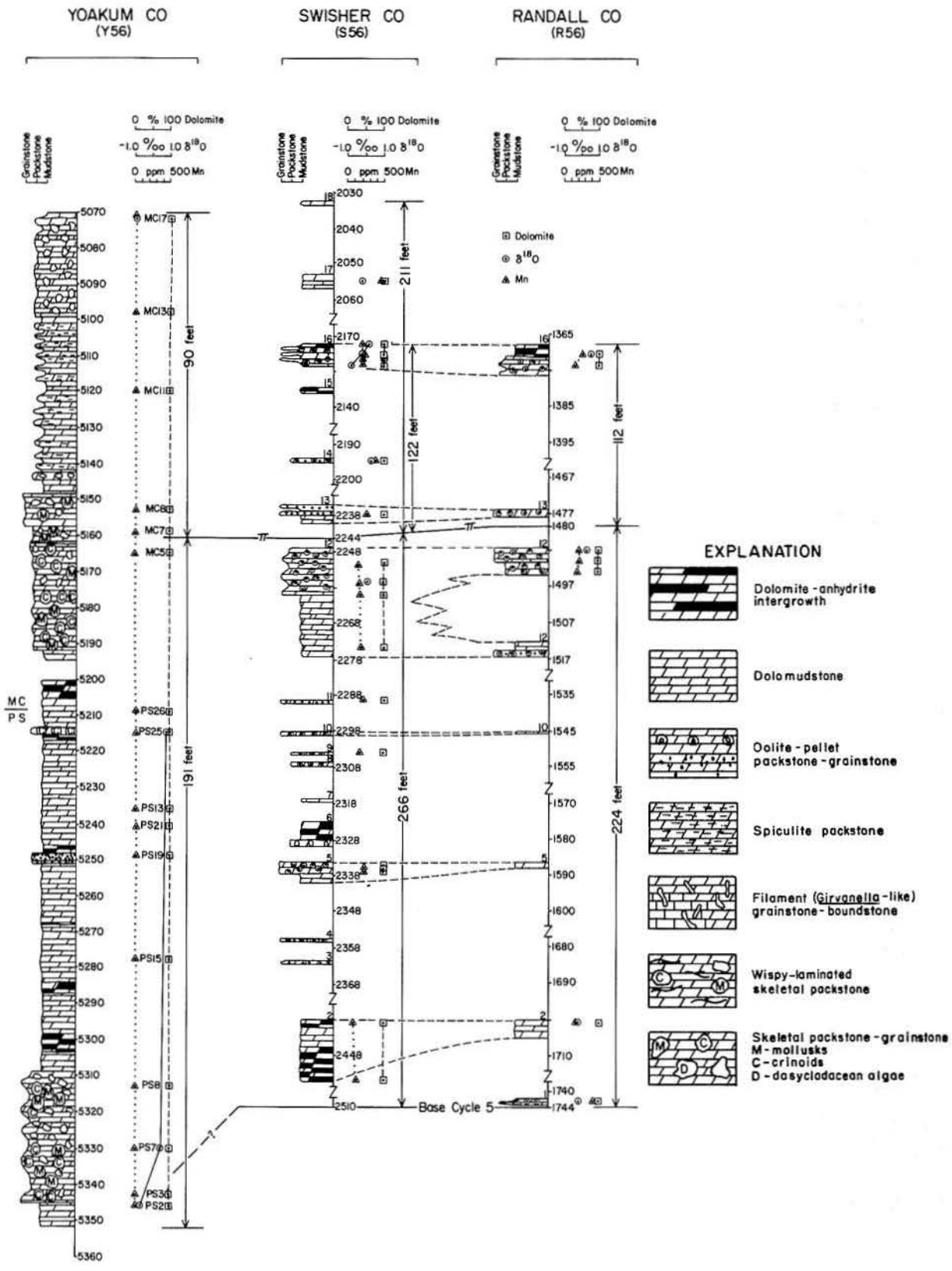

Figure 6. Lithofacies distribution of YSR56 rock units. Y56 description composite from PS and MC wells.

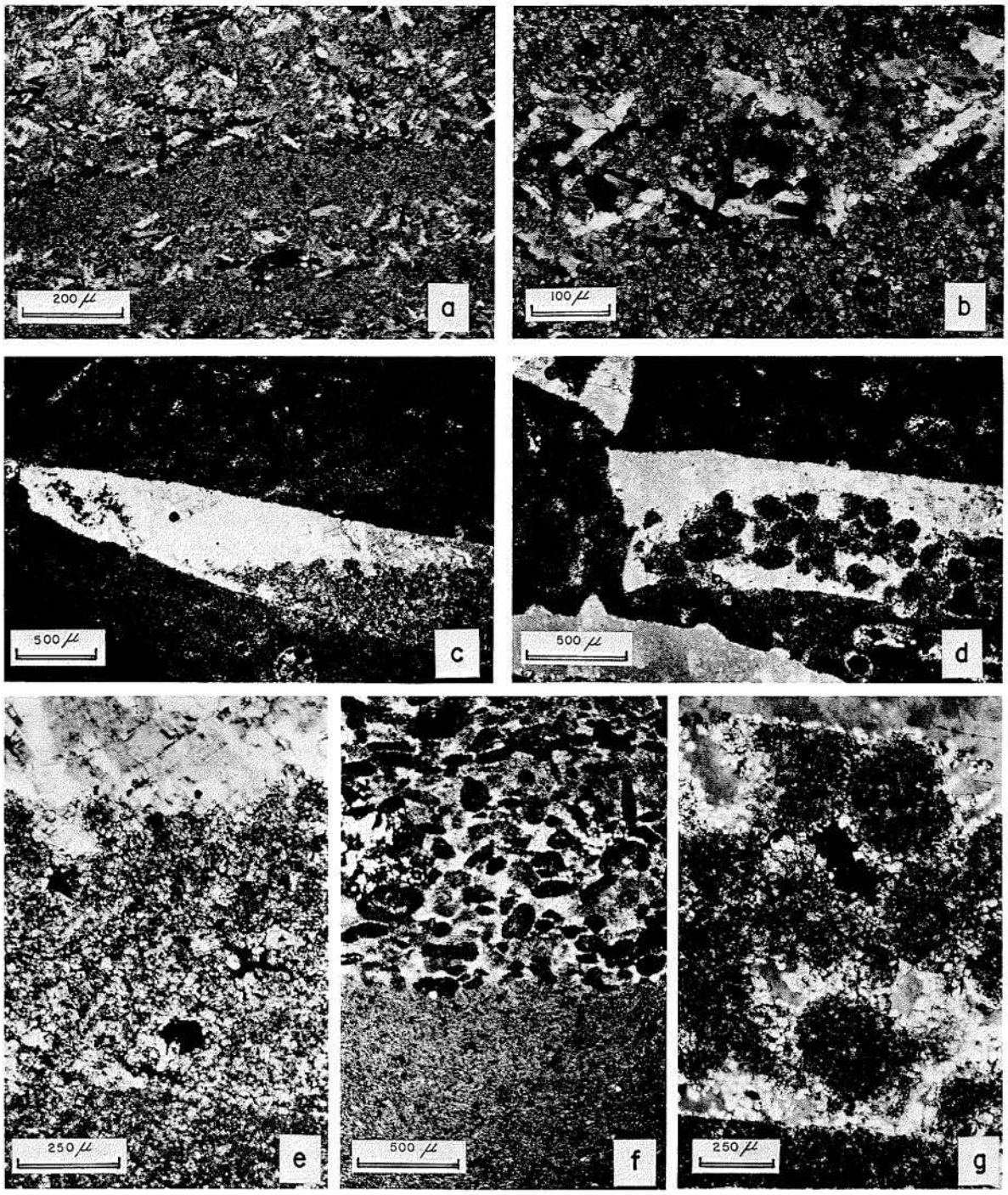

Figure 7. Photomicrographs of San Andres rocks.(a) Laminated dolomite-anhydrite intergrowth. (b) Detailed view of a. Dolomite fabric is hypidiotopic to idiotopic. (c) Geopetal dolomud and anhydrite cement in an early skeletal mold. (d) Geopetal pelletal grainstone and anhydrite cement in an early skeletal mold. Some pellet outlines also can still be recognized outside the mold. (e) Detailed view of c. Geopetal mud is less compacted and contains more anhydrite intermud cement than groundmass mud. (f) Dolomudstones alternate with pelletal grainstone. (g) Detailed view of d.

lacking this kind of fringe cement are those few that are cemented by anhydrite. Original textures of the ooids and of the cements were mostly obliterated through micritization, recrystallization, and dolomitization, and thus no information is available regarding primary mineralogy or crystal orientation.

The high-energy environment of formation and accumulation of ooids documented from many ancient and recent oolitic deposits also existed during deposition of most of the San Andres examples. The coarse, well-sorted, cross-laminated ooids in grainstones characterize the highest current regime in the depositional basin. The less-sorted ooids associated with muds indicate a more moderate current regime in which suspension and bed-load ooid populations coexisted (Sass and others, 1972; Heller and others, 1980). Smaller, dense-textured ooids were apparently carried as suspension load. At a certain size they were transferred into the bed load, where they accreted additional concentric layers but in a somewhat different crystal fabric. The 150μm grain size appears to be the approximate size break between the suspension- and bed-load populations. Comparing this figure with the 100μm size break observed in a protected, low-energy, Recent lagoon (Sass and others, 1972) and the 600μm size break documented for some Cambrian ooids (Heller and others, 1980) may provide a relative measure of energy conditions at the depositional site of the San Andres oolitic rocks. Because of the high salinities and densities of the water in which these oolites were formed, less energy than needed in normal seawater may have been required to keep oolites as large as 150μm in suspension.

The mode of ooid and pellet deformation suggests that the grains were still in a plastic, prelithified state while deformation took place. Cement that apparently avoided the "welding" of adjacent ooids in the deformed rocks must have been introduced before deformation. Cement also precipitated between concentric ooid layers (fig. 9b), which suggests that either the layers were not too dense or that the cement grew when ooid growth ceased. Cement growth before mud accumulation in some of the packstones further corroborates the early introduction of the cement, which probably originated as magnesium-calcite or aragonite. Prelithification oolite deformation has not been observed in recent oolite deposits. San Andres oolites, unlike other oolites, must have been extremely soft if they could be deformed to such an extent with apparently little overburden. The possibility that these oolites were formed and diagenetically altered in highly saline water may imply that some evaporite minerals coprecipitated with the carbonate concentric coats. These, together with the high-saline interstitial water, may have introduced higher plasticity and also may have retarded lithification.

Sponge Spicule Packstones

San Andres rocks are characterized by closely packed siliceous sponge spicules (fig. 9d, 9f). Few other skeletal particles, mostly calcispheres (fig. 9d) and some mollusks and crinoids, are associated with the spiculitic rocks. The spicules, which are 100 to 250μm long and about 50μm wide, accumulated parallel to the bedding plane, with some directional orientation. Most spicules consist of microquartz, but a few were replaced by dolomite and anhydrite. The dense groundmass of the spicule packstones is partly silicified dolomitic mud; dolomite is about 20 to 30 percent of the whole rock.

Spicule packstones occur as irregular bands a few centimeters thick, alternating with equally thin dolomite mudstones. The lower parts of spicule layers normally are in erosional contact with the mudstones. These mudstones are also somewhat silicified. The closely packed, oriented spicules combined with erosional contacts at their lower bed boundaries indicate that accumulation was current controlled.

The spicule packstone-mudstone alternation pattern and the abundant mud associated with the spicules indicate that currents were short-lived. Well-preserved, fine, elongated spicules indicate that, although allochthonous, they were transported only over short distances and that their accumulation site was not far from their habitat. No sponge biolithites were observed in the San Andres Formation, and only a single sponge fragment was identified. The absence of sponge megafossils is attributed to spontaneous skeletal disintegration to single spicules. Siliceous sponge spiculitic carbonates have been described from a broad range of water depths and are thus not clear-cut environmental indicators. Nevertheless, their association with calcispheres that are almost identical to the Cretaceous "open-marine" calcispheres *Pithonella* (Bein, 1976) and not to the recent shallow-water calcisphere produced by the

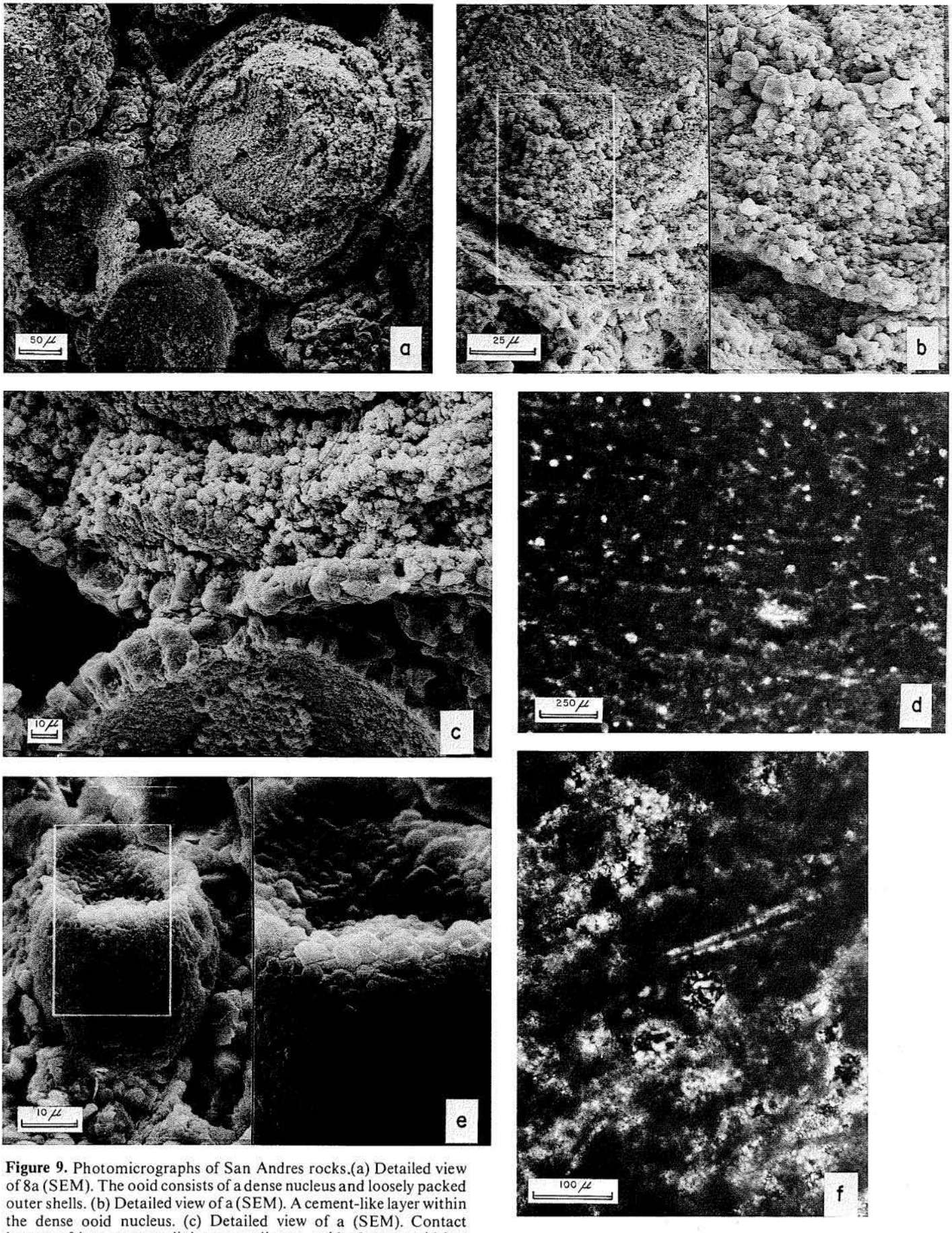

Figure 9. Photomicrographs of San Andres rocks.(a) Detailed view of 8a (SEM). The ooid consists of a dense nucleus and loosely packed outer shells. (b) Detailed view of a (SEM). A cement-like layer within the dense ooid nucleus. (c) Detailed view of a (SEM). Contact between fringe cements lining two adjacent ooids. Lower ooid has been entirely leached. (d) Sponge spicule packstone. (e) Calcispheres associated with some of sponge spicule packstone (SEM). (f) Detailed view of d. Microquartz in sponge spicule molds.

Gradation between wispy laminations and well-developed stylolites and the large amount of skeletal material truncated by them (fig. 11d) indicate that both are pressure solution effects. Considering the observed amount of material lost from single skeletal fragments and the large amount of insoluble residue accumulated along the stylolites and the wispy laminations, it appears that much of the rock (30 to 40 percent) has been lost. This effect is confined almost exclusively to rocks in Yoakum and Lamb Counties. The same rock types in the Swisher core at a much shallower depth do not exhibit significant pressure solution effects. Shallower burial depth or early plugging of porosity by salt and anhydrite in the Swisher rocks, or both, may account for this difference. Mudstone and spicule packstone found at the same burial depth in Yoakum and Lamb Counties display little pressure dissolution except at boundaries of anhydrite nodules. Differing intensity of pressure solution must be related to differences in fabric, composition of rock constituents, and permeability.

Skeletal Packstones and Grainstones

Under this category, all rocks composed of several skeletal types are discussed.

Dasyclad packstone: Rare and scattered dasycladaceae fragments were observed in some of the rocks already described. In a few Swisher core samples (S4) these organisms are the main rock constituents. The dasyclad fragments, most probably *Mizzia* (fig. 11a, 11c), are closely packed and oriented perpendicularly to bedding. Blocky calcite cement and some celestite are associated with the sedimentary sequence in which these rocks are included (fig. 12f, 12g). Dolomitization in this part of the sequence is incomplete, and various amounts of calcite (other than the blocky cement) occur in these rocks. Increased amounts of *Mizzia* in the rocks further shoreward from the Capitan Reef was described by Toomey and Cys (1977). Limited biota and abundant non-skeletal grains in these rocks are suggestive of a restricted, somewhat hypersaline depositional environment (Toomey and Cys, 1977). The flourishing of this alga during a short period of time in the Swisher area may have resulted from certain salinity conditions (somewhat higher than normal marine) that prevailed locally.

Mollusks and unidentified skeletal packstones and grainstones: Most of the skeletal fragments in these rocks are preserved as micrite envelopes with anhydrite infilling. Pressure solution, as evidenced by stylolites and wispy laminations, is less pronounced here than in the wispy-laminated crinoid rocks. The depositional environment of these rocks was similar to that of the crinoid rocks, but some change in ecological control, such as salinity, depth, or energy, favored dominance of one skeletal population over the other.

ANHYDRITE-DOLOMITE ASSOCIATION AND SILICIFICATION

Anhydrite-dolomite associations occur in four forms that apparently followed different diagenetic sequences. These associations are dolomite-anhydrite intergrowth, nodular anhydrite, replacement anhydrite, and blocky anhydrite cement.

Dolomite-Anhydrite Intergrowth

In some rocks, intergrowth follows a laminate pattern similar to algal wavy lamination, but in others,intergrowth is random or arranged in simple laminations. Single lanceolate, elongate, and flat crystals are scattered within the dolomite groundmass and have a subvertical to subhorizontal orientation. In laminated rocks, lamination is expressed by different amounts of anhydrite within the dolomite groundmass. Lamination of some of these rocks resembles bedding, which implies crystallization and settling within a water body. The subvertical orientation of many crystals (fig. 7a, 7b), however, suggests an interstitial growth within the host carbonate sediment. The clear, undamaged brittle anhydrite crystals must have formed by

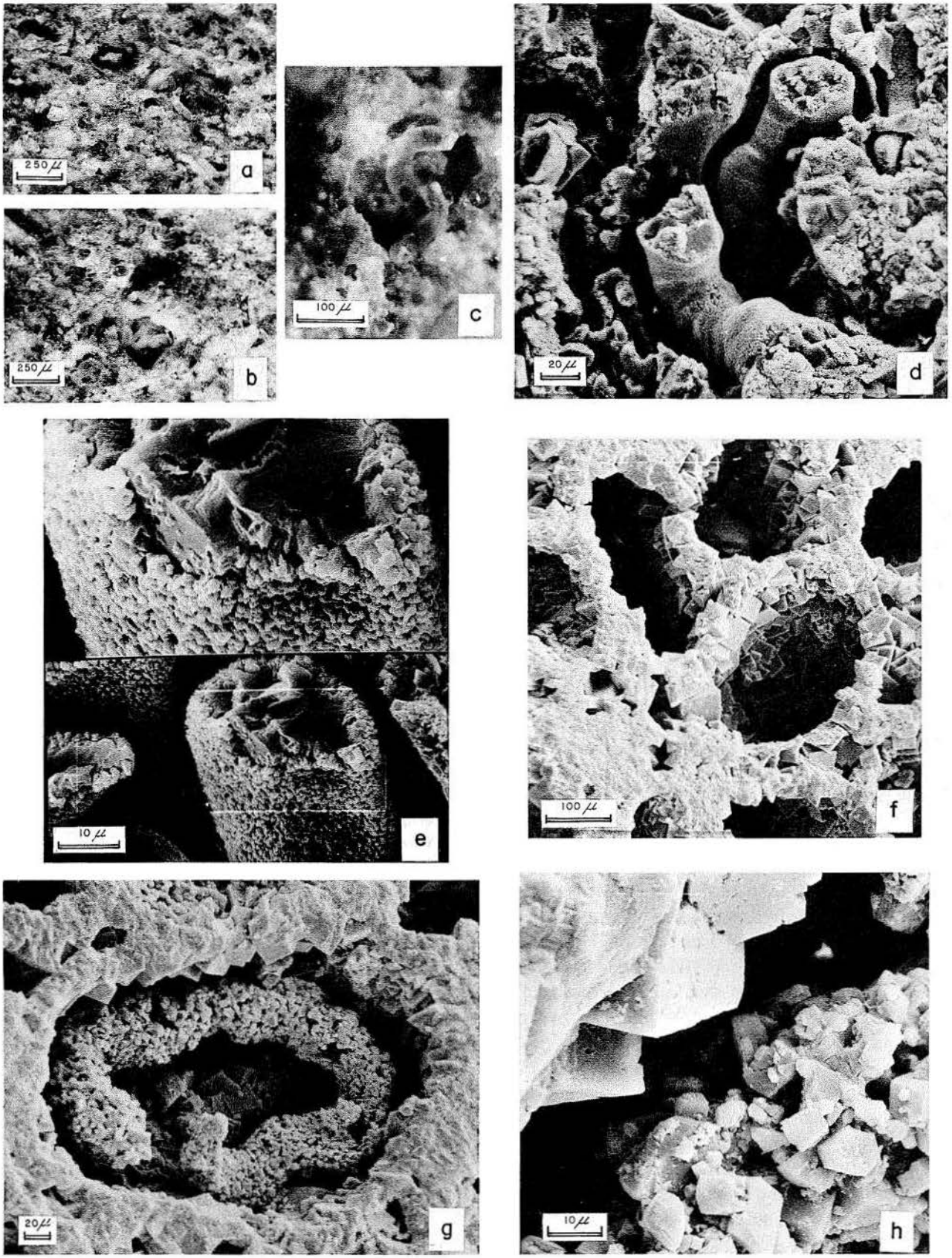

Figure 10. Photomicrographs of San Andres rocks.(a) and (b) *Girvanella*-like filaments as main rock constituents. (c) Detailed view of b. (d) and (e) Detailed view of b (SEM). Filament tube infilled with large blocky calcite crystals. (f) Dolomitized *Girvanella*-like rock (SEM). Filaments have been leached. (g) Same as in f (SEM). A few filaments have been preserved and dolomitized. (h) Detailed view of g (SEM).

displacing a soft, water-saturated sediment, apparently at an early diagenetic stage. Laminations resulted from fluctuations in the anhydrite saturation level of the water body, which also affected the chemistry of the interstitial water.

Anhydrite Nodules

Anhydrite nodules range in size from a few millimeters to several centimeters and may occur as single or subhorizontal clusters of nodules. The host carbonate includes dolomitized mudstone, pellet packstone, and skeletal and spiculite packstone. Internal structures range from cleavage flakes that are oriented tangential to the surface of the nodule to massive, granular anhydrite fabrics. Shearman (1966) and Shearman and Fuller (1969) reasoned that the evolution of similar nodules was by displacive growth before lithification and response to compaction. Because such nodular growth has been observed in the capillary zone above the water table in modern supratidal sabkhas (Shearman, 1966; Kinsman, 1966), it has been widely applied as evidence of sabkha deposition. However, since such nodules have been also described from deeper water sediments, it appears that they are merely diagenetic growth fabrics that occur when mud is in contact with highly saline brines (Dean and others, 1975; Holser, 1979a).

Replacement Anhydrite

Replacement anhydrite consists of large, cloudy crystals (2 to 15 mm) that include relics of the original host rock texture and constituents (fig. 12a, 12b, 12c). Such anhydrite, found only in mudstones and spiculite packstone, was termed "replacement anhydrite" by Murray (1964). The replacement nature rather than the displacive growth of the nodules and intergrowth may point to a growth stage in which the sediment was no longer susceptible to displacement. Since the relict dolomite crystals are similar to those composing the entire rock and since no displacement is evident, the timing of the replacement postdates the final dolomitization stage. The sediment was already lithified to a certain degree. It is unclear how such a replacement could start and proceed in one large crystal in a dense, fine-grained sediment. Possibly the anhydrite precipitated in some local secondary porosity. Open sites could have resulted from oxidation of organic matter, causing partial dissolution of adjacent dolomite crystals. Anhydrite growth in such cases may have been a cement associated with megascopic dissolution and not a true replacement by anhydrite.

Blocky Anhydrite Cements

Blocky anhydrite cements occur in some grainstones, mostly as infillings of skeletal molds. The space is typically occupied by single or a few large anhydrite crystals. The early diagenetic origin of these cements is demonstrated by the absence of fringing carbonate cement in those pellet-oolite grainstones cemented by anhydrite. Growth of the carbonate cements of early marine origin was apparently prevented by early anhydrite growth. Blocky anhydrite cements in skeletal molds may also have formed during an early diagenetic stage; early leaching of skeletons is evident from the infilling of geopetal molds that preceded precipitation of some of these cements.

Silicification of Anhydrite

Silicification of anhydrite affects mostly the nodules and replacement anhydrite. In nodules most silica occurs as large quartz crystals that engulf each anhydrite lath (fig. 12e). As silicification advances, the engulfed anhydrite crystals are leached, leaving empty lath-shaped molds in dense, blocky quartz (fig. 12d). Some molds are later infilled by silica. It appears that silicification of the nodules starts in voids left between the elongated anhydrite crystals. In some nodules, length-slow, spherulitic quartzine replaces anhydrite along outer boundaries and in fractures cutting the nodules.

Silicification of replacement anhydrite takes place only when the anhydrite is in contact with silicified nodules. Silicification along such boundaries appears to advance into the anhydrite following a "reaction rim" in which the dolomite relicts are selectively leached from the anhydrite (fig. 12a, 12b).

The silicification of anhydrite extends beyond the silica-rich sponge spicule packstone but is limited to zones in which these rocks are intercalated in the San Andres sequence (Yoakum and Lamb Counties). Farther north (Swisher and Randall Counties), there is little evidence of silicification in anhydrite nodules. The source of silica for silicification is probably the abundant, siliceous sponge spicules originally composed of opal.

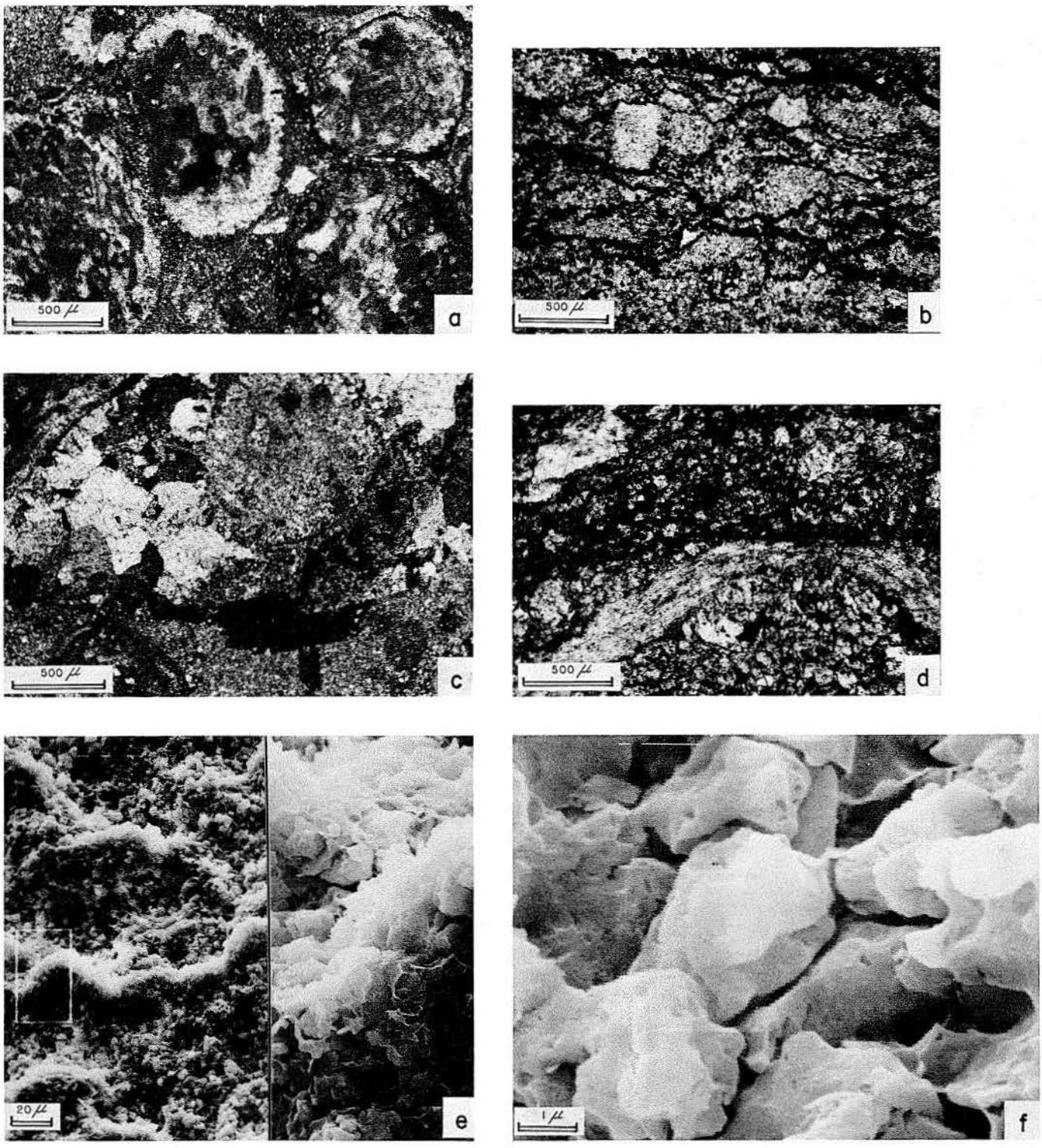

Figure 11. Photomicrographs of San Andres rocks.(a) Dasycladaceae (*Mizzia*-like) packstone. (b) Wispy-laminated crinoid packstone. Skeletal boundaries closely follow packed stylolites. (c) Detailed view of a. Blocky calcite cement. (d) Pressure solution effects along wispy laminations. (e) A wispy-laminated rock (SEM). Clay along crystal boundaries. (f) Grain-to-grain compromise boundaries in a wispy-laminated rock (SEM).

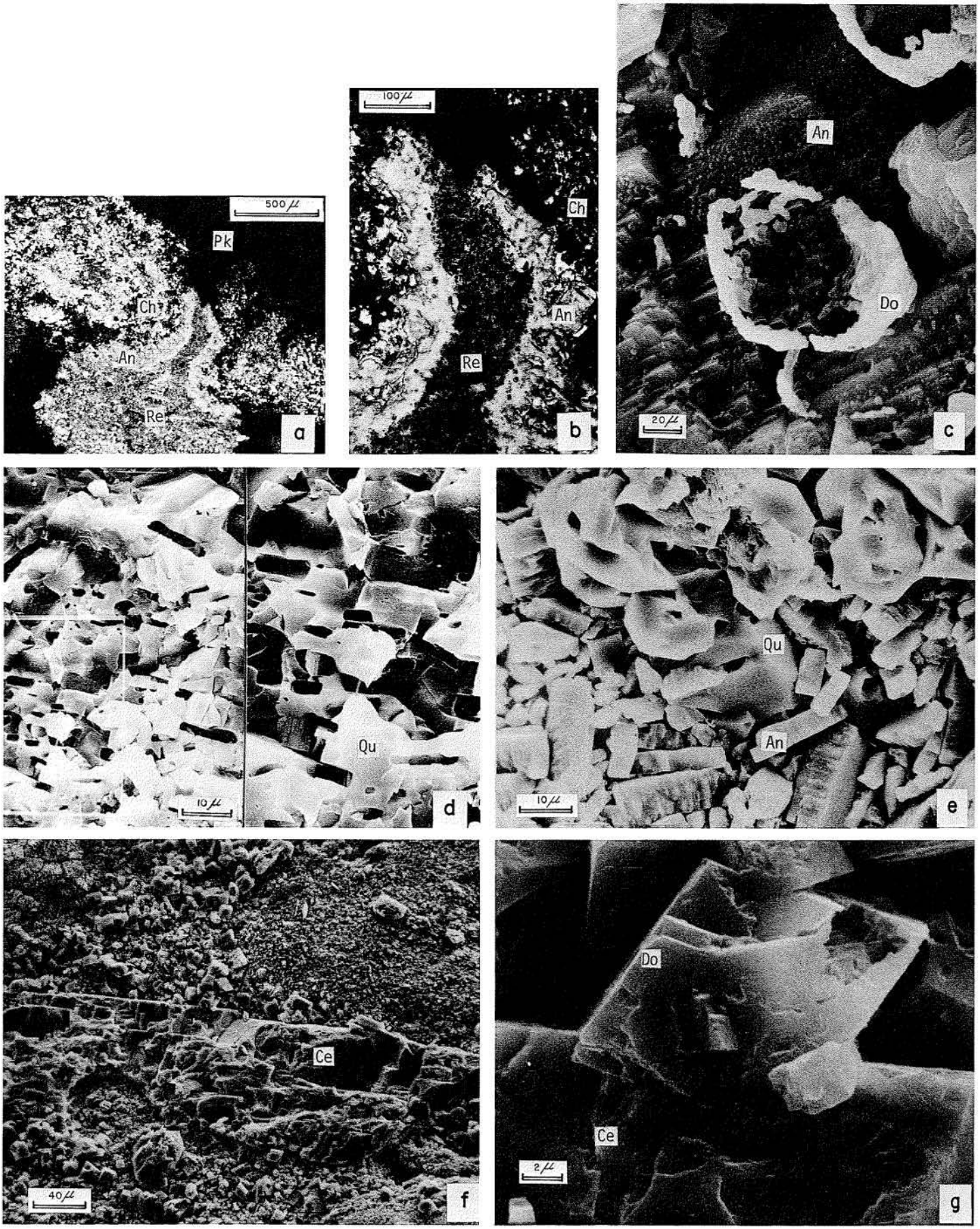

Figure 12. Photomicrographs of San Andres rocks. (a) Silicification of replacement anhydrite. Replacement anhydrite (Re) within a sponge spicule packstone (Pk) is affected along boundaries by chert (Ch) nodules. Silicification follows a "reaction rim" (An) in which relict dolomite crystals have been leached selectively from anhydrite. (b) Detailed view of a. (c) Detailed view of replacement anhydrite in b (SEM). Relict dolomite crystal (Do) in large anhydrite crystal (An). (d) Silicification of nodular anhydrite (SEM). Quartz crystals (Qu) with elongated molds after anhydrite. (e) Silicification of nodular anhydrite (SEM). Large quartz crystals (Qu) engulf anhydrite crystals (An). Advanced stage of silicification results in mold formation seen in d. (f) Dolomite and celestite (Ce) in dasyclad packstone (SEM). (g) Detailed view of f (SEM). Dolomite (Do) and celestite (Ce) intergrowth.

GEOCHEMICAL DATA

Organic Matter Associated with Carbonates

The amount of total indigenous organic carbon (TOC) in the San Andres carbonates is low in the north (Swisher well) and somewhat higher in the south (Lamb area) (table 2). Due to shallow burial depth, the maturation of the organic matter is low, as revealed from low vitrinite reflectance values and coloration indices (Dutton, 1980; Ramondetta, in press). The low maximum burial temperature of about 40°C (105°F), which corresponded to such low maturation values ($R_o = 0.4$), left some of the early organic characteristics intact.

Table 2. Pristane/phytane ratio and total organic carbon in San Andres carbonates.

Sample	Pristane/Phytane	Total Organic Carbon %
L - CB	0.99	0.87
L - HF	0.91	0.63
L - ARA	0.88	0.57
L - FGA	0.89	0.43
L - SMA	1.01	0.33
S4 (composite)	1.34	0.26
S - 2275.0	1.57	0.14
S - 2933.9	1.82	0.13
S - 2756.7	1.96	0.24
S - 2715.0	2.27	0.12
S - 2733.0	2.58	0.15
S - 2085.0	2.78	0.11
S - 2126.0	3.06	0.10

Gas chromatograms (GC) of saturated hydrocarbons from S2 and lower S4 samples (dolomite mudstones) (fig. 13) reveal organic matter of marine origin. The lower gas chromatogram (S2756.7) is characteristic of organic matter, probably algal, which was altered microbially early during diagenesis. The absence of light hydrocarbons in these samples is attributed to evaporation. Organic matter in the filamentous and crinoid skeletal rocks of S4 (S2715) is characteristic of marine organic matter containing limited terrigenous compounds (carbon preference index CPI [Cooper and Bray, 1963] up to 1.19) and low maturation (high amount of compounds at the triterpane-sterane region). Samples from S56 (S2275 and S2085) contain organic matter of mixed marine (mostly algal) and terrigenous origin (CPI - 1.33 to 1.43).

The relatively low nC17/pristane and nC18/phytane ratios (fig. 13) appear to be caused by low maturation rather than by biodegradation. Excellent preservation of light n-alkanes in almost all samples is sufficient evidence to reject biodegradation as a process by which the nC17, nC18, and other light n-alkanes were differentially eliminated.

In all Swisher County samples, pristane concentration significantly exceeds phytane (figs. 13, 14, and 15; table 2). In Lamb County samples, phytane surpasses or equals pristane (fig. 14). These two isoprenoids, abundant in many sediments, are mostly early diagenetic derivatives of the phytol side chain of chlorophyll (Cox and others, 1970). Sufficient oxygen supply during early diagenesis favors the formation of pristane over phytane, whereas deficiency in oxygen favors phytane over pristane generation (Welte and Waples, 1973).

Cross-plotting the pristane/phytane ratio over TOC (fig. 15) shows a good correlation ($R = -0.75$, and -0.89 for log-log correlation). One way to interpret this correlation is to assume that the relatively high oxygen flux (proximity to meteoric influx) that favored pristane formation was sufficient to oxidize the organic matter in the Swisher area. Lower oxygen availability favored phytane generation and caused less oxidation of the organic matter in the Lamb County area. Varying amounts of input of organic matter over the area may explain the high correlation shown in figure 15 in a different way. Assuming there was similar limited oxygen flux in both Swisher and Lamb San Andres sediments, large amounts of organic matter available for oxidation in Lamb sediments may have reduced and maintained low oxygen values. Oxidation of initially low amounts of organic matter in the Swisher area would, however, consume only part of the oxygen available, and the environment would become less reducing. In any case, oxidation-reduction conditions in the early diagenetic environment were different in the northern and southern parts of the area. Although the organic matter in S24 and S56 units is of different types and sources, similar early diagenetic oxidation-reduction conditions prevailed throughout the deposition of the entire rock sequence in the Swisher County area.

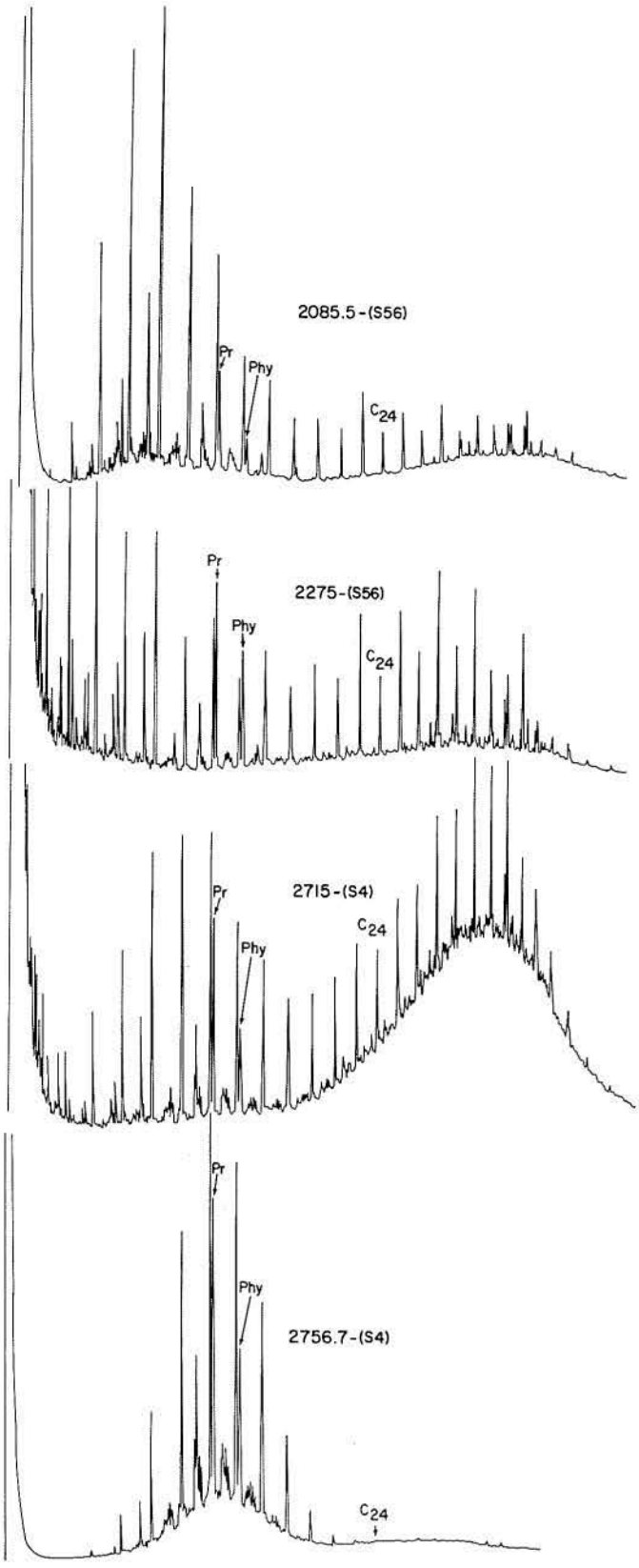

Figure 13. Gas chromatogram of saturated hydrocarbons in the Swisher County core. Pristane (Pr) exceeds phytane (Phy) in all samples. Strong odd-over-even preference in the heavy n-alkanes in S56 samples indicates large amounts of terrestrial organic matter.

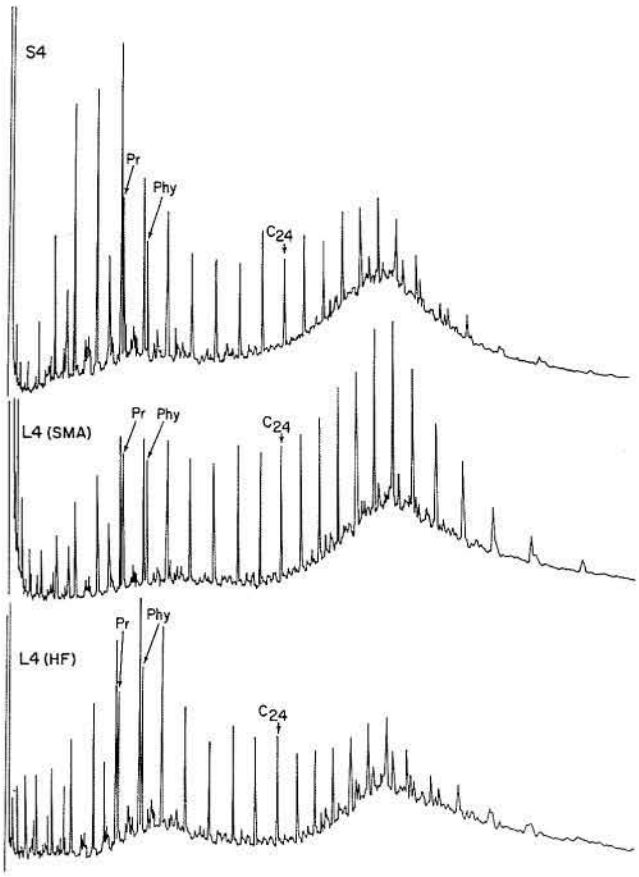

Figure 14. Gas chromatogram of saturated hydrocarbons in S4 and L4 rock units indicates similar marine-derived organic matter. Increase in early diagenetic oxidation conditions from bottom to top is evidenced by increase of pristane/phytane ratio.

Trace Elements in Associated Evaporites

Bromide in Halite

Halite in R2, R3, and R4 units is significantly enriched in bromide relative to the halite in R56 units. Halite in R4, in particular, exhibits several high values (table 3). Bromide content in halite has been proven to be a sensitive indicator of evaporation-crystallization histories. In evaporating seawater, the bromide concentration builds up in the brine to about 510 ppm before halite precipitation takes place. The distribution coefficient of about 0.04 controls the intake of bromide by halite from about 65 to 75 ppm in the earliest precipitated halite to about 200 ppm, at which point potash-magnesia minerals start to crystallize (Holser, 1979b). Bromide values below this range indicate that the salt-precipitating solution reached halite saturation as a result of dissolution of previously deposited halite in addition to normal evaporation of seawater. In most

salt basins the water regime is controlled by the amount and composition of inflow, reflux, and evaporation. Smooth and continuous changes in bromide content in a salt rock sequence[1] indicate that the controls were almost constant throughout deposition. In general, the larger and deeper the water body, the less pronounced are the frequent fluctuations in either of these controls reflected by the bromide content (Holser, 1979b).

The low bromide values in most of the R56 samples indicate that salt saturation and precipitation were accomplished in part by salt remobilization. Relatively small depletion in bromide content in most of the R56 samples indicates, however, that salinity rarely dropped below five times that of seawater. Higher bromide values in R234 units indicate that halite saturation was maintained over the entire precipitation period and that inflow of marine water rarely exceeded evaporation rates. High bromide values in R234 rock units reflect normal evaporation cycles under relatively steady conditions. The continuous and relatively homogeneous halite rock sequences of R234 (90 to 92 percent halite in SR4, point counted; P. Ramondetta, personal communication, 1981) are interrupted only by some thin anhydrite and mud streaks, and are consistent with such steady depositional conditions. Halite in the R56 unit, in contrast, is interbedded with many carbonate, anhydrite, and mud units. The many abrupt lithologic changes within thicker units probably reflect events of rapid, short-lived water inflow into the salt basin, which also resulted in salt dissolution. The sensitivity of the basin to inflow fluctuation apparently implies that the basin receiving R56 halite was shallower and less extensive than the basin in which R234 units were deposited. An increase in the number of such fluctuations may have resulted from different rates of seawater

[1]Raw bromide data, which frequently fluctuate within a range of several tens of ppm, are usually smoothed by a moving average of several adjacent data points (Raup and Hite, 1977).

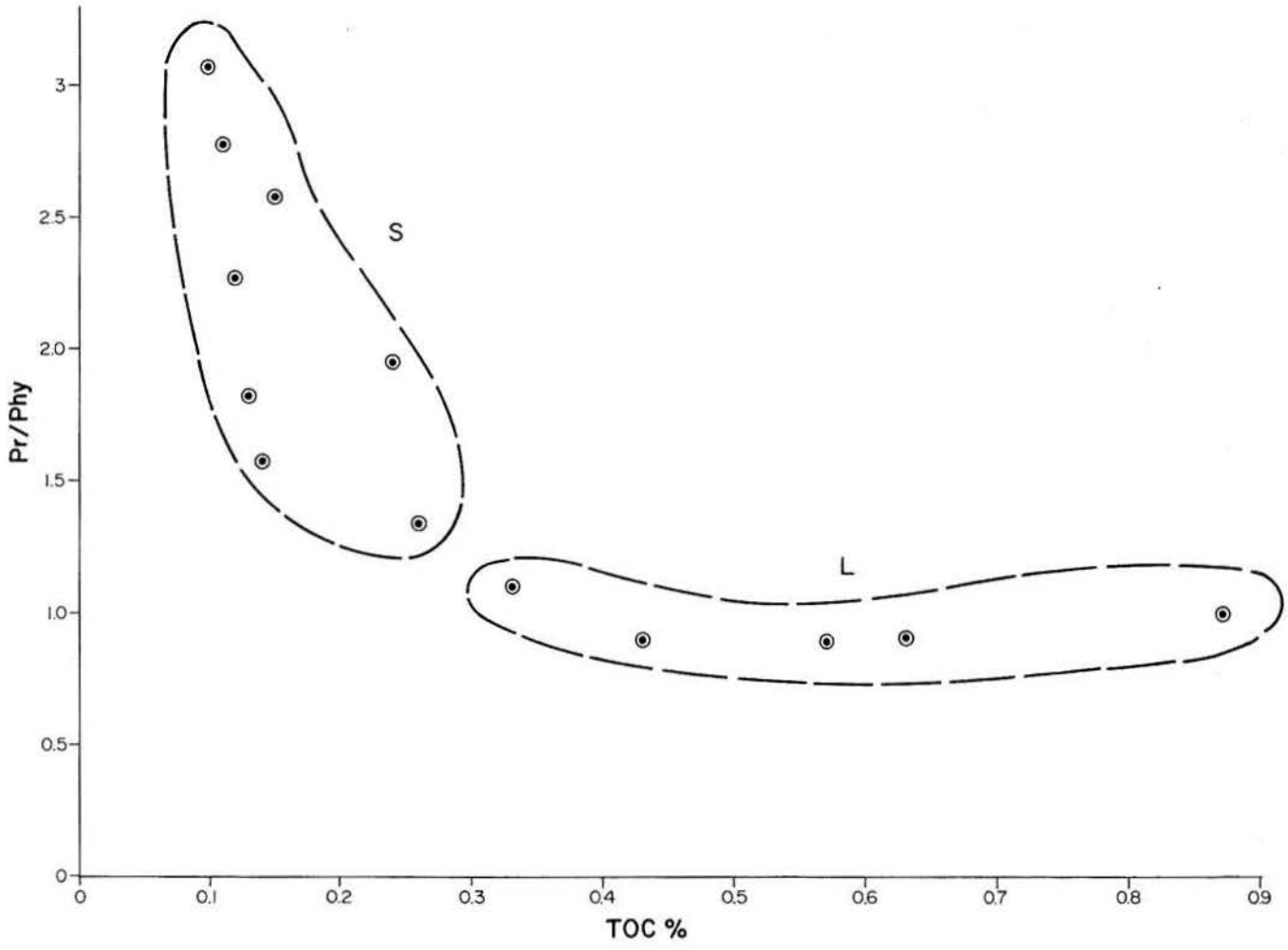

Figure 15. Relation between pristane/phytane ratio and total organic carbon in Swisher County (S) and Lamb County (L) samples.

inflow. Another explanation is that large volumes of fresh water intermittently flooded the salt basin and interrupted the steady-state evaporating conditions. Such floods may have resulted in temporary, slightly undersaturated conditions with respect to halite; following further evaporation, carbonate-, sulfate-, and bromide-depleted halite may have precipitated.

Strontium in Anhydrite

The strontium content of anhydrite is controlled by the Sr/Ca ratio in the solution and the distribution coefficient of Sr in anhydrite, or gypsum in the case of replacement anhydrite. The mass ratio of strontium/calcium in brines saturated with respect to aragonite and calcium-sulfates and celestite stabilizes at 0.022 over a broad range of salinities, probably beyond halite saturation. Dolomitization can reduce the ratio to about 0.010 (Butler, 1973). Advanced dolomitization, which may depress sulfate concentration to nearly zero by enhancing additional calcium-sulfate precipitation, allows strontium to rise in the brine beyond the limit of a 0.022 ratio for strontium/calcite (Butler, 1973; Kinsman, 1966). A high precipitation ratio of calcium-sulfates to celestite, caused by rapid increase in salinity from leaching of halite, also may result in high strontium/calcium ratios (Butler, 1973). Distribution coefficients of about 0.18 for gypsum and 0.37 for anhydrite (Butler, 1973) yield a strontium content of gypsum and anhydrite crystals from such brines (strontium/calcium = 0.010 to 0.022) within the range of about 400 to 1,000 ppm and 1,050 to 2,400 ppm, respectively. Replacement anhydrite after gypsum may be characterized by depletion of strontium as compared to primary anhydrite. Deviation from this range will result from higher or lower strontium/calcium ratios in the solution and the dependence of the distribution coefficient on temperature, brine concentration, and growth rate of the crystals (Kushnir, 1980).

The strontium content of all the San Andres massive and carbonate-associated nodular anhydrite (table 3) points to a primary rather than to a replacement origin. Strontium values of the San Andres anhydrite are well within the range of primary recent and many ancient anhydrites (Butler, 1973; Dean and Tung, 1974). Considering the approximate stability fields of anhydrite and gypsum at normal surface temperatures (Butler, 1973; Hardie, 1967), the primary origin of the anhydrite implies that salinities in the basin did not drop much below seven times that of seawater. This

Table 3. Bromide content in halite and strontium and magnesium content in anhydrite nodules and massive anhydrite beds.

Anhydrite

Sample	ppm Sr	ppm Mg
2,118.2	1,573	2,416
2,183.7	1,452	269
2,248.6	1,773	148
2,265.7	1,507	210
2,286.7	1,487	1,345
2,321.0*	2,390	1,000
2,329.6*	1,350	500
2,508.4	1,377	5,000
2,547.0	1,257	1,298
2,601.0	1,387	3,259
2,638.0	2,835	145
2,707.4	1,780	1,872
2,711.6	1,790	11,185
2,818.0*	2,070	800
2,826.0	2,088	3,474
2,893.0	2,287	41,784
2,897.0*	1,750	800
1,490.5	1,770	576
1,493.5*	1,270	250
1,711.8*	1,430	550
1,963.0*	1,670	500
1,963.4*	2,390	800
2,005.0	1,368	594
CB 66	1,554	946
CB 87	1,554	93
CB 94	1,574	302
CB 97*	2,700	1,300
HF 11*	2,150	800

Halite

Sample	ppm Br
1,165	22
1,175	32
1,240	89
1,252	40
1,270	55
1,288	76
1,304	51
1,313	43
1,326	71
1,342	66
1,358	49
1,396	30
1,408	26
1,424	48
1,465	44
1,635	79
1,641	81
1,674	48
1,751	79
1,772	133
1,783	138
1,803	101
1,815	67
1,833	94
1,836	71
1,850	124
1,866	85
1,900	75
1,913	68
1,919	67
1,934	67
1,949	80
2,004	75
2,062	84
2,106	93
2,115	75
2,131	74
2,146	70
2,162	73
2,037	74
2,805	68

reasoning is compatible with the relatively small depletion in bromide content in the R56 halites, indicating that salinities below the halite saturation level also were limited during the precipitation of the closely associated anhydrite nodules and carbonates.

Sodium and Chloride in Carbonates

Interpretation of sodium (Na) data revealed by whole-rock analysis is difficult owing to interference between sodium derived from salt and/or brine inclusions and sodium substituted in the carbonate lattice. The main problems in this regard are small liquid and halite inclusions that cannot be removed by any technique. To compensate for this limitation, two different analytical procedures were undertaken. First, chloride and sodium were analyzed after a complete dissolution of the rocks. Plotting chloride versus sodium/chloride for all samples (table 4) yields almost no correlation.

Plotting single-unit data separately displays fair correlation (figs. 16, 17, and 18). Assuming a constant volume and composition for the inclusions and constant sodium substitution in the dolomite lattice, a theoretical correlation between these two parameters should exhibit the pattern shown in figure 16a (inset). The sodium/chloride ratio approaches constant low values once the contribution of sodium from lattice substitution becomes negligible relative to sodium contributed from inclusions. In contrast, sodium/chloride approaches infinity once the contribution of inclusions becomes negligible. Where high correlation exists (Y56 unit, fig. 16a), the sodium/chloride value at the lower right (0.7, circled area) is the closest to the composition of inclusions, whereas those values to the upper left indicate limited contribution from inclusions. The lower correlations for the other units (figs. 16, 17, and 18) indicate variability in the volume of inclusions, their composition, and different amounts of sodium substituted in the dolomites of the same unit.

Assuming that the sodium/chloride mean ratio of the samples (circled) at the right of each correlation (or the group mean of the entire unit, where no correlation is shown) is the closest approximation of inclusion composition of each unit, the sodium contribution from inclusions can be calculated. Subtracting the sodium derived from inclusions from the total mean Na content in each unit may approximate sodium substituted in the different dolomites (appendix A).

To evaluate these inferences further, a second procedure was undertaken. Samples were ground in

Table 4. Carbonate constituents, trace elements, and stable isotopes in San Andres carbonates. Do-dolomite; Ca-calcite; An-anhydrite; Ir-insoluble residue. *Electron probe data.

		% rock constituents				% mole	ppm										$\delta^{18}O$		$\delta^{13}C$	
	Sample	Do	Ca	An	Ir	Ca in Do	Na	K	Al	Fe	Mn	Zn	Sr	P	Na/Cl (eq.)	Cl (eq.)	Do	Ca	Do	Ca
	2,813.0	91	—	—	9	50	360	3,168	10,243	5,570	113	14	116	272	0.91	19	—	—	—	—
	2,819.0	97	2	—	1	51	180	193	531	806	70	—	191	—	0.31	25	1.11	—	4.80	—
	2,822.0	95	2	—	3	51	97	367	1,022	1,580	67	8	129	280	0.21	20	0.78	—	4.46	—
S3	2,846.4	91	2	—	7	51	431	2,912	6,177	3,813	74	12	104	167	0.76	25	—	—	—	—
	2,855.0	87	2	—	11	51	373	607	1,488	5,210	171	—	70	—	0.67	24	—	—	—	—
	2,857.0	78	1	—	21	51	296	4,319	11,008	8,147	233	17	91	238	0.51	25	0.02	—	4.19	—
	2,897.0	97	3	—	—	52*	121	112	324	987	124	7	265	—	0.24	22	0.89	—	4.78	—
	2,916.0	16	81	1	2	—	78	761	1,797	2,169	106	11	7,700	—	0.23	15	—	—	—	—
S2	2,917.9	23	54	—	23	—	189	3,606	8,083	4,345	148	20	698	209	0.42	20	-0.79	-2.61	4.52	3.57
	2,931.8	76	6	—	18	—	319	6,246	14,304	9,467	310	18	1,458	332	0.39	35	—	—	—	—
	2,933.9	61	38	—	1	—	45	991	2,686	2,792	234	7	137	245	0.15	14	-0.9	-3.22	4.32	3.36
	CB57	85	7	2	6	—	304	1,222	3,925	1,349	44	6	534	237	1.42	9	—	—	—	—
	CB68	93	2	—	5	51	182	373	1,364	680	32	16	80	328	0.65	12	1.47	—	3.58	—
	CB97	94	4	—	2	51*	234	453	1,051	924	28	7	271	—	0.33	31	—	—	—	—
	ARA19	92	4	1	3	—	217	151	321	386	32	—	152	291	0.64	15	—	—	—	—
	ARA16	86	5	—	9	—	253	578	1,218	1,222	32	—	90	356	0.39	29	—	—	—	—
	ARA11	90	4	—	6	—	333	699	1,447	903	43	11	105	229	0.69	21	—	—	—	—
	ARA2	89	5	1	5	—	213	721	1,730	1,074	42	6	413	313	—	—	—	—	—	—
L4	ARA1	72	26	1	1	—	198	987	2,408	1,605	40	—	151	155	—	—	—	—	—	—
	FGA14	98	—	—	2	50	236	399	805	761	31	31	107	264	—	—	—	—	—	—
	FGA11	88	7	—	5	—	225	876	2,094	1,646	37	5	88	541	—	—	—	—	—	—
	FGA6	18	82	—	—	—	218	316	714	491	17	6	272	230	0.45	21	-0.52	-2.84	4.08	2.86
	FGA1	86	8	—	6	—	160	802	1,734	1,603	58	6	98	—	0.42	17	—	—	—	—
	HF2	86	7	—	7	—	220	703	1,751	1,434	31	12	77	499	0.28	34	—	—	—	—
	HF5	85	5	—	10	—	417	347	852	231	19	9	162	225	0.46	39	—	—	—	—
	HF11	91	3	3	3	50*	183	162	480	351	26	8	229	360	0.51	16	1.34	—	3.16	—
	HF18	60	3	35	2	—	159	140	647	567	21	7	990	139	0.55	13	1.49	—	3.08	—
L3	SMA12	98	—	—	2	50	751	676	1,379	660	26	25	137	183	—	—	1.79	—	3.79	—
	MC17	95	1	2	2	50	359	122	392	172	12	11	190	182	1.61	10	0.01	—	4.26	—
	MC13	95	1	—	4	50	315	125	397	112	14	15	118	—	1.01	14	—	—	—	—
	MC11	65	—	—	35	50	419	271	658	271	15	9	131	—	0.85	21	—	—	—	—
	MC8	94	—	1	5	50	429	159	387	189	16	13	128	156	0.93	20	—	—	—	—
	MC7	95	1	—	4	50	445	313	741	380	15	6	104	196	1.02	19	—	—	—	—
	MC5	97	1	—	2	50	460	129	273	153	9	41	77	169	0.97	21	—	—	—	—
	PS26	95	1	—	4	50	372	926	2,006	639	31	16	99	209	0.75	22	—	—	—	—
Y56	PS25	94	1	—	5	50	368	1,085	2,333	576	31	10	99	276	1.93	8	1.81	—	5.25	—
	PS23	99	1	—	—	50	401	360	862	318	19	10	96	235	1.27	14	—	—	—	—
	PS21	97	1	—	2	50	408	391	881	360	27	15	105	173	1.05	18	—	—	—	—
	PS19	98	1	—	1	50	300	608	1,427	725	29	13	101	194	0.66	20	—	—	—	—
	PS15	94	1	—	5	50	357	700	1,685	684	24	32	121	529	0.72	22	—	—	—	—
	PS8	96	1	—	3	50	453	108	274	144	16	8	90	142	1.41	14	—	—	—	—
	PS7	97	1	—	2	50	461	139	374	161	11	14	93	131	1.43	14	1.54	—	5.80	—
	PS3	97	1	—	2	50	453	134	410	162	12	10	89	—	1.16	17	—	—	—	—
	PS2	95	1	—	4	50	362	400	920	275	23	15	164	158	1.18	13	0.44	—	5.31	—

Table 4 (cont.)

	Sample	% rock constituents Do	Ca	An	Ir	% mole Ca in Do	ppm Na	K	Al	Fe	Mn	Zn	Sr	P	Na/Cl (eq.)	Cl (eq.)	$\delta^{18}O$ Do	Ca	$\delta^{13}C$ Do	Ca
	1,371.0	93	2	—	5	49*	149	350	977	1,211	261	16	121	—	0.23	29	0.76	—	6.14	—
	1,374.0	94	2	—	4	51	248	378	950	910	166	14	198	—	0.22	46	—	—	—	—
	1,487.0	94	2	—	4	50*	168	421	1,129	1,846	218	17	102	—	0.28	27	0.64	—	5.09	—
R56	1,490.0	94	2	—	4	51	124	412	1,041	1,820	211	9	489	—	0.22	25	—	—	—	—
	1,493.3	89	4	3	4	—	152	627	1,682	2,185	188	10	788	—	0.34	19	—	—	—	—
	1,701.0	95	2	—	3	51	216	328	853	1,108	149	8	180	—	0.26	37	0.39	—	6.54	—
	1,743.0	93	3	—	4	51	157	290	897	3,342	405	14	267	—	0.17	41	0.43	—	5.33	—
	1,963.4	82	6	6	6	50*	214	1,322	3,104	2,256	65	—	341	—	0.43	21	0.66	—	4.52	—
	1,965.0	88	4	2	6	—	318	439	1,036	1,477	52	—	—	—	0.60	23	—	—	—	—
	1,969.0	95	4	—	1	—	182	211	526	1,156	51	—	174	—	0.34	23	—	—	—	—
	1,977.0	64	29	—	7	53*	184	500	1,294	1,264	52	—	172	—	0.36	22	—	—	—	—
R4	1,981.0	94	6	—	—	—	158	260	663	985	58	—	98	—	0.24	28	—	—	—	—
	1,995.0	86	14	—	—	53*	88	174	471	718	54	—	102	—	0.16	23	—	—	—	—
	2,005.0	9	90	—	1	—	50	241	780	745	32	111	617	—	—	—	—	-4.5	—	3.60
	2,007.7	73	26	—	1	—	86	806	2,049	2,430	67	7	170	166	0.15	25	—	—	—	—
	2,014.0	23	76	—	1	—	232	1,256	2,714	1,776	56	12	355	—	0.74	14	—	—	—	—
	2,020.0	24	75	—	1	—	139	768	1,767	1,366	50	5	3,868	—	0.27	22	0.25	-3.51	5.07	4.60
R3	2,096.5	88	3	5	4	49*	475	572	1,819	1,796	272	7	1,628	—	0.66	31	1.12	—	4.93	—
	2,100.0	80	—	—	20	48	414	3,154	11,478	7,500	346	28	164	250	0.66	27	—	—	—	—
	2,170.7	90	6	—	4	—	176	152	456	1,402	152	11	80	145	0.24	32	—	—	—	—
	2,174.5	90	9	—	1	52*	326	62	228	1,608	197	361	92	—	0.47	30	-0.20	—	5.14	—
	2,175.4	90	9	—	1	—	226	95	366	2,168	242	33	57	—	0.43	23	—	—	—	—
R2	2,189.4	82	7	—	11	—	212	860	2,167	2,777	194	14	102	—	—	—	—	—	—	—
	2,194.0	77	7	—	16	52*	427	3,348	8,417	6,624	212	17	99	769	0.50	37	-0.35	—	2.94	—
	2,204.0	81	10	—	9	—	287	1,749	4,592	4,316	174	11	452	239	0.40	31	—	—	—	—
	2,204.8	55	4	—	41	51*	290	2,634	6,359	5,898	270	23	108	362	0.40	32	-2.45	—	3.67	—
	2,085.5	90	—	—	10	50*	220	1,624	4,514	3,288	447	12	107	—	0.34	28	0.05	—	4.16	—
	2,122.8	97	—	—	3	50	185	289	728	643	216	—	130	—	0.32	25	0.49	—	6.07	—
	2,126.0	97	—	—	3	50*	211	229	607	677	206	7	154	—	0.34	27	0.18	—	6.10	—
	2,127.0	96	—	—	4	50	169	339	939	960	215	7	88	—	1.01	7	—	—	—	—
	2,128.8	96	—	—	4	50	174	350	951	929	209	11	88	—	0.41	19	-0.74	—	5.63	—
	2,196.4	90	1	—	9	50	292	2,009	5,546	4,076	379	19	129	—	0.45	28	0.67	—	4.87	—
	2,237.0	99	1	—	—	50	149	165	321	4,273	288	—	138	—	0.21	31	—	—	—	—
	2,252.0	100	—	—	—	50	—	204	504	1,891	158	—	5,100	—	—	17	—	—	—	—
S56	2,257.7	97	—	—	3	50	63	1,069	2,629	2,587	159	11	267	—	0.14	20	0.32	—	5.33	—
	2,260.3	89	—	—	11	50	274	1,985	5,077	4,966	172	16	91	—	0.62	19	—	—	—	—
	2,275.0	91	—	—	9	50	42	2,123	5,799	5,006	183	11	70	143	0.18	10	—	—	—	—
	2,290.0	98	2	—	—	51	272	241	395	3,672	214	8	101	—	0.30	40	—	—	—	—
	2,304.0	91	1	3	5	50	290	748	2,354	2,306	164	10	181	—	0.43	29	—	—	—	—
	2,336.2	93	1	—	6	50	202	698	1,916	3,129	223	15	81	—	0.37	24	1.58	—	5.95	—
	2,337.4	85	—	—	15	50	322	3,297	9,225	6,469	220	18	102	—	—	—	—	—	—	—
	2,439.0	96	—	—	4	50	314	477	1,002	1,133	88	15	115	—	0.37	37	—	—	—	—
	2,455.0	94	—	—	6	50	271	1,479	3,472	2,320	108	17	96	—	0.36	33	—	—	—	—
	2,697.3	15	5	77	3	—	—	388	1,398	955	43	58	1,668	—	—	—	—	—	—	—
	2,704.9	54	6	36	4	—	—	849	2,118	1,873	61	7	1,376	—	—	—	1.74	—	2.49	—
	2,715.0	86	6	—	8	52*	340	706	1,479	1,521	49	6	388	193	0.65	23	-0.62	—	4.69	—
	2,733.6	2	98	—	—	—	155	168	351	444	29	5	346	—	0.74	9	—	-2.59	—	4.05
S4	2,741.5	3	96	—	1	—	261	103	271	367	22	6	7,314	—	0.60	19	—	—	—	—
	2,744.8	8	92	—	—	—	265	239	453	519	25	8	502	130	0.76	15	—	—	—	—
	2,756.7	6	82	—	12	—	393	1,553	3,363	2,287	44	12	4,478	—	0.90	19	—	—	—	—
	2,767.7	8	90	—	2	—	117	876	2,048	1,184	40	8	288	—	0.41	12	—	—	—	—
	2,778.0	22	69	—	9	—	416	2,570	5,377	3,346	82	11	300	—	0.93	25	—	—	—	—
	2,785.0	77	5	—	18	—	786	4,445	9,422	6,927	198	17	130	152	1.18	33	0.57	—	3.72	—

small water volumes and after removal of the solid, the solutions were analyzed for calcium, magnesium, sodium, chloride, sulfate, and bicarbonate content. It was assumed that sodium derived from the dolomite lattice through dissolution will be balanced with calcium and magnesium by bicarbonate, whereas sodium and other cations released to the solution through mechanical breakdown of inclusions will be balanced by chloride. Table 5 presents the composition of these solutions. The low concentration of most compounds resulted in a somewhat high analytical error (table 5). The excess magnesium in the calcium + magnesium that is balanced by the HCO_3 and SO_4 is considered to be an artifact of a situation in which anhydrite and dolomite dissolved, but some $CaCO_3$ precipitated during the experiment. In all samples, deficiency of sodium relative to chloride is evident, and the excess chloride is balanced by excess calcium + magnesium over HCO_3 + SO_4 (table 5). Using the same procedure (appendix A), sodium substitution in the

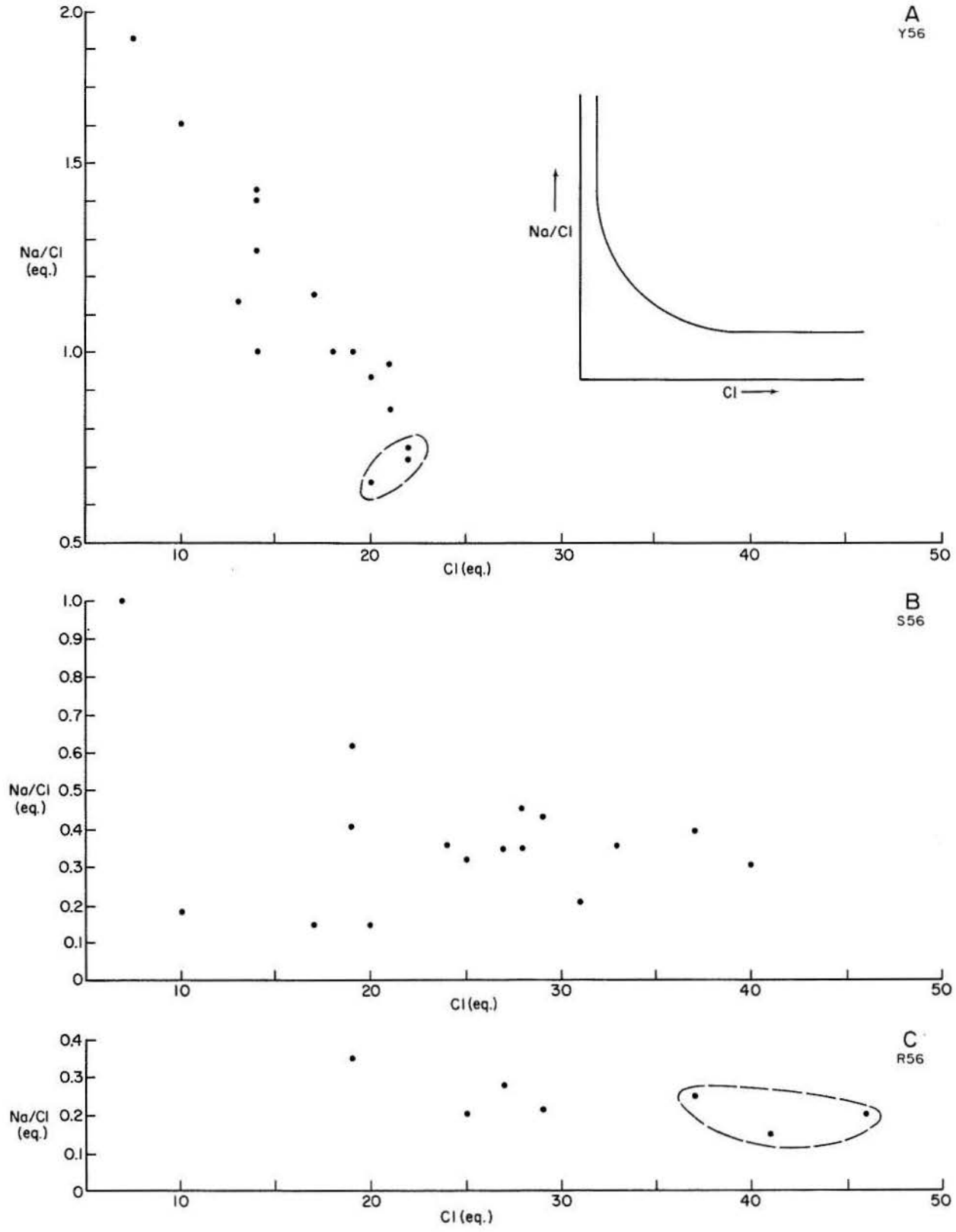

Figure 16. Relation between sodium/chloride (equivalent ratio) and chloride (equivalent) in YSR56 samples. Inset figure in A describes theoretical relation between parameters. Circled points used to calculate low mean sodium/chloride ratios used in calculations described in appendix A.

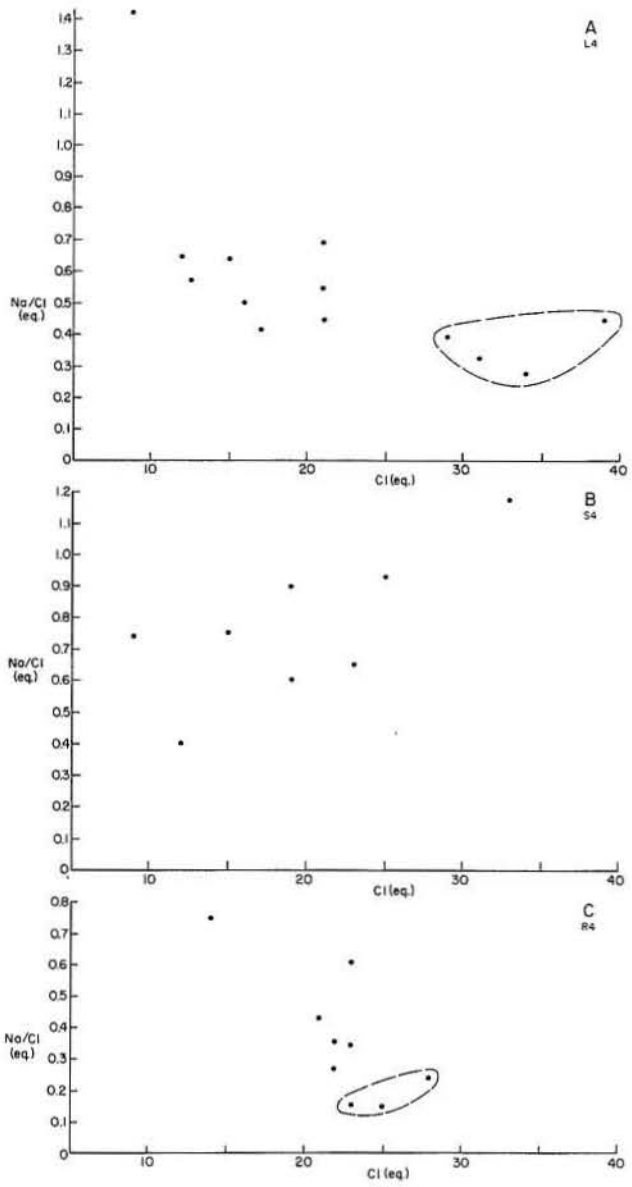

Figure 17. Relation between sodium/chloride (equivalent ratio) and chloride (equivalents) in LSR4 sample. Circled points used to calculate low mean sodium/chloride ratios used in calculations described in appendix A.

dolomite lattice was evaluated (appendix B). But even considering the wide margins of error involved in these procedures, the results are similar, and they indicate exceptionally high sodium in the dolomite lattice in the Y56 unit samples and an overall sodium deficiency in almost all the liquid inclusions.

Plotting mean values of chloride over sodium/chloride (fig. 19) results in a trend similar to that indicated for some of the separate units (figs. 16, 17, and 18). Assuming a constant total volume of inclusions in all units, the increase in chloride content corresponds to an increase in the total salinity of the included fluids. Comparing sodium/chloride values corresponding to the same chloride value in the different units (fig. 19) indicates a decrease in this ratio with increasing salinity. Sodium in dolomite lattices in units of the same stratigraphic level appears to increase from north to south from 13 ppm in R56 to 38 ppm in S56 to 125 ppm in Y56 and from 0 ppm in R4 to 66 ppm in S4 to 111 ppm in L4.

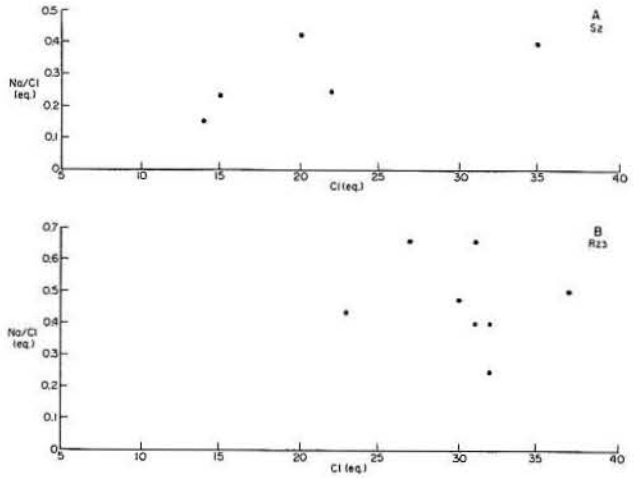

Figure 18. Relation between sodium/chloride (equivlent ratio) and chloride (equivalents) in SR23 sample.

The extremely low and consistent sodium/chloride ratios in the San Andres samples and their high potassium/chloride ratios indicate that evaporation of these fluids continued far into the halite precipitation stage. Abundant salt in the Permian sequence in the Palo Duro Basin and the San Andres Formation in particular indicates that large amounts of sodium-depleted brines must have been present throughout the basin. It is assumed that the dense brine, highly enriched in magnesium relative to calcium and refluxing through the sediment, caused the dolomitization and was entrapped within the crystals as fluid inclusions.

It is impossible to measure the salinity of the inclusions directly, but the small possible volume of the samples that were ground into powder before analysis implies very high salinities. By assuming salinities 10 times that of seawater, the chloride content of 1,000 ppm measured in many samples accounts for a volume of fluid inclusions of about 0.5 percent of the total rock volume.

Sodium substitution for cations in the dolomite lattice is controlled by an extremely low distribution coefficient (about 10^{-5}; White, 1978), but since sodium is a major constitutent in marine basins, it still might be found in measurable amounts in dolomites. The sodium content of dolomites, reportedly as high as 1,000 ppm, has been used in many studies as a tool for estimating paleosalinity (Fritz and Katz, 1972; Land and Hoops, 1973; Veizer and others, 1978). Our study verifies the possibility that most sodium analyzed and reported (regardless of whether analyzed on whole-rock samples or by electron probe) may have been derived from inclusions rather than from the carbonate lattice.

The higher amounts of sodium in the dolomite lattice in the southern rock sequences (Y56, L4) may be related to the paleodepositional environment. The northerly increase in salt in San Andres rocks must have been reflected by a northerly deficiency in sodium in the residual brine. This trend of sodium deficiency appears justified, given the composition of fluid inclusions. In the north the concentrated brine was consistently above halite saturation, with relatively low sodium/calcium + magnesium ratios, whereas salinity of the brine in the south was usually below halite saturation; thus, more sodium remained in the water. The sodium concentration in the brine might have been lower in the northern area as a result of the extremely low sodium/calcium + magnesium ratios even if the total salinity were higher. Lower sodium/calcium + magnesium ratio in the refluxing brines in the north caused the formation of dolomites low in Na as compared to the dolomites in the south.

Potassium in Carbonates

Plotting potassium (K) versus aluminum (Al) values (table 4, fig. 20) results in an excellent correlation (R = 0.98), which indicates that most of the potassium was derived from clays. A positive intercept on the potassium axis at zero aluminum suggests, however, that some potassium is combined in the carbonate system. The intercept value of 24 ppm potassium (a standard error of 28 indicates that some samples may have no potassium in the carbonate system, but others may have values higher than 24 ppm) is considered an approximation of the average potassium content in the carbonate system. Plotting potassium versus aluminum in separated units further corroborates this approximation. In SR56 with low sodium/chloride ratios the potassium intercept value is 20 ppm, whereas in Y56 with higher sodium/chloride ratios the intercept value is negative.

As in the case of sodium, there is no direct method for evaluating whether the potassium substitutes for cations in the dolomite lattice or whether it is derived from liquid inclusions. Assuming a liquid

Table 5. Chemical composition of water used to leach ground dolomite samples.

Sample	R-1969 (R4)		S-2085 (S56)		S-2715 (S4)		MC-5 (Y56)		PS-7 (Y56)	
	ppm	eq.	ppm	eq.	ppm	eq.	ppm	eq.	ppm	eq.
Na^+	1.62	0.07	1.78	0.08	2.04	0.09	1.36	0.06	3.72	0.16
Ca^{++}	8.90	0.45	10.24	0.51	8.96	0.45	6.16	0.31	13.60	0.68
Mg^{++}	9.46	0.79	10.62	0.89	9.58	0.80	4.74	0.40	9.06	0.76
Cl^-	5.10	0.14	10.50	0.30	5.30	0.15	3.10	0.09	14.40	0.41
HCO_3^-	64.50	1.06	61.50	1.01	68.80	1.13	40.50	0.66	53.00	0.87
SO_4^{--}	3.46	0.07	4.62	0.10	4.04	0.08	2.88	0.06	8.66	0.18
analytical error	3%		4.7%		1.5%		5%		8%	
mNa/Cl	0.50		0.27		0.60		0.67		0.39	
	$Ca + Mg = 1.24$		$Ca + Mg = 1.40$		$Ca + Mg = 1.25$		$Ca + Mg = 0.71$		$Ca + Mg = 1.44$	
	$HCO_3 + SO_4 = 1.13$		$HCO_3 + SO_4 = 1.11$		$HCO_3 + SO_4 = 1.21$		$HCO_3 + SO_4 = 0.72$		$HCO_3 + SO_4 = 1.05$	
	Ca + Mg (excess) = 0.11		Ca + Mg (excess) = 0.29		Ca + Mg (excess) = 0.04		—		Ca + Mg (excess) = 0.39	
	$Na = 0.07$		$Na = 0.08$		$Na = 0.09$		$Na = 0.06$		$Na = 0.16$	
	$Na + Mg = 0.18$		$Na + Mg = 0.37$		$Na + Mg = 0.13$		—		$Na + Mg = 0.55$	
	$Cl = 0.14$		$Cl = 0.30$		$Cl = 0.15$		$Cl = 0.09$		$Cl = 0.41$	

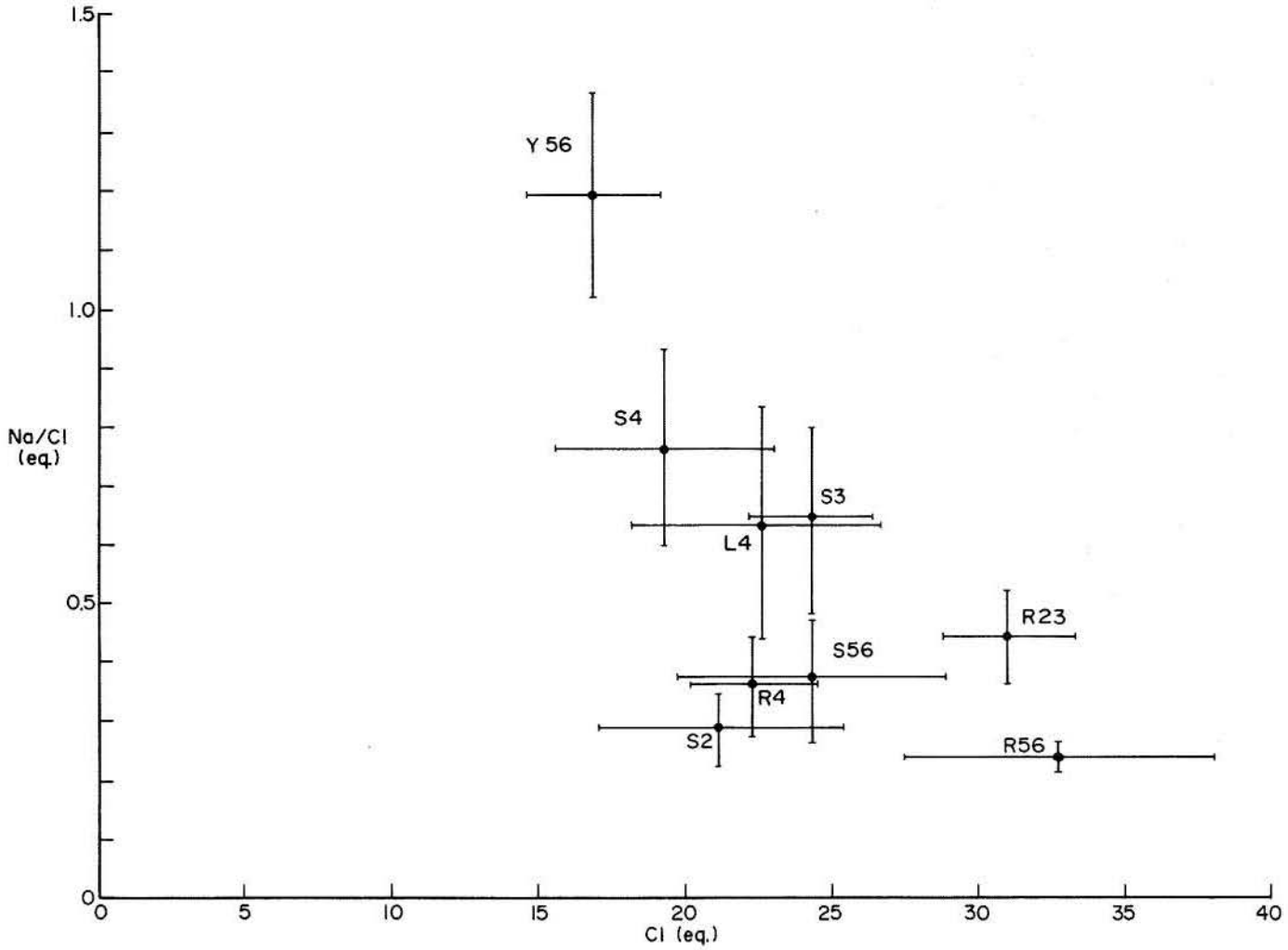

Figure 19. Relation between Na/Cl (equivalent ratio) and Cl (equivalents) mean values of each unit. Bars through the points equal one standard deviation.

inclusion source for all the potassium in the samples implies that the molar potassium/chloride ratio in inclusions is approximately 2.7 x 10^{-2}. This ratio, which is significantly higher than that in normal marine waters (1.8 x 10^{-2}), is within the expected range for solutions characterized by extensive halite precipitation.

Strontium in Carbonates

The strontium content of the dolomites is mostly in the range of 100 to 400 ppm, whereas calcites contain about 900 to 1,200 ppm (table 4). Frequent high values are due to small amounts of celestite mostly associated with the calcite cements. No clear-cut trend in the strontium distribution has been found; there is no spatial, lithologic, or stratigraphic control of strontium, and its correlation with other elements or isotopes is generally poor. Lack of good correlation may be due to interference of celestite, even in samples with relatively small amounts of strontium. A frequency distribution diagram of strontium values in dolomite samples (fig. 21), excluding those exceeding 1,400 ppm (proven celestite contamination), displays a maximum of 36.5 percent at 100 to 150 ppm, and 83.8 percent of the samples contain between 50 and 200 ppm strontium.

Like most ancient dolomites, the San Andres dolomites are depleted in strontium relative to most Holocene marine dolomites, which contain 500 to 700 ppm strontium. The low strontium content has been explained either by primary formation in nonmarine fluids or by fresh-water diagenesis of marine dolomites (Land, 1973). Theoretical modeling of burial diagenesis through successive recrystallization stages has been used by Land (1980) to demonstrate that strontium depletion during seawater diagenesis is conditioned on a very low D^{Sr} value. This approach requires several

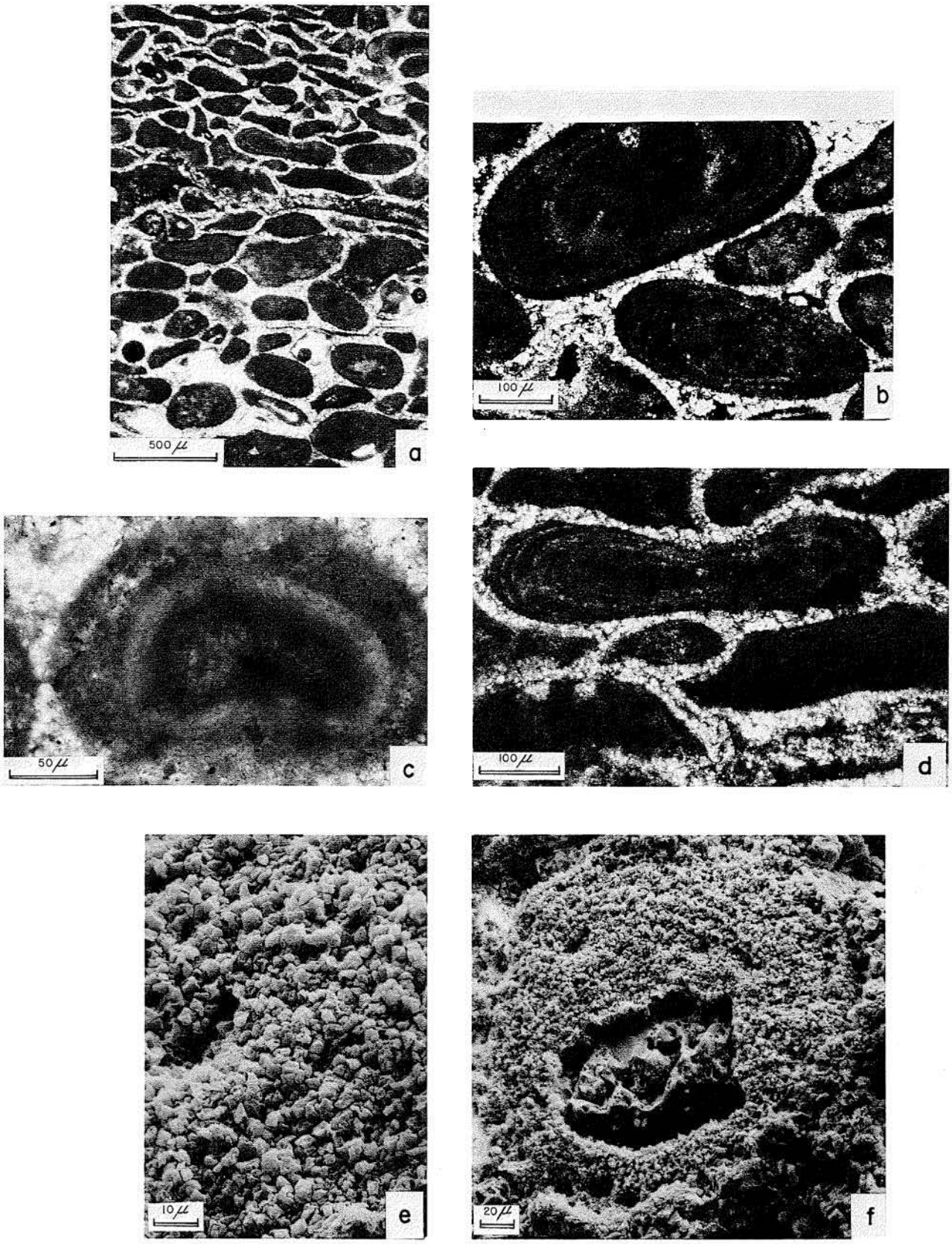

Figure 8. Photomicrographs of San Andres rocks.(a) Deformed oolites and pellets in a grainstone. (b) Detailed view of a. Ooids are fringed by a cement one crystal thick. (c) A small, dense ooid. (d) Detailed view of a. Each deformed ooid is surrounded by a fringe cement one crystal thick. (e) and (f) Detailed view of c (SEM). Ooid laminae consist of closely packed equant dolomite crystals.

alga *Acetabularia,* and their confinement to the southern part of the area during San Andres deposition indicate some environmental control, most likely prevalence of more normal marine salinities or a certain depth limit. The position of these rocks in the vertical succession of Lamb and Yoakum Counties (figs. 5 and 6) may, however, suggest a somewhat higher tolerance for salinity increase than do the highly diverse skeletal rocks found below them.

Filamentous (*Girvanella*-Like) Grainstones and Boundstones

The main constituent of these rocks is filaments or tubes, 15 to 30μm in diameter and 150 to 300μm in length. The filaments may be single or associated in groups forming a complex network (fig. 10a, 10b, 10c, 10d). In calcitic rocks the tubes are made of a single crystal calcite layer, up to 10μm thick. The internal space of the tube is commonly cemented by large calcite (fig. 10d, 10e), anhydrite, or salt crystals.

Dolomitization affects most of these rocks. In highly dolomitized rocks the entire groundmass consists of a network of large—up to 40μm—euhedral dolomite crystals (fig. 10f). The filaments themselves are mostly dissolved, leaving molds partly infilled by halite or anhydrite. Some tubes that escaped leaching are dolomitized by euhedral crystals significantly smaller (10 to 12μm in size) than the surrounding cement crystals (fig. 10g, 10h).

The filaments in these rocks are similar to *Girvanella* filaments found worldwide in many Paleozoic rocks, including the Permian of Texas and New Mexico (Johnson, 1961). The origin of these problematic organisms was discussed by Riding (1975), who supported the idea that *Girvanella* represents the calcified filaments of blue-green algae. The low biotic diversity in these filamentous rocks and the possible association with blue-green algae, combined with their lateral and stratigraphic restriction to cycle 4 in the northern part of the area, suggest a depositional environment slightly more saline than seawater.

Wispy-Laminated Crinoid Packstones

The main allochem constituents are crinoids, mollusks, and a very few bryozoans, brachiopods, foraminifers, ostracods, and calcareous algae. Fragment size ranges between 50μm and a few centimeters. In many of the rocks some sorting and rounding of the skeletal material is observed. Sorted grainstones of the same skeletal composition commonly exist between the packstones. Crinoid packstones are commonly intensively burrowed and devoid of any original depositional texture. Most of the rocks display a wispy-laminated network of clay and organic matter (fig. 11b, 11d, 11e). Close inspection of grain contacts (fig. 11b, 11d, 11e) reveals that many of them are stylolites of various sizes and forms.

Almost all these rocks are entirely dolomitized. Some calcite is present, most as crinoid and some as pelecypod fragments. Many of the skeletal fragments other than crinoids have been leached, leaving micritic-enveloped molds infilled by blocky anhydrite crystals. In some of the shell fragments the blocky anhydrite cement formed after the deposition of geopetal mudstone and pelletal grainstone. The highly diverse skeletal assemblage characterizing these rocks is suggestive of a normal marine subaqueous depositional environment. Fragmentation of all shells, their slight abrasion and sorting, and the grainstone streaks between the packstones indicate a moderate current regime that is normally favorable for such a dense population.

Leaching of skeletal fragments and a micrite-enveloped moldic stage commonly characterize the process by which the early unstable carbonate minerals were replaced by stable ones. Such transformation may take place during diagenesis in the presence of meteoric water; mold formation and small amounts of calcite precipitates characterize the vadose zone; mold formation and intensive calcite precipitation characterize the phreatic zone. Owing to fluctuations of the water table, diagenesis in both regions typically overlaps. Thus, intensive calcite precipitation is common in most places after aragonite and high magnesium calcite removal.

The scarcity of such calcite cements or their dolomitized replacements and the evidence of leaching associated with anhydrite precipitation point to a different solution composition that controlled San Andres diagenesis. Geopetal infillings provide evidence of an early, almost contemporaneous process of skeletal-fragment leaching and subsequent anhydrite infilling, and must have occurred in a brine that was nearly anhydrite saturated. Mold formation and anhydrite filling and its relation to dolomitization will be discussed further after presentation of geochemical data.

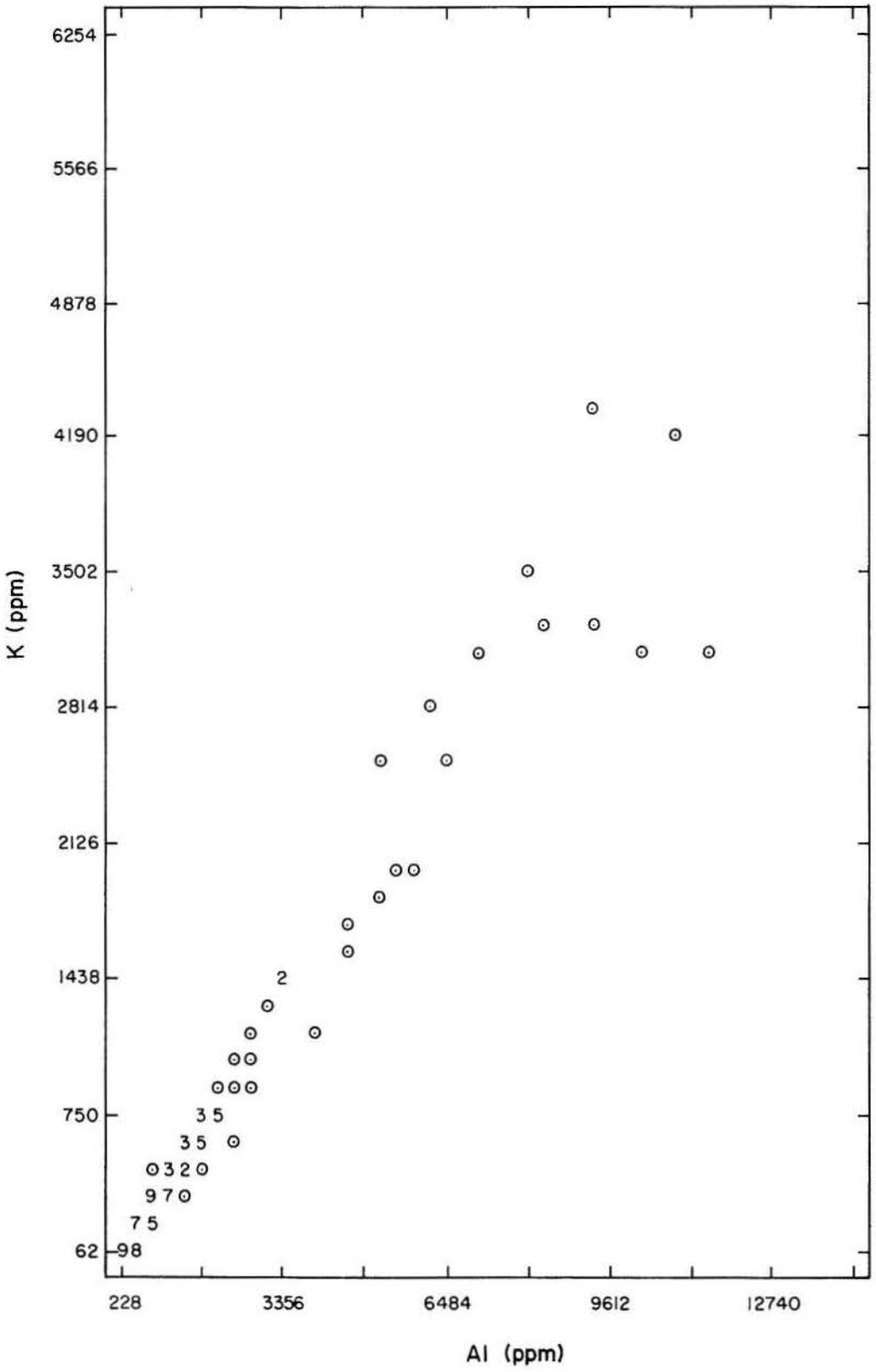

Figure 20. Relation between potassium and aluminum in all San Andres rocks (correlation factor, R, is 0.98, and intercept value of potassium for zero aluminum is 24 ppm; standard error of intercept is 28).

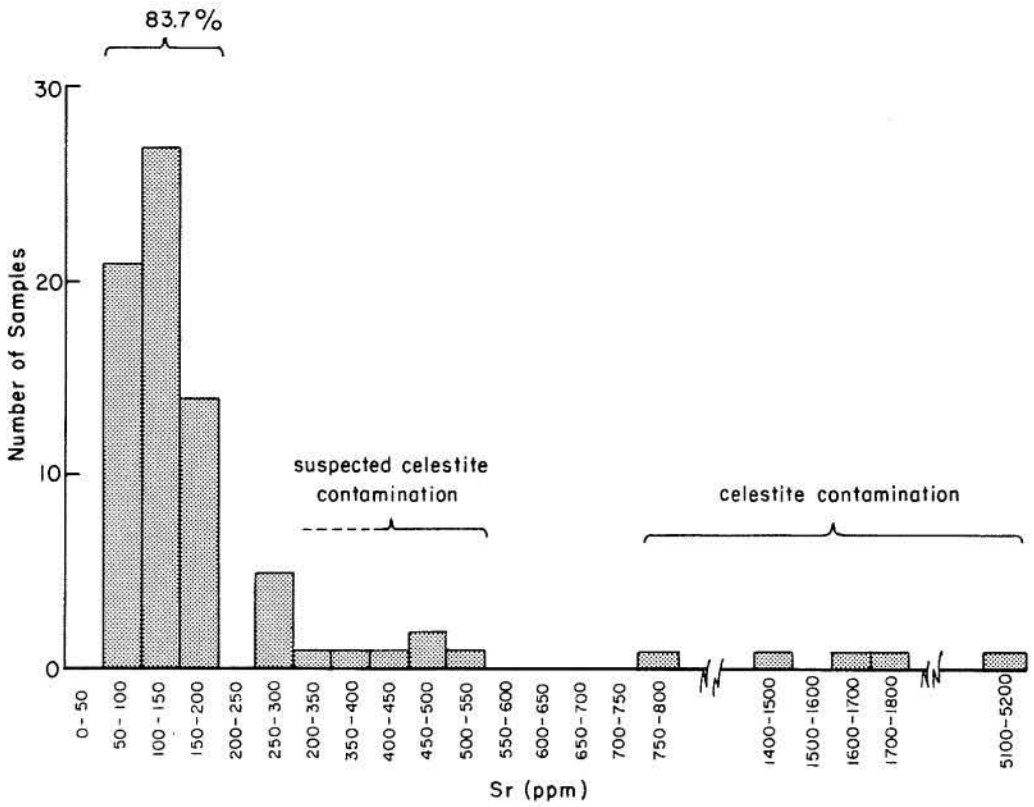

Figure 21. Frequency histogram of strontium content in dolomite samples.

recrystallization stages of dolomite and the application of two different D^{Sr} values; the first, in which about 500 to 700 ppm strontium enters early diagenetic dolomites (or protodolomites) and the second, much lower, value that controls the strontium distribution during later diagenesis.

The apparent isolation of many San Andres dolomites in thick salt and anhydrite rock sequences and the absence of any associated fresh-water cements are sufficient evidence for rejecting fresh-water diagenesis as a cause of strontium depletion. Periods of possible fresh-water inflow into the depositional basin have already been proposed for SR56, but the apparent proportion deduced from bromide content in most of the salts and the strontium content in anhydrite is insufficient to reduce the strontium/calcium ratio to sufficiently low levels. Furthermore, similarly low strontium values in the cements, allochems, muds, and in the different dolomite units exhibiting apparently different depositional brine histories also negate the possibility of meteoric-marine water mixing to account for the strontium depletion.

A rejection of late fresh-water diagenesis and early fresh-water and marine-water mixing raises the possibility of diagenesis by the marine-derived brines. Because of the noticeable changes that occur in the structure and the composition of dolomites with time, such a diagenetic process appears to be feasible. The Holocene dolomites containing 500 to 700 ppm strontium and the ancient dolomites containing only 100 to 200 ppm strontium are, in fact, different in their degree of order, unit cell dimensions, and magnesium/calcium ratio. These differences clearly point to a stabilization or recrystallization phase through which the dolomites pass. Patterson (1972), citing Kinsman's (1966) data that only 2 to 3 ppm strontium occur in magnesite, concluded that strontium does not occupy magnesium sites in the rhombohedral carbonates, and, therefore, the strontium replaces the calcium only in the dolomite lattice (Behrens and Land, 1972). The change toward stoichiometric composition, higher order, and contraction of the cell unit makes a reduction in D^{Sr} between these two dolomite phases quite likely. The relatively large strontium ion ($Sr^{++} = 1.13$Å; $Ca^{++} = 0.99$Å; $Mg^{++} = 0.65$Å) fits poorly in the contracted and more ordered magnesium-enriched lattice of late-phase dolomite.

Kinetic effects also may reduce the D^{Sr} during diagenesis. It was shown that D^{Sr} decreases with decreasing rate of calcite precipitation (Kinsman and Holland, 1969; Lorens, 1981) and that the most rapid change occurs at comparatively slow precipitation rates. The rate effect has been explained to result from the presence of cation sites at the surface of the crystals at a lower degree of coordination than ideal sites within the lattice. Intake of large strontium ions into these sites is relatively easy and is controlled by a D^{Sr} larger than that at higher degree coordination sites. During increase in degree of coordination in these sites, changing from surface to internal positions, slow growth rates enable equilibrium to develop between the solution and the crystal at the new higher coordination, controlled by the lower D^{Sr}. Insufficient time for equilibration at high growth rates will result in strontium content as controlled by the high D^{Sr} at the low-surface coordination sites (Lorens, 1981). Evidently the change from early diagenetic dolomite to stoichiometric and ordered dolomite is a slow process (presumably much slower than initial dolomite formation) and thus may explain a significant D^{Sr} reduction during this transformation.

We propose that the strontium content in San Andres dolomite and in other ancient dolomite followed a two-stage diagenesis in a marine-derived brine. During the first early diagenetic stage of dolomite formation, a relatively high D^{Sr} dictated an intake of 500 to 700 ppm strontium into the poorly ordered dolomite crystals. During the second stage of slow transformation into ordered dolomite, a much lower D^{Sr} value controlled an intake of only 100 to 200 ppm strontium into the dolomite. After the second stage, the strontium/calcium and the calcium/magnesium ratios in the expelled pore water increased and caused precipitation of strontium-rich calcite, celestite, and some of the anhydrite associated with the dolomite. The apparent isotopic equilibrium in $\delta^{18}O$ between dolomite and the associated calcite (discussed later) supports such a cogenetic model.

Iron and Manganese in Carbonates

Plotting iron versus aluminum concentrations (table 4) results in a good correlation ($R = 0.86$), whereas manganese versus aluminum results in a poor correlation ($R = 0.39$). Plotting manganese versus aluminum in separate rock units yields high correlations where manganese content is low (fig. 22c, 22d), and in no correlation where manganese content is high (fig. 22a, 22b). These data indicate that in dolomite, which contains small amounts of manganese (intercept values for zero aluminum in high correlation plots are 8 and 9 ppm manganese, fig. 22c, 22d), the manganese measured is mostly derived from clay (a few tens of ppm). On the other hand, high manganese contents in other dolomite units are derived mostly from the dolomite.

Plotting iron versus aluminum for the same dolomite units results in good correlations and demonstrates that in all samples a large proportion of iron is derived from clay. The intercept values for zero aluminum for the different units, which are considered to account for the average iron content in the carbonate system, fall into two distinct categories: 567 to 630 ppm (fig. 23a, 23b) and 18 to 37 ppm (fig. 23c, 23d). Plotting manganese values of each unit versus its iron intercept value (fig. 24) reveals two distinct groups: SR23 and SR56 rock units, which are relatively rich in manganese and iron, and LSR4 and Y56 units, which are depleted in both elements.

The D^{Mn} value of calcite, which is about 15 to 17 (Bodine and others, 1965; Pingitore, 1978), dictates a diagenetic manganese concentration trend opposing that of sodium and strontium. Kinetic effects, which have been shown to affect the D^{Mn} value in a reverse manner to that of D^{Sr} (D^{Mn} increases with decrease in crystal growth rate; Lorens, 1981), may amplify these opposed diagenetic trends. The D^{Mn} value of dolomite is not known, but the small Mn^{2+} radius (midway between that of magnesium and calcium) and the presence of mixed manganese, calcium, and magnesium carbonates (Calvert and Price, 1977) imply similar manganese content for calcite and dolomite.

The instability of Mn^{4+} in diagenetic reducing environments and the upward diffusion of Mn^{2+} (Elderfield, 1977) can significantly increase the manganese concentration, causing formation of manganoan carbonates around the oxic-anoxic boundary in shallow-water environments (Calvert and Price, 1977). Another source of manganese is meteoric water, which normally contains 10 to 20 times more manganese than does seawater, having a manganese/calcium ratio of about 35×10^{-5} as compared with 0.05×10^{-5} in seawater.

Unlike the strontium content in the San Andres dolomite, the manganese content varies significantly among the various rock units, reflecting either different parent solutions or different diagenetic

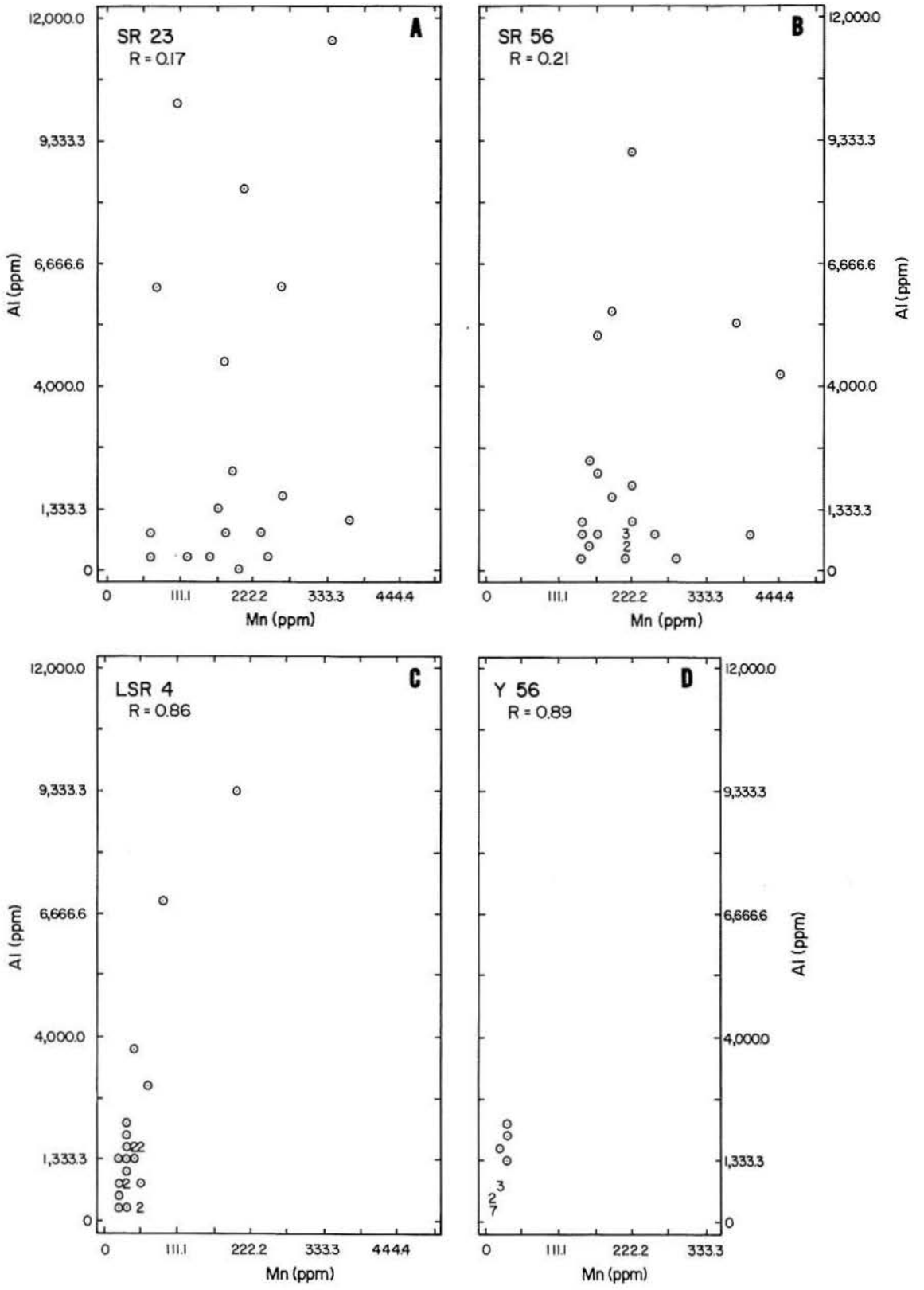

Figure 22. Relation between aluminum and manganese in rock samples. Intercept manganese values for zero aluminum are 9 ppm in C and 8 ppm in D.

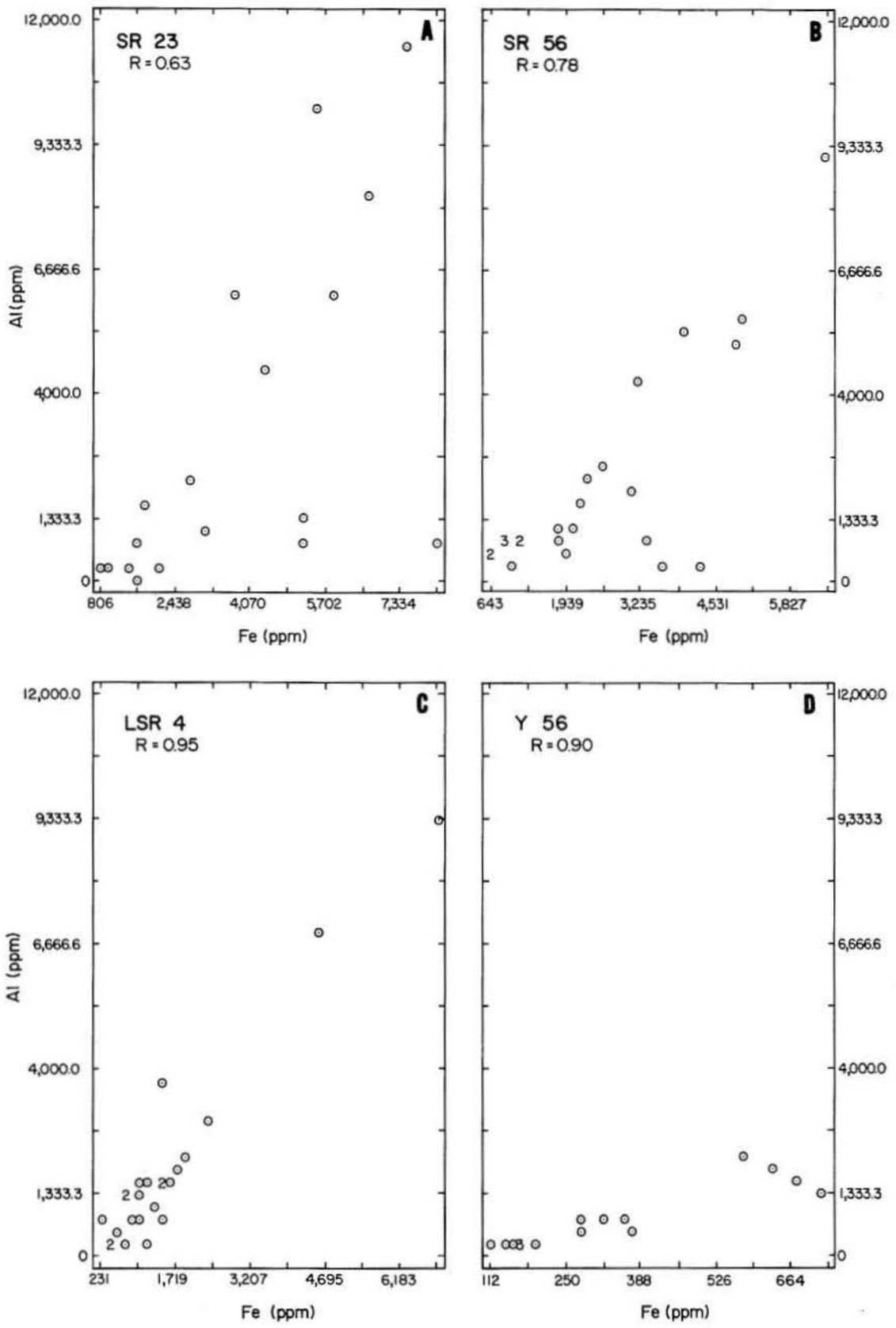

Figure 23. Relation between aluminum and iron in rock samples. Intercept iron values for zero aluminum are 567 ppm in A, 630 ppm in B, 37 ppm in C, and 18 ppm in D.

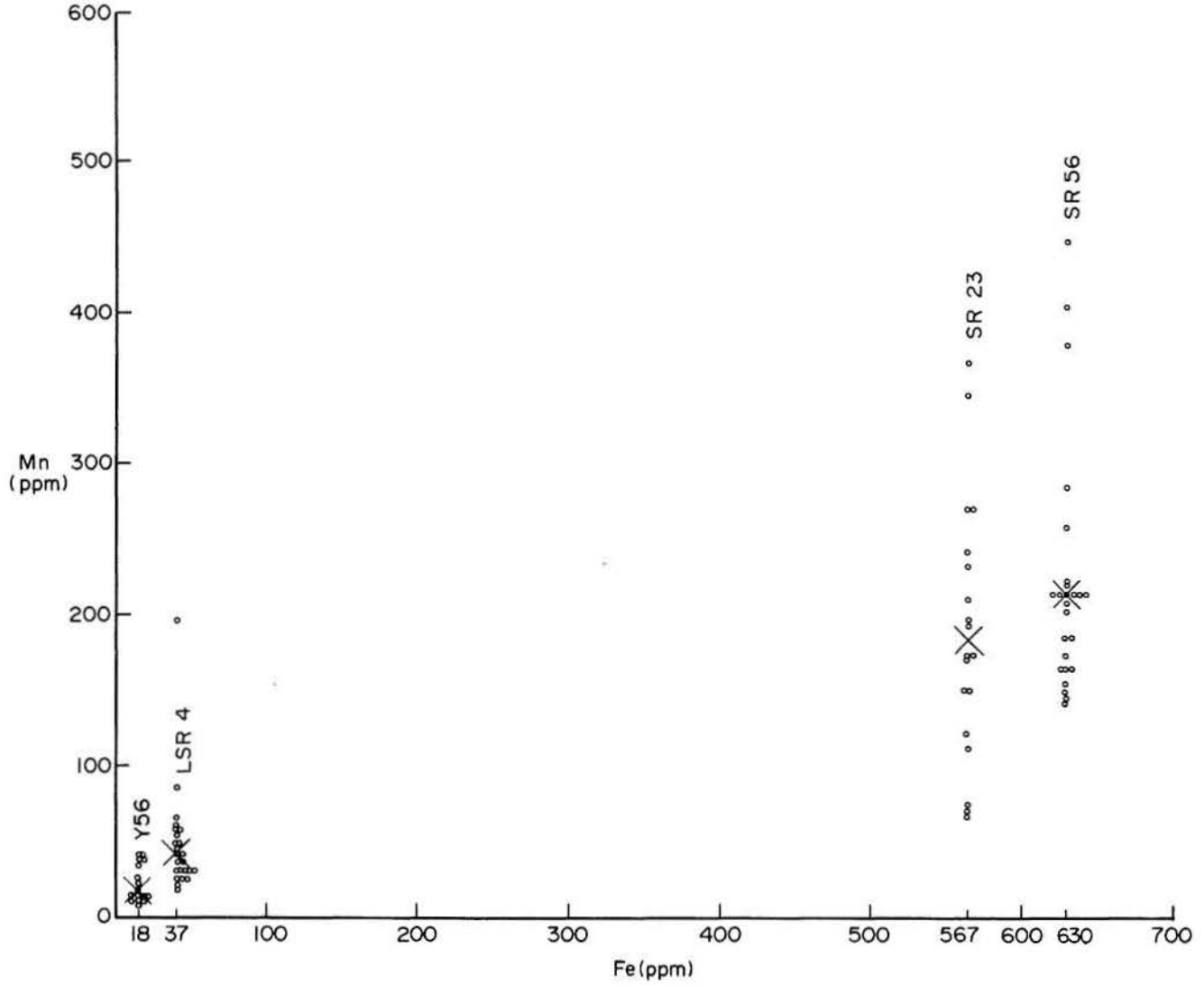

Figure 24. Relation between manganese and iron intercept value for zero aluminum (fig. 23). Cross represents mean manganese values in each unit.

sequences, or both. Differences in the early diagenetic Eh conditions that have been deduced from pristane/phytane ratios do not overlap the significant manganese increase in samples from S4 to S56 units (fig. 24). The change from low-manganese to high-manganese rock units, however, coincides with a marked change in the source of the organic matter, from mostly marine in S4 to mostly terrestrial in S56 (fig. 13). It appears, therefore, that the variation in manganese and iron content reflects different water sources rather than changes in the early diagenetic Eh conditions. The relatively high manganese and iron content of SR56 as compared with Y56 may have resulted from higher meteoric water input into the principally marine-derived brine. The paleogeographic setting corroborates such an explanation; Y56 is located about 130 km (80 mi) farther south from the basin margin than SR56 is, and therefore Y56 was less influenced by fresh water.

Other Trace Elements in Carbonates

The ICP analytical method provides data on many other elements in San Andres rocks. Several elements are below or near detection limits, including (with detection limits in ppm): Co-2, Ni-5, Mo-5, As-10, Cd-2, V-5, Pb-20, Sb-20, Se-25, Sn-5, Be-0.5, U-10, Th-10, and B-20. Other elements, having measured concentrations well within the ICP resolution, do not indicate any correlation with other parameters. Elements in this category and their measured concentration range in ppm are: Cr 7-23, Cu 5-350, Zn 7-35, and Li 6-40. Barium

correlates highly with aluminum with a negative intercept value for zero aluminum, which indicates that most barium measured (2 to 60 ppm) is derived from clay.

Phosphorus concentration ranges between the detection limit (~100 ppm) and 520 ppm (table 4). Almost all L-4 samples (14 out of 16) contain phosphorus above detection limits; their mean value is 298 ppm. In Y56, 13 of 15 samples contain phosphorus concentrations above detection limits, and the mean value is 190 ppm. In SR56, in contrast, almost all samples (24 of 25) contain phosphorus levels below the detection limit of about 100 ppm. In SR234, 16 of 40 samples contain phosphorus above the detection limit. Petrographic observation and organic carbon measurements clearly correlate phosphorus content with organic carbon content; the high phosphorus values of L4 and Y56 are associated with relatively high organic matter content, whereas the low phosphorus content in SR56 coincides with almost no organic matter. It is unknown whether the measured phosphorus is derived directly from organic matter, from dissolution of phosphate minerals, or from phosphorus-carbonate association.

Stoichiometry and Order of Dolomite Crystals

Stoichiometric evaluation is based on a whole-rock and electron probe chemical analysis. In almost all LRS56 samples in which dolomite is the only carbonate mineral detected by X-ray diffraction (39 of 40 samples), the calculated molar percent of $MgCO_3$ is 50 to 49 percent, indicating an almost ideal stoichiometric composition. In other parts of the sequence studied, an additional 11 samples have ideal compositions. In all other samples (46) of which the majority contain a proven calcite phase (X-ray diffraction and petrography), the molar percent of $MgCO_3$ ranges between 48 percent and 2 percent. To estimate stoichiometry in these dolomites and to estimate order of all samples, several electron probe analyses and detailed X-ray diffraction analyses were conducted. The probe data indicate that all dolomites associated with calcites are also close to stoichiometric composition in the range of 47 to 51.5 molar percent $MgCO_3$ (table 4 and fig. 25).

Calculated hexagonal unit cell parameters of all but one sample (14 of 15) clearly indicate contraction of the unit cell beyond the dimensions of disordered synthetic dolomites and Holocene natural dolomites (fig. 25) and even beyond synthetic stoichiometric ones. The dolomites may be grouped according to their unit cell parameters as (1) YSR56 samples overlapping natural stoichiometric dolomite dimensions and deviating slightly toward magnesite parameters and (2) LSR4 and SR2 samples overlapping natural stoichiometric dolomites and deviating slightly toward calcite dimensions.

The relative degree of ordering was approximated by comparing an ordering peak height (015) with a reference peak (110). Most of the YSR56 samples (in which unit cell parameters deviate toward magnesite) indicate a relatively higher degree of ordering than do the LSR4 and SR2 samples (fig. 25).

Stable Isotopes in Carbonates and Cherts

The $\delta^{18}O$ and $\delta^{13}C$ values of all carbonate samples are given in table 4, and $\delta^{18}O$ in quartz is given in table 6. Cross plots of $\delta^{18}O$ versus $\delta^{13}C$ indicate that YSR56 can be grouped separately from LSR4 and SR23 mainly on the basis of $\delta^{13}C$ composition (fig. 26). Both groups overlap slightly, but the YSR56 samples are significantly enriched in ^{13}C ($\delta^{13}C$ mean values of the groups are 5.46‰ and 4.14‰, respectively).

Table 6. $\delta^{18}O$ values in quartz separated from partially silicified anhydrite nodules and sponge spicule packstone.

Sample	$\delta^{18}O$	Remarks
CB 67	31.8	Sponge spicule packstone
CB 74	31.6	Partly silicified anhydrite nodule
HF 7	31.8	Partly silicified anhydrite nodule
ARA 11	30.8	Partly silicified anhydrite nodule
PS 1	31.8	Partly silicified anhydrite nodule

Calcite associated with dolomites in the same samples is 1.8 to 3.75‰ depleted in $\delta^{18}O$ and 0.5 to 1.2‰ depleted in $\delta^{13}C$. Possible interference of coexisting calcite and dolomite CO_2 during the analytical procedure may have shifted some of the dolomite to lighter compositions and some of the calcite to heavier compositions. The fractionation effect of 2 to 4‰ in $\delta^{18}O$ between dolomite and calcite (Fritz and Smith, 1970; Aharon and others, 1977; Land, 1980) implies that both minerals in LSR4 and SR2 are apparently in equilibrium and in a cogenetic relation. Carbon values are also apparently near equilibrium.

$\delta^{18}O$ and $\delta^{13}C$ do not correlate, either in all data cross plots or in any separate data group. Data from units that had been stratigraphically analyzed in several places reveal that $\delta^{18}O$ values decrease with depth (figs. 3, 4, 5, and 6). Cross plotting $\delta^{18}O$ over manganese clearly demonstrates this trend (fig. 27). In three of seven rock units, a negative correlation is indicated between manganese and $\delta^{18}O$, whereas in another three rock units an increase of $\delta^{18}O$ is followed by almost constant manganese values. A general negative correlation is also indicated collectively for all these units (fig. 27).

The proposed diagenetic model by which the dolomite and calcite evolved implies that the $\delta^{18}O$ composition of the rocks could have been shaped by equilibrium with at least three solutions. Such a complex diagenetic history may prevent direct determination of the brine compositions involved. However, the constraint of the proposed model, resulting in relatively light $\delta^{18}O$ compositions, can be evaluated. Some of the observed compositions still bear recognizable early prints attributed to the depositional environment. Many of the other samples have only some average equilibrated composition between the latest fluids in which they stabilized and some earlier inherited composition.

The sodium/chloride and potassium/chloride ratios ascribed to fluid inclusions in the dolomite, their estimated salinity, and the lack of almost any fresh-water cements indicate that the latest diagenetic stage took place in highly saline brines. These brines, which originated from evaporation of seawater beyond the halite precipitation level with or without some additional meteoric or seawater mixture, were originally trapped or later refluxed within the sediment.

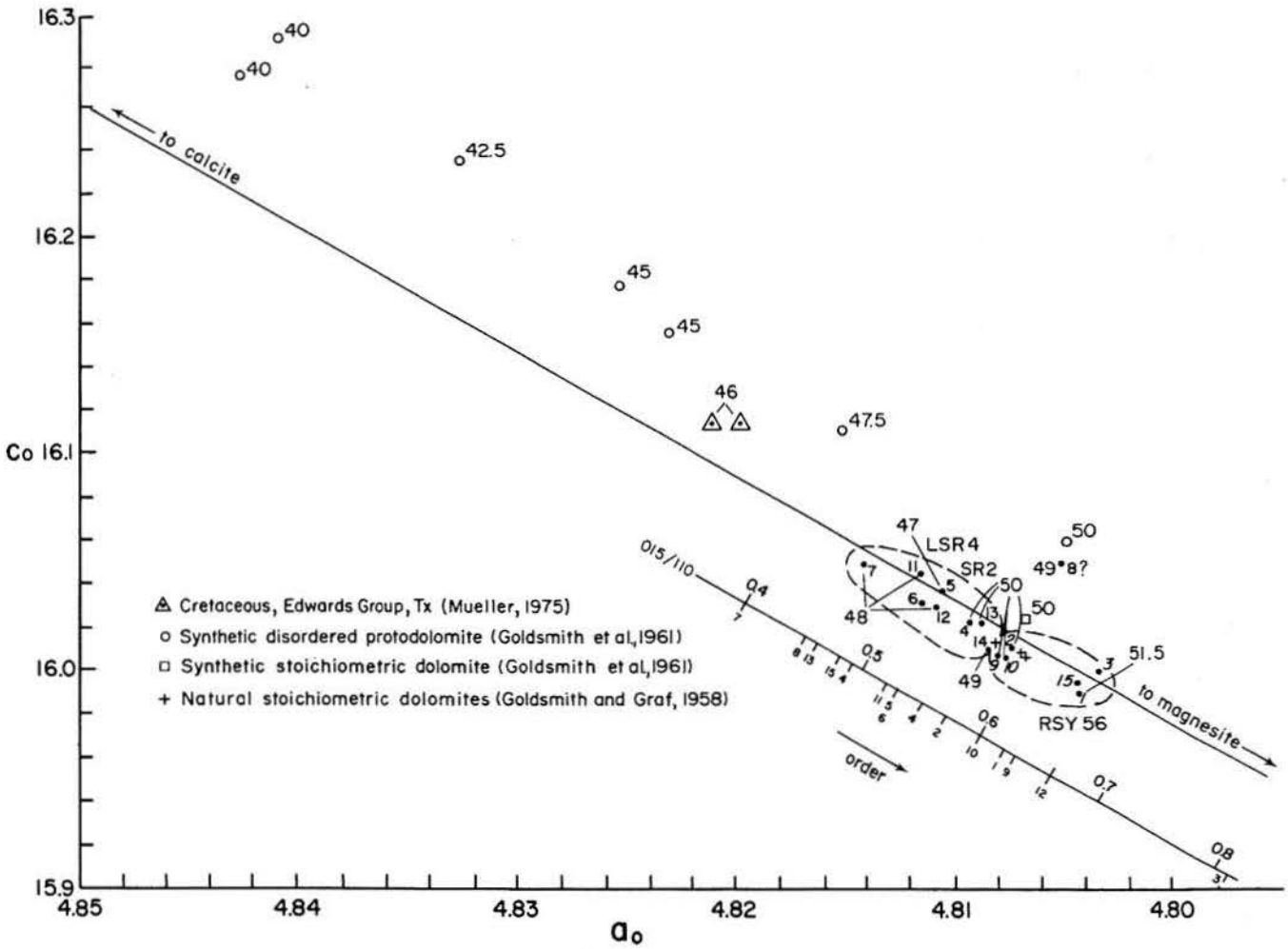

Figure 25. Hexagonal unit cell parameters a_o and c_o (in Å) calculated from X-ray diffraction. Sample identification is as follows:

1 R-1371	4 R-1963	7 R-2194	10 S-2126	13 HF-11
2 R-1487	5 R-1995	8 R-2204	11 S-2715	14 CB-97
3 R-1493	6 R-2170	9 S-2085	12 S-2897	15 PS-15

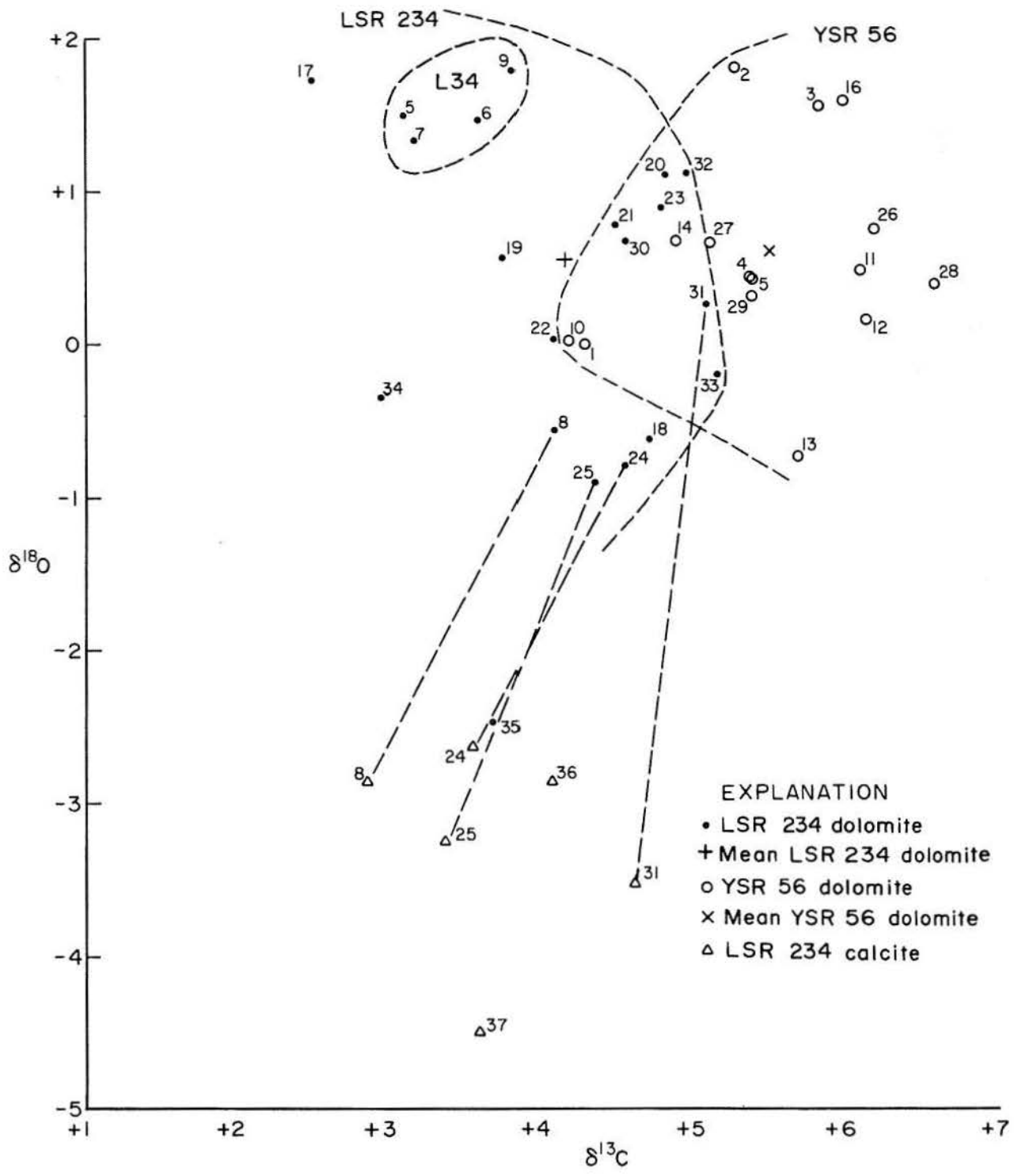

Figure 26. Relation between $\delta^{18}O$ and $\delta^{13}C$ in dolomites (circles) and calcites (triangulars). Sample identification is as follows:

1-MC17	6-CB68	11-S2122	16-S2236	21-S2822	26-R1371	31-R2520	36-R2733
2-PS25	7-HF11	12-S2126	17-S2704	22-S2857	27-R1487	32-R2096	37-R2005
3-PS7	8-FG6	13-S2128	18-S2715	23-S2897	28-R1701	33-R2174	
4-PS2	9-SMA12	14-S2196	19-S2785	24-S2917	29-R1743	34-R2194	
5-HF18	10-S2085	15-S2257	20-S2819	25-S2933	30-R1963	35-R2204	

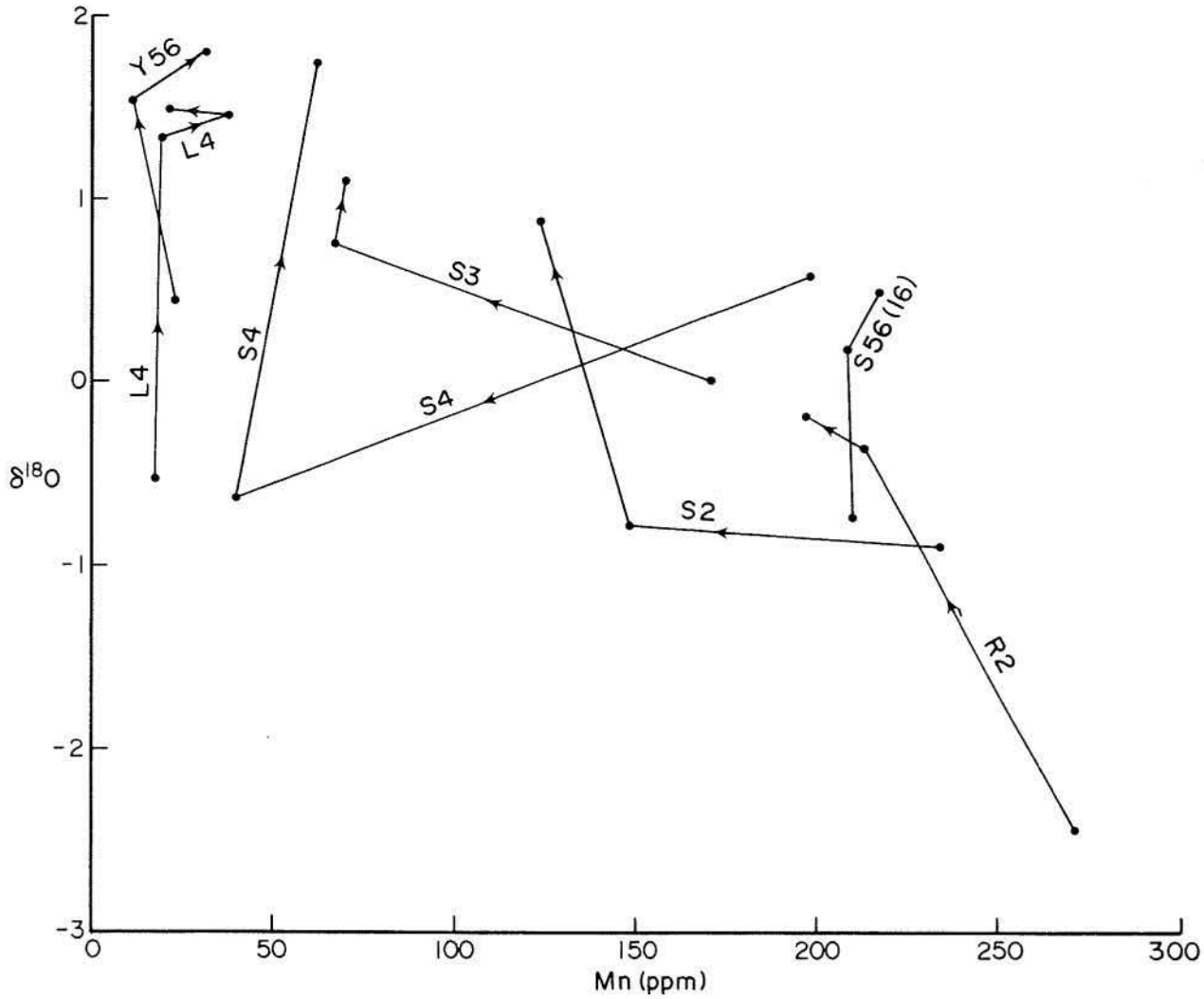

Figure 27. Relation between $\delta^{18}O$ and manganese in stratigraphically related samples.

Equilibrium relations between the carbonates, solutions, and temperatures can be calculated (table 7) by applying $\Delta^{18}O$ of about 3‰ for the CO_2 evolved from cogenetic dolomite and calcite and using the experimental equation (Epstein and others, 1953; Craig, 1965):

$$T(°C) = 16.9 - 4.2\ (\delta c - \delta w) + 0.13\ (\delta c - \delta w)^2 \quad (1)$$

or by using the experimental equation derived for protodolomites (Fritz and Smith, 1970):

$$1000 \ln \alpha = 2.62 \times 10^6 T^{-2} + 2.17. \quad (2)$$

Similar equilibrium relations between the cherts, solutions, and temperatures can be calculated using Knauth and Epstein's (1975) equation (table 8):

$$1000 \ln \alpha = 3.09 \times 10^6 T^{-2} - 3.29. \quad (3)$$

The rock sequence that is under discussion is currently buried at a depth between 370 and 1,620 m (1,110 to 5,010 ft). Geologic reconstruction of the area, bottom-hole temperatures, and vitrinite reflectance (Dutton, 1980; Ramondetta, 1981) indicate that the rock sequence was never more deeply buried; thus, diagenesis under high temperature can be rejected. Original brine temperature might have been quite high. Concentrated brines are less transparent than seawater, absorb more solar energy, and may thus reach higher temperatures than does normal seawater. Temporary or long-term water stratification, which frequently develops even in shallow water, may amplify the heating of the dense brine, as in a greenhouse. Considering these effects, original brine temperatures might have been as high as 40° to 45° C. Similar temperatures currently exist at all depths at which the rocks are buried.

The $\delta^{18}O$ values in evaporating marine brine are known to increase to 4 to 6‰ during the first stages of evaporation (Gat, 1979; Lloyd, 1966). The upper limit of $\delta^{18}O$ depends upon the relative humidity over the evaporating brine; the higher the humidity, the lower the $\delta^{18}O$. High humidity is expected over most marine brines even in desert areas. In the desert Qatar Peninsula, for example, humidities of 75 to 100 percent limit the $\delta^{18}O$ to about 4‰ (Lloyd, 1966). At high water salinities (above approximately four times that of seawater), $\delta^{18}O$ values generally decrease again with increasing salinity to about 2 to 4‰ at the initial point of halite precipitation (Gonfiantini, 1965; Lloyd, 1966; Sofer and Gat, 1972; Holser, 1979b; Nadler and Magaritz, 1980). This reversal has been explained to result from the decrease in the activity of the water in highly saline brines, which affects the relative rates of evaporation and condensation (Gonfiantini, 1965). Interaction and isotopic fractionation between free water and the large amount of water in the hydration sphere of the cations in such brines have also been considered to affect the reversal (Holser, 1979b; Taube, 1954; Sofer and Gat, 1972).

Given these considerations, it appears that the San Andres dolomites, calcites, and cherts may have been stabilized and equilibrated with a brine having a $\delta^{18}O$ of 2 to 4 ‰ at a temperature of 35° to 45° C (tables 7 and 8). Such a brine could have been formed within the frame of the proposed depositional-diagenetic model.

The relative increase in $\delta^{18}O$ with decreasing depth in several dolomite units is considered to reflect an initial depositional trend of the presumed aragonite precursor. These changes followed increased evaporation of the water that caused the deposition of these thin carbonate layers. Decreased manganese in the same direction (fig. 27) is explained by the high D^{Mn}, which gradually depleted the brine in manganese as carbonate precipitation continued. The mean lighter $\delta^{13}C$ composition of the LSR234 and the L34, in particular, as compared with the YSR56 (fig. 26), may be explained best by the higher proportion of organic-derived carbon released through the oxidation of the more abundant organic matter in these rock units.

The $\delta^{18}O$ composition of the studied San Andres dolomites is significantly depleted relative to exposed Permian dolomites in the Guadalupe Mountains. Rudolph (1978) reported $\delta^{18}O$ values of 2.2 to 3.2‰ and $\delta^{13}C$ of 5 to 6.5‰ in back-reef Tansill dolomites a few kilometers shoreward from the Capitan Reef. Three samples from the Seven Rivers Formation, about 32 km (20 mi) shoreward from the reef trend, were analyzed during the present study (table 9).

Table 7. $\delta^{18}O$ equilibrium relations between water and carbonates as a function of temperature. (1) and (2) refer to equations used for calculation (see text).

	$\delta^{18}O$ water (SMOW)						
Equation	1	2	3	4	5		
(1)	28°C	33°C	38°C	44°C	50°C	1.5	
(2)	29°C	34°C	40°C	46°C	52°C		
							$\delta^{18}O$ dolomite
(3)	33°C	38°C	44°C	50°C	56°C	0.5	(PDB)
(4)	34°C	40°C	46°C	52°C	59°C		

Table 8. $\delta^{18}O$ equilibrium relation between water and cherts as a function of temperature.

$\delta^{18}O$ water (SMOW)						
1	2	3	4	5		
30°C	35°C	40°C	45°C	50°C	31.8	
31°C	36°C	41°C	46°C	51°C	31.6	$\delta^{18}O$ chert (SMOW)
35°C	40°C	45°C	50°C	55°C	30.8	

Table 9. $\delta^{18}O$ and $\delta^{13}O$ values in the Seven Rivers Formation, Guadalupe Mountains. The extremely light $\delta^{18}O$ value in sample 1 is may be an analytical error caused by the small amount of dolomite in the sample.

Sample	$\delta^{18}O$	$\delta^{13}C$	Remarks
1	-12.85	+4.2	dolomite lamina (1 mm) in thick-bedded gypsum
2	+4.2	+5.3	dolomite bed (10 to 15 cm) in thick-bedded gypsum
3	+3.4	+6.4	dolomite unit (5 to 6 m) on top of gypsum beds

An explanation for the isotopically lighter composition of the San Andres dolomite relative to Tansill and Seven River dolomites may be related to the different history of the dolomitizing brines. In dolomite from the exposed Guadalupe Mountains, the dolomitizing fluid was derived from a marine brine that had been evaporated up to the point of gypsum precipitation, and attained the heaviest $\delta^{18}O$ composition possible. The brine that dolomitized the Palo Duro dolomites, in contrast, had much more advanced evaporation, presumably beyond the halite precipitation stage. Considering the reversal effect noted in the $\delta^{18}O$ compositions in highly concentrated brines, the $\delta^{18}O$ of this brine might have been lighter than that which formed the Guadalupe Mountains dolomite.

DISCUSSION

The San Andres Formation may be divided into two parts, the lower sequence including cycles 2, 3, and 4, and the upper sequence (termed here YSR56), in which no clear-cut large cycles can be differentiated. The lower part, and cycle 4 in particular, consists of carbonate, anhydrite, and salt, which accumulated mostly under subaqueous conditions (Handford and others, in press; Presley, 1981; this study). Bromide content in the halite is consistently high and indicates continuous salt deposition without intermittent dissolution. Some of the salt units are thick and extend over large areas; cycle 4 salt forms a continuous salt unit about 50 to 70 m (150 to 200 ft) thick with an areal extent of over 100 by 200 km in the area studied (Presley, in press). Halite accumulation of such an extent without potash-magnesia mineral precipitation and with no dissolution record indicates that deposition occurred in a large water body with an efficient circulation pattern that enabled continuous fresh marine-water supply and dense brine outflow. Increased salinity may have resulted from the large size of the water body relative to its depth and evaporation rate. Circulation may have been affected by local bar formation at the Northern Shelf margin of the Midland Basin (such as oolite shoals [Todd, 1976] or differential subsidence overlapping former shelf margin trends [Ramondetta, in press]). Salinity fluctuations could have resulted from a change in the configuration of those bars and their effects on the water circulation and/or from relative sea-level changes. Under the proposed depositional model, deposition of cycles 2, 3, and 4 occurred subaqueously in a large shelf basin or lagoon. Lithologic changes are ascribed to the increase in water salinity followed by only small bathymetric changes. The mudstone units are also considered to be subaqueous deposits of terrigenous material derived from the adjacent desert land. The deltaic and fluvial-deltaic systems (Smith, 1974) of the San Angelo Formation (early San Andres time; M. Presley, personal communication, 1981) northwest of the study area were deposited at the margins of the subaqueous basin. Mud was carried and dispersed over the basin mostly as suspension load in the dense brine.

Sedimentological as well as geochemical properties of the upper San Andres rocks in the Palo Duro Basin (SR56) indicate a change in the depositional regime. The interbedded salt, anhydrite, carbonate, and mud units are much thinner and laterally less persistent than those of the lower part of the formation. The lithologic change is followed by a significant increase in the manganese, iron, and terrestrial organic matter associated with the carbonates, and by bromide depletion in many halites. Water that controlled sedimentation during this period apparently decreased in volume and may have been divided into several smaller and shallower basins. Since halite saturation during this period was achieved partially through dissolution of previously deposited salt, the precipitation of potash-magnesia minerals was precluded even when the expected circulation pattern became less efficient. The change of the basin configuration from a relatively deep, large water body to shallower, smaller, separated water bodies was reflected also by a change in the basin-margin terrigenous sedimentation. The formerly deltaic and fluvial-deltaic systems of the San Angelo Formation (early San Andres time) changed into a mud-rich tidal-flat system of the Blaine Formation (middle to late San Andres time; Smith, 1974; M. Presley, personal communication, 1981). Many of the thin carbonate beds between the evaporites and mudstones in SR56 may have been deposited by introduction of meteoric water rather than by increased marine carbonate supply (a process that may be compared to the whiting - aragonite precipitation in the Dead Sea following inflow of meteoric water and after continuous evaporation; Neev and Emery, 1967). The predominance of chemically precipitated carbonates and their association with primary anhydrite indicates that salinity of the water in the Palo Duro Basin remained high during carbonate deposition.

Handford and others (in press) and Presley (1979, 1981) concluded that the Permian sequence including the San Andres Formation in the Palo Duro Basin accumulated in a coastal sabkha and salt pan complex along an arid coastline. Most of the salt and anhydrite was interpreted as

subaqueous brine pan precipitates. Their paleogeographic model described the brine pans as being located landward of a narrow supratidal strip that contained standing water and, similar to some recent brine pans, was at sea level. Mixtures of salt and red-brown mudstones, termed "chaotic mudstone-salt," were considered to be salt-flat deposits in which most of the salt grew displacively within the muds.

The salt-flat/brine pan model adapted from recent environments by Handford and others (in press) and Presley (1981) provides an analogy for processes involved in evaporite deposition; however, many criteria given to define such environments are ambiguous. Subaqueous anhydrite and salt may precipitate from brine pans; chaotic mudstone-salt may evolve in playa-like areas by displacive growth of salt from a high ground-water table, and nodular anhydrite may occur in the capillary zone of supratidal environments. On the other hand, displacive hopper growth was found in muddy sediments at the bottom of the Dead Sea (Gornitz, 1965); nodular anhydrite is found in subaqueous, deeper-than-sabkha environments (Dean and others, 1975; Holser, 1979), and subaqueous evaporite sequences in general are found in many settings other than supratidal brine pans (Schrieber, 1977). Holocene models do not provide a setting in which all the different lithological associations are found at one place. Dimensions of most partial analogs are by far smaller than the San Andres setting. In current usage the term "sabkha" refers to a flat deflation surface in arid zones that is in equilibrium between wind erosion and the capillary fringe above a ground-water table. Standing water on sabkhas may result from either rapid rise of the ground-water table or from flooding. In both cases, large open water bodies are temporary, usually lasting less than a year. Chemical precipitation over the sabkha complex occurs interstitially under vadose and phreatic conditions. The temporary nature of the open water bodies results in some thin, intermittent subaqueous evaporite veneer or some sporadic, thicker, localized units.

Our data appear to negate the application of such a depositional regime to the lower San Andres Formation and to cycle 4 in particular. Shallow brine pans in a sabkha (salt-flat) model that flooded periodically are neither compatible with the required continuous widespread circulation pattern nor able to precipitate thick continuous salt sequences without salt recycling. The high proportion of subaqueous to interstitial chemical sediments in the sequence requires another hydrogeological setting, namely a shelf basin or lagoon.

Despite the proposed differences in the depositional regime between the lower and upper part of the San Andres Formation, the similarity of all the dolomite indicates that diagenesis occurred in similar brines. Considering all data previously discussed, it appears that the brines in which the carbonates were stabilized and dolomitized were basically magnesium-calcium-chloride brines. The abundance of halite in the sequence explains the predominance of such brines throughout the entire diagenetic period. The initial brine composition that evolved through $CaCO_3$, $CaSO_4$, and sodium chloride precipitation was most likely saturated with respect to anhydrite but undersaturated with respect to $CaCO_3$ and apparently also to dolomite. The solubility product of $CaCO_3$ in hypersaline waters is higher than that of normal sea water, and it increases with increasing salinity (Sass and Ben-Yaakov, 1977). During the first stages of brine reflux through the carbonate sediments, dissolution of $CaCO_3$ and consequent $CaSO_4$ precipitation were the main processes. The abundant molds and their cementation by anhydrite is attributed to this stage. Dissolution of aragonite and subsequent gypsum precipitation in sediments affected by saline "potentially dolomitizing fluids" in a recent Persian Gulf sabkha were described by Patterson (1972). After this process, calcium and magnesium concentrations were maintained at approximately constant levels, whereas SO_4 concentration decreased. At the same time carbonate concentration must have increased until dolomite saturation occurred. Sulfate reduction and organic matter consumption may have also affected the process (Berner, 1971; Patterson, 1972). Continuous dolomitization reduced the magnesium/calcium ratio of the solution. After $CaSO_4$ dissolution and diagenetic magnesium intake by clays (Handford and others, in press), the brine may have shifted from dolomite to calcite saturation. Such brines in contact with earlier dolomitized rocks induced some dedolomitization (in R4), and, when in contact with $CaCO_3$ sediments, caused aragonite-to-calcite transformation, calcite recrystallization, and calcite cement precipitation (in R4, S234). After dolomitization, stabilization of early dolomite to ordered dolomite, and aragonite-to-calcite transformation, strontium was released to the solution from the precursor minerals and may have

caused celestite saturation and precipitation (S2, R4, and in many other parts of the sequence). The high strontium content of the brine is reflected in the high-strontium calcite in the San Andres Formation. The abundant calcite in SR4 and S2 rock units, as compared with almost pure dolomite in all other parts of the San Andres Formation, may have resulted from a higher carbonate rock-to-brine volume ratio. The higher the ratio, the faster the magnesium-to-calcium ratio in the brine dropped below dolomite supersaturation. The thin carbonate beds in SR56 were entirely dolomitized because of their small volume compared with the brine volume. The intensive dolomitization of the thick Y56 rock units was presumably achieved due to the high amount of brine reflux through them. Their location at the seaward margin of the basin reduced the amount of evaporite deposition that plugged some of the pore space and increased significantly the efficiency of the heavy brine reflux back to the sea. The apparent $\delta^{18}O$ equilibrium relations among the calcite, dolomite, and chert with similar brine composition over the same temperature range indicate that opal dissolution and subsequent quartz precipitation was cogenetic with carbonate diagenesis.

The diagenetic sequence by which the Palo Duro and the Northern Shelf San Andres carbonates evolved was basically the same. In both, diagenesis followed isothermally and isochemically in association with highly saline magnesium-calcium-chloride brines. Continuous contact between the Palo Duro carbonates and these halite-saturated brines resulted in almost complete plugging of the original pore space and of the space left after the early $CaCO_3$ dissolution and the subsequent anhydrite deposition. To the south, over the Northern Shelf, the dolomitizing brine apparently became undersaturated with respect to halite owing to mixture with marine water. Superimposed on such initial brine differences, higher proportions of skeletal lithofacies more susceptible to pressure solution and pore space not plugged by halite resulted in higher porosity in this area. The proposed diagenetic model implies that after early diagenetic processes, the Palo Duro sequence remained a closed (but compacting) system, basically unchanged by later fluid influx.

CONCLUSIONS

The San Andres evaporitic sequence in the Palo Duro Basin includes thick carbonate units in its lower part (SR234) and many thin units in its upper part (SR56). To the south, the evaporites pinch out and carbonates predominate.

Six basic lithofacies were differentiated in the carbonates, namely, dolomudstone, pellet-oolite packstone-grainstone, filamentous (*Girvanella*-like) grainstone, sponge spicule packstone, wispy-laminated crinoid packstone, and skeletal packstone-grainstone. Facies distribution was controlled mostly by the salinity of the water body, which most of the time increased from south to north.

Carbonates in the upper part of the formation consist of pure dolomite; in the lower part of the formation the dolomites are accompanied by some calcite in the form of unreplaced skeletal fragments and cements commonly associated with celestite.

Anhydrite associated with carbonates is in four forms: (1) dolomite-anhydrite intergrowth; and (2) nodular anhydrite, both of early displacive origin; (3) replacement anhydrite, which postdates dolomitization and lithification and apparently follows early dissolution, presumably owing to organic matter oxidation; and (4) blocky anhydrite cement, which is in skeletal molds that formed after dissolution of $CaCO_3$.

Organic matter in L4 and S24 is mostly derived from a marine source, whereas in S56, most of the organic matter is terrestrial in origin. The pristane-to-phytane ratio is low in L4 and high in both S24 and S56, pointing to more reducing, early diagenetic conditions in L4.

Consistent bromide values higher than 70 ppm in R234 and mostly lower values in R56 indicate steady-state conditions during R4 deposition and non-steady-state conditions during R56 depositions. Water saturation with respect to halite owing to some salt dissolution in R56 apparently implies a smaller and shallower water body than that of R4.

High strontium content in all anhydrite types indicates primary anhydrite precipitation in highly saline water (greater than seven times that of sea water).

Sodium/chloride and potassium/chloride ratios attributed to liquid inclusions in the carbonates indicate a dolomitizing brine of magnesium-calcium-chloride composition derived from marine water evaporated beyond halite saturation. High sodium substitution for cations in dolomite in L4 and Y56 is attributed to higher sodium/calcium + magnesium ratios in the southern brine. The lower sodium/calcium + magnesium ratio in the northern brine caused by extensive halite precipitation resulted in lower sodium concentrations in dolomite to the north.

Manganese and iron content in S56 is characteristically higher than in most other parts of the formation. The high manganese and iron values correlate with high amounts of terrestrial-derived organic matter and not with different early diagenetic Eh conditions, and are attributed to increased influence of meteoric water in the basin to the north.

The 500 to 200 ppm strontium range, which accounts for 84 percent of all dolomite, indicates depletion relative to Holocene dolomite. This depletion is attributed to kinetic effects and contraction of the cell unit that accompanies the change toward stoichiometric composition and reduces the D^{Sr} during the transformation of metastable dolomite to ordered, stoichiometric phases.

$\delta^{18}O$ values of coexisting calcite, dolomite, and chert apparently indicate equilibrium with a brine having $\delta^{18}O$ values of 2 to 4‰ over a temperature range of 35° to 45° C. The relatively light $\delta^{18}O$ values are explained by the observed reversal in the dependence of $\delta^{18}O$ on increased evaporation in highly saline brine.

The lower part of the San Andres Formation was subaqueously deposited in a broad shelf basin or lagoon, deep enough to maintain long periods of steady-state circulation and to prevent potash-magnesia concentration in the brine. Cyclic changes in the carbonate facies and in the evaporitic sequence are attributed to changes in water salinity without significant changes in water depth.

The upper part of the formation was deposited in a much smaller water body sensitive to inflow fluctuations. The increased meteoric water inflow evidenced by high manganese and iron and terrestrial organic matter also accounts for a bicarbonate source for the deposition of many thin carbonate units in SR56.

Diagenesis of carbonates occurred in contact with high-saline magnesium-calcium-chloride brines that evolved through anhydrite and halite precipitation. Skeletal mold formation and subsequent anhydrite cementation, dolomitization, and calcite cementation associated with celestite and dedolomite are all cogenetic products of such a brine-rock interaction. Dissolution of siliceous sponge spicules and subsequent chertification apparently occurred in contact with the same brines.

The San Andres carbonates in the Palo Duro Basin were deposited in water ranging from normal marine to ten times normal concentrations, and were diagenetically changed essentially isochemically in a highly saline magnesium-calcium-chloride brine in a closed sedimentary basin.

ACKNOWLEDGMENTS

Clara Ho contributed much to the chemical procedures undertaken in this study. The manuscript benefited from thorough and critical reviews by R. L. Bassett, L. F. Brown, Jr., C. R. Handford, J. H. McGowen, M. W. Presley, S. C. Ruppel, and W. D. Wiggins.

Funding for this research was provided by the U.S. Department of Energy under Contract No. DE-AC97-80ET-46615 and the National Science Foundation, Contract No. EAR-7824081 (LSL). The publication was typed by Margaret Chastain and typeset by Charlotte J. Frere, under the supervision of Lucille C. Harrell, and edited by Amanda R. Masterson. Figures were drafted by Thomas M. Byrd, Jeffrey Horowitz, and Jamie McClelland, under the supervision of Dan F. Scranton, and photographic printing was by Jim Morgan. Cover and design were by Barbara Jezek.

REFERENCES

Aharon, P., Kolodny, Y., and Sass, E., 1977, Recent hot brine dolomitization in the "solar lake," Gulf of Elat; isotopic, chemical, and mineralogical study: Journal of Geology, v. 85, no. 1, p. 27-48.

Behrens, E. W., and Land, L. S., 1972, Subtidal Holocene dolomite, Baffin Bay, Texas: Journal of Sedimentary Petrology, v. 42, no. 1, p. 155-161.

Bein, A., 1976, Shelf basin sedimentation: mixing and diagenesis of pelagic and clastic Turonian carbonates, Israel: Journal of Sedimentary Petrology, v. 47, no. 1, p. 382-391.

Berner, R. A., 1971, Principles of chemical sedimentology: New York, McGraw-Hill, 240 p.

Bodine, M. W., Holland, H. D., and Borcsik, M., 1965, Coprecipitation of manganese and strontium with calcite, *in* Problems of postmagmatic ore deposition: Prague, Geological Survey of Czechoslovakia, v. 2, p. 40-46.

Butler, G. P., 1973, Strontium geochemistry of modern and ancient calcium sulfate minerals, *in* Purser, B. H., ed., The Persian Gulf: New York, Springer-Verlag, p. 423-452.

Calvert, S. E., and Price, N. B., 1977, Shallow water continental margin and lacustrine nodules, distribution and geochemistry, *in* Glasby, G. P., ed., Marine manganese deposits: Elsevier Oceanography Series 15, p. 45-86.

Chuber, S., and Pusey, W. C., 1972, Cyclic San Andres facies and their relationships to diagenesis, porosity and permeability in the Reeves field, Yoakum County, Texas, *in* Elam, J. G., and Chuber, S., eds., Cyclic sedimentation in the Permian Basin: West Texas Geological Society, p. 135-150.

Clayton, R. N., and Mayeda, T. K., 1963, The use of bromine pentafluoride in the extraction of oxygen from oxides and silicates for isotopic analysis: Geochimica et Cosmochimica Acta, v. 27, p. 43-52.

Cooper, J. E., and Bry, E. E., 1963, A postulated role of fatty acids in petroleum formation: Geochimica et Cosmochimica Acta, v. 27, p. 1113-1127.

Cox, R. E., Maxwell, J. R., Eglinton, G., Phillinger, C. T., Ackman, R. G., and Hooper, S. N., 1970, The geological fate of chlorophyll: the absolute stereochemistry of acyclic isoprenoid acid in a 50 million year lacustrine sediment: Chemical Comm., p. 1639-1641.

Craig, H., 1965, The measurement of oxygen isotope paleotemperature: Proceedings, Spoleto conference on stable isotopes in oceanographic studies and paleotemperatures, p. 161-182.

Dean, W. E., and Tung, A. L., 1974, Trace and minor elements in anhydrite and halite, Supai Formation (Permian), east-central Arizona, *in* Coogan, A. H., ed., Fourth symposium on salt: Northern Ohio Geological Society, v. 1, p. 275-285.

Dean, W. E., Davies, G. R., and Anderson, R. Y., 1975, Sedimentological significance of nodular and laminated anhydrite: Geology, v. 3, no. 7, p. 367-372.

Dutton, S. P., 1980, Petroleum source rock potential and thermal maturity, Palo Duro Basin, Texas: The University of Texas at Austin, Bureau of Economic Geology Geological Circular 80-10, 48 p.

Elderfield, H., 1977, The form of manganese and iron in marine sediments, *in* Glasby, G. F., ed., Marine manganese deposits: Elsevier Oceanography Series 15, p. 269-290.

Epstein, S., Bucksbaum, R., Lowenstam, H. A., and Urey, H. C., 1953, Revised carbonate-water isotopic temperature scale: Geological Society of America Bulletin, v. 64, p. 1315-1326.

Fritz, P., and Katz, A., 1972, The sodium distribution of dolomite crystals: Chemical Geology, v. 10, no. 3, p. 237-244.

Fritz, P., and Smith, D. G. W., 1970, The isotopic composition of secondary dolomites: Geochimica et Cosmochimica Acta, v. 34, no. 11, p. 1161-1173.

Gat, J. R., 1979, Isotope hydrology of very saline surface waters, *in* Isotopes in lake studies: International Atomic Energy Agency, Vienna, p. 151-162.

Goldsmith, J. R., and Graf, D. L., 1958, Relation between lattice constants and composition of the Ca-Mg carbonates: American Mineralogist, v. 43, no. 1-2, p. 84-101.

Goldsmith, J. R., Graf, D. L., and Heard, H. C., 1961, Lattice constants of the calcium-magnesium carbonates: American Mineralogist, v. 46, p. 453-457.

Gonfiantini, R., 1965, Effetti isotopi nell'evaporazione di acque salate: Atti Soc. Tosc. Sci. Nat., Ser. A., v. 72, p. 1-22.

Gornitz, V. M., 1965, A study of halite from the Dead Sea: New York, Columbia University, Master's thesis.

Handford, C. R., Wiggins, W. D., Palmer, D. P., and Bassett, R. L., in press, Sedimentology, petrography, and diagenesis of Permian evaporites, Randall County, Texas: The University of Texas at Austin, Bureau of Economic Geology Report of Investigations.

Hardie, L. A., 1967, The gypsum-anhydrite equilibrium at one atmosphere pressure: American Mineralogist, v. 52, p. 172-200.

Heller, P. L., Komar, P. D., and Pevear, D. R., 1980, Transport processes in ooid genesis: Journal of Sedimentary Petrology, v. 50, p. 943-952.

Holser, W. T., 1979a, Mineralogy of evaporites, *in* Burns, R. G., ed., Marine minerals: Mineralogical Society of America, Short Course Notes, p. 211-294.

_____ 1979b, Trace elements and isotopes in evaporites, *in* Burns, R. G., ed., Marine minerals: Mineralogical Society of America, Short Course Notes, p. 295-346.

Jacka, A. D., and Franco, L. A., 1973, Deposition and diagenesis of Permian evaporites and carbonates and clastics on shelf areas of the Permian Basin, *in* Coogan, A. H., ed., Fourth symposium on salt: Northern Ohio Geological Society, v. 1, p. 67-89.

Johnson, J. H., 1961, Limestone-building algae and algal limestones: Colorado School of Mines, Boulder, Colorado, 297 p.

Kinsman, D. J. J., 1966, Gypsum and anhydrite of Recent age, Trucial Coast, Persian Gulf, *in* Rau, J. L., ed., Second symposium on salt: Northern Ohio Geological Society, p. 302-326.

Kinsman, D. J. J., and Holland, H. D., 1969, The co-precipitation of cations with $Ca\text{-}CO_3$ - IV; the co-precipitation of Sr^{2+} with aragonite between 16° and 96°C: Geochimica et Cosmochimica Acta, v. 33, no. 1, p. 1-17.

Knauth, L. P., and Epstein, S., 1975, Hydrogen and oxygen isotope ratios in silica from the JOIDES Deep Sea Drilling Project: Earth and Planetary Science Letters, v. 25, p. 1-10.

Kushnir, J., 1980, The co-precipitation of strontium, magnesium, sodium, potassium and chloride ions with gypsum; an experimental study: Geochimica et Cosmochimica Acta, v. 44, no. 10, p. 1471-1482.

Land, L. S., 1973, Contemporaneous dolomitization of middle Pleistocene reefs by meteoric water, North Jamaica: Bulletin of Marine Sciences, v. 23, p. 64-92.

———— 1980, The isotopic and trace element geochemistry of dolomite: The state of the art *in* Zenger, D. H., Dunhum, J. G., and Ethington, R. L., eds., Concepts and models of dolomitization: Society of Economic Paleontologists and Mineralogists, Special Publication No. 28, p. 87-110.

Land, L. S., and Hoops, G. K., 1973, Sodium in carbonate sediments and rocks: a possible index to the salinity of diagenetic solutions: Journal of Sedimentary Petrology, v. 43, no. 3, p. 614-617.

Lloyd, R. M., 1966, Oxygen isotope enrichment of sea water by evaporation: Geochimica et Cosmochimica Acta, v. 30, no. 8, p. 801-814.

Lorens, R. B., 1981, Sr, Cd, Mn, and Co distribution coefficients in calcite as a function of calcite precipitation rate: Geochimica et Cosmochimica Acta, v. 45, no. 4, p. 553-561.

McCrea, J. M., 1950, On the isotopic chemistry of carbonate and a paleotemperature scale: Journal of Chemical Physics, v. 18, p. 849-857.

Meissner, F. F., 1972, Cyclic sedimentation in Middle Permian strata of the Permian Basin, West Texas and New Mexico, *in* Elam, J. G., and Chuber, S., eds., Cyclic sedimentation in the Permian Basin: West Texas Geological Society, p. 203-232.

Mejia, D. P., 1977, Facies and diagenesis of Permian lower San Andres Formation, Yoakum County, West Texas: The University of Texas at Austin, Master's thesis, 137 p.

Milner, S., 1976, Carbonate petrology and syndepositional facies of the lower San Andres Formation (Middle Permian), Lincoln County, New Mexico: Journal of Sedimentary Petrology, v. 46, p. 463-482.

Murray, R. C., 1964, Origin and diagenesis of gypsum and anhydrite: Journal of Sedimentary Petrology, v. 34, no. 3, p. 512-523.

Nadler, A., and Magaritz, M., 1980, Studies of marine solution basins – isotopes and compositional changes during evaporation, *in* Nissenbaum, A., ed., Hypersaline brines and evaporitic environments: Elsevier, Developments in Sedimentology 28, p. 115-129.

Neev, D., and Emery, K. O., 1967, The Dead Sea depositional processes and environments of evaporites: Geological Survey of Israel Bulletin 41, 147 p.

Patterson, R. J., 1972, Hydrology and carbonate diagenesis of a coastal sabkha in the Persian Gulf: Princeton University, Ph.D. dissertation, 473 p.

Pingitore, N. E., Jr., 1978, The behavior of Zn^{2+} and Mn^{2+} during carbonate diagenesis: theory and applications: Journal of Sedimentary Petrology, v. 48, p. 799-814.

Presley, M. W., 1979, Upper Permian evaporites and red beds, *in* Geology and geohydrology of the Palo Duro Pasin, Texas Panhandle: The University of Texas at Austin, Bureau of Economic Geology Geological Circular 79-1, p. 39-49.

———— 1981, Middle and Upper Permian salt-bearing strata of the Texas Panhandle—lithologic and facies cross sections: The University of Texas at Austin, Bureau of Economic Geology, Cross Section, 10 p.

Ramondetta, P. J., in press, Genesis and emplacement of oil in San Andres Formation, Northern Shelf of the Midland Basin, Texas: The University of Texas at Austin, Bureau of Economic Geology Report of Investigations.

Raup, O. B., and Hite, R. J., 1977, Bromide distribution in marine halite rocks, *in* Dean, W. E., and Schreiber, B. S., eds., Marine evaporites: Society of Economic Paleontologists and Mineralogists Short Course 4, p. 105-123.

Riding, R., 1975, *Girvanella* and other algae as depth indicators: Lethaia, v. 8, no. 2, p. 173-179.

Rudolph, K. W., 1978, Diagenesis of back reef carbonates: an example from the Capitan complex: The University of Texas at Austin, Master's thesis, 159 p.

Sass, E., Weiler, Y., and Katz, A., 1972, Recent sedimentation and oolite formation in the Ras Matarma Lagoon, Gulf of Suez, *in* Stanley, D. J., ed., The Mediterranean Sea: a natural sedimentation laboratory: Stroudsburg, Pennsylvania, Dowden, Hutchinson and Ross, p. 279-292.

Sass, E., and Ben-Yaakov, S., 1977, The carbonate system in hypersaline solutions: Dead Sea brines: Marine Chemistry, v. 5, no. 1, p. 83-199.

Schreiber, B. C., 1977, Environments of subaqueous gypsum deposition, *in* Dean, W. E., and Schreiber, B. C., eds., Marine evaporites: Society of Economic Paleontologists and Mineralogists Short Course 4, p. 43-73.

Shearman, D. J., 1966, Origin of evaporites by diagenesis: Institute of Mining and Metallurgical Engineers, Transactions, Section B, v. 75, p. 208-215.

Shearman, D. J., and Fuller, J. G., 1969, Anhydrite diagenesis, calcitization, and organic laminates, Winnipegosis Formation, Middle Devonian, Saskatchewan: Bulletin of Canadian Petroleum Geology, v. 17, p. 496-525.

Smith, G. E., 1974, Depositional systems, San Angelo Formation (Permian), north Texas: The University of Texas at Austin, Bureau of Economic Geology Report of Investigations No. 80, 73 p.

Sofer, Z., and Gat, J. R., 1972, Activities and concentrations of oxygen-18 in concentrated aqueous salt solutions: analytical and geophysical implications: Earth and Planetary Science Letters, v. 15, p. 232-238.

———— 1975, The isotope composition of evaporating brines: effect of the isotopic activity ratio in saline solutions: Earth and Planetary Science Letters, v. 26, p. 179-186.

Syers, J. K., Chapman, S. L., Jackson, M. L., Rex, R. W., and Clayton, R. N., 1968, Quartz isolation from rocks, sediments and soils for determination of oxygen isotopic composition: Geochimica et Cosmochimica Acta, v. 32, p. 1022-1025.

Taube, H., 1954, Use of oxygen isotopes effects in the study of hydration of ions: Journal of Physical Chemistry, v. 58, p. 523-528.

Todd, R. G., 1976, Oolite bar progradation, San Andres Formation, Midland Basin: American Association of Petroleum Geologists Bulletin, v. 60, no. 6, p. 907-925.

Toomey, D. F., and Cys, J. M., 1977, Rock/biotic relationships of the Permian Tansill-Capitan facies exposed on the north side of the entrance to Dark Canyon, Guadalupe Mountains, southeastern New Mexico, *in* Upper Guadalupian facies, Permian Reef complex, Guadalupe Mountains, New Mexico and West Texas: Society of Economic Paleontologists and Mineralogists, Permian Basin Section, Publication 77-16, p. 133-150.

Veizer, J., Lemieux, J., Jones, B., Gibling, M. R., and Savelle, J., 1978, Paleosalinity and dolomitization of a lower Paleozoic carbonate sequence, Somerset and Prince of Wales Islands, Arctic Canada: Canadian Journal of Earth Science, v. 15, no. 9, p. 1448-1461.

Welte, D. H., and Waples, D., 1973, Ueber die Bevorzugung geradzahleger n-Alkane in Sedimentgesteinen (The preference for even-numbered n-alkanes in sedimentary rocks): Naturwissenschaften, v. 60, no. 11, p. 516-517.

White, A. F., 1978, Sodium coprecipitation in calcite and dolomite: Chemical Geology, v. 23, no. 1, p. 65-72.

Wickman, J., 1978, The southern Oklahoma Aulacogen, *in* Structural style of the Arbuckle region: Geological Society of America, South Central Region, Field Trip 3, p. 8-41.

Appendix A. Calculation of sodium content in dolomite lattice based on whole-rock analysis.

APPENDIX A

Rock unit	Y56	S56	R56	L4	S4	R4	S2	R23
Mean Na (total)	398	206	176	229	341	160	150	303
Mean Cl	592 (16.7 eq.)	872 (24.6 eq.)	1163 (32.8 eq.)	787 (22.2 eq.)	688 (19.4 eq.)	790 (22.3 eq.)	752 (21.2 eq.)	1070 (30.2 eq.)
Mean low Na/Cl eq.	0.71 (fig. 16a)	–	0.18 (fig. 16c)	0.37 (fig. 17a)	–	0.18 (fig. 17c)	–	–
Mean Na/Cl eq.	–	0.36	–	–	0.71	–	0.29	0.44
Na derived from liquid inclusion	0.71 = Na 16.7	0.36 = Na 24.6	0.18 = Na 32.8	0.37 = Na 22.2	0.71 = Na 19.4	0.18 = Na 22.3	0.29 = Na 21.2	0.44 = Na 30.2
	Na = 273 ppm	Na = 203 ppm	Na = 138 ppm	Na = 111 ppm	Na = 316 ppm	Na = 94 ppm	Na = 141 ppm	Na = 305 ppm
Na in dolomite lattice	398 -273 125 ppm	206 -203 3 ppm	176 -138 38 ppm	229 -111 118 ppm	341 -316 25 ppm	160 - 94 66 ppm	150 -141 9 ppm	303 -305 0 ppm

Appendix B. Calculation of sodium content in dolomite lattice based on mechanical crushing of dolomite in water.

APPENDIX B

	1969	2085	2715	MC5	PS7
Sample	(R4)	(S56)	(S4)	(Y56)	(Y56)
Na in sample	182 ppm	225 ppm	340 ppm	460 ppm	461 ppm
Cl in sample	815 ppm (23 eq.)	993 ppm (28 eq.)	815 ppm (23 eq.)	244 ppm (21 eq.)	496 ppm (14 eq.)
Na/Cl eq.	0.50	0.27	0.60	0.67	0.39
Na in liquid inclusion	0.50 = Na 23 Na = 265 ppm	0.27 = Na 28 Na = 173 ppm	0.60 = Na 23 Na = 317 ppm	0.67 = Na 21 Na = 324 ppm	0.39 = Na 14 Na = 126 ppm
Na in dolomite lattice	~0 ppm	220 -173 47 ppm	340 -317 23 ppm	460 -324 136 ppm	461 -126 335 ppm